Aristotle University of Thessaloniki

ARCHMAT
(ERASMUS MUNDUS MASTER IN ARCHaeological MATerials Science)

Archaeomagnetic characterization and possible dating based on archaeointensity values, of prehispanic ceramics from the Nueva Esperanza archaeological site - TCE Sector (Sabana de Bogotá, Colombia)

Luis Felipe Navarro Páez

Dr. Professor Emeritus Despina Kondopoulou – Aristotle University of Thessaloniki; Geophysics Department.

Dr. Assist. Professor Elina Aidona – Aristotle University of Thessaloniki; Geophysics Department.

Dr. Assoc.Professor Lambrini Papadopoulou – Aristotle University of Thessaloniki; Geology Department.

Thessaloniki – Greece; December 2021

Contents

Acknowledgments

I would like to dedicate these words to all those people who not only helped to build the ideas embodied in this document, but also helped to form me as a person during these times. That in one way or another influenced my life, both private and academic.

First, I want to thank the ARCHMAT project for grant me a scholarship, and hence giving me the opportunity to approach to the field of Archaeometry. Thanks to this, I will be able to open the boundaries of the archaeological applications in my country.

Second, I want to thank all people who opened the doors of their institutions to me and dedicated time and interest in collaborating with the development of this work. To the company Transmisora Colombiana de Energía S.A.S E.S.P., the Universidad Minuto de Dios and the Agroparque Sabio Mutis; all being institutes that were the backbone of the Nueva Esperanza-TCE sector excavation and the management of the archaeological findings, who gave the materials with which this project was built. From here I want to thank Hector Lopez, Julieth Rodriguez, of the Agroparque Sabio Mutis, and specially Sebastian Rivas, who was the connection to all the institutions and persons related to Nueva Esperanza-TCE.

Third, I want to thank all the Professors who participated in the development of this project. Assoc.Professor Lambrini Papadopoulou, for the petrographic analyzes carried out, and the leap of faith in approaching Colombian geology. Assist. Professor Elina Aidona for the immense patience she had throughout the laboratory work and whenever I appeared in her office with a question. And to Professor Emeritus Despina Kondopoulou, for risking accepting me as a thesis candidate with an idea on archaeomagnetism in Colombia and helping to focus on the work during these hard times. Eternal thanks for trusting in this project and for all your efforts to make it come true.

Fourth, I want to thank all the people that shared with me all these years in an important manner. Daniela, whom I love and admire. We decided to venture into a pretty crazy idea that I can say worked. And now what is probably the best part, enjoy life while the future unfolds. Thank you for all the support, patience and encouragement given during this time. We will always have Crete (and Santorini). To my family and friends in Colombia. Even though we endure a pandemic with an ocean apart, you kept supporting me, no matter what. And to my new family, my dear ARCHMAT friends. Together we overcome the absolute unexpected, creating bonds beyond nations. Thank you for the last two years that were full of everything.

And last, but not least, my sister Juanita. Thank you for everything.

Introduction

The development of archaeometrical research has been characterized by interdisciplinary fields. Thus, different approaches and new subfields of knowledge and applications are created. In the case of geophysics, with particular interest in the geomagnetic field (hereafter GMF), the study of the past magnetic field of the Earth and its evolution, called Palaeomagnetism, gave important information on its history through geological periods. Researchers found out that the principles and methods used in Palaeomagnetism can be applied on archaeological materials, especially those made from baked clay. These methods help to understand better the GMF in recent times, that is around the last 9000 years, with the appearance of artifacts made from baked clay. The geomagnetic information obtained can help to date the last moment when the artifact was heated and cooled. Hence, the studies of archaeomagnetism evolved in the common ground of different disciplines (for an overview see Brown et al.,2021).

In the last two decades, a considerable amount of archaeomagnetic studies have been published worldwide, but the majority come from Europe, and in general, the North Hemisphere (Hervé, et al., 2019; Brown et al.,2021). This is a serious disadvantage since it is very important to have a homogeneous distribution of the data if a researcher wants to build reliable models of the geomagnetic field and apply them for archaeological purposes. Even so, in the resent years there has been progress in acquiring data from places all over the world, like Middle East (Gallet, et al., 2015; Shaar, et al., 2016; Ben-Yosef et al., 2017), Africa (Di Chiara, 2020), China (Cai, et al., 2020), South East Asia (Cai, et al., 2021), New Zealand (Turner, et al., 2020), Mesoamerica (Mahgoub, et al, 2019b; García, et al., 2021), South America (Goguitchaichvili, et al., 2019) and the Caribbean (Cejudo, et al., 2019).

For the Colombian case, to date, four investigations have been published on archaeomagnetism, specifically on intensity (Berkovich, et al., 2017; Cejudo, et al., 2019; Obregón, et al., 2019; Rojas, et al., 2020). Due to the situation described, these publications take important first steps to understand the characteristics of archaeomagnetic data obtained in northern South America, their relationship with surrounding regions of the continent, the magnetic attributes of the archaeological artifacts, and to establish the interest in the future development of a secular variation curve for the country.

In order to contribute to this problematic, in the present project thirty-nine (39) ceramic fragments excavated from three funerary contexts of the archaeological site of Nueva Esperanza - Sector TCE (municipality of Soacha, in the Sabana de Bogotá) were selected as follows: 10 fragments from TCE06-(B-2)-VI-R57-T21, 20 fragments from TCE14-H10-II-R6-T30 and 9 fragments from TCE04-H3-III-R13-T43. The archaeological data and the samples used are part of the work reported by Rivas (2021). From these contexts, TCE14-H10-II-R6-T30 had previous radiocarbon dating information available. Thus, the general objective of this research was focused, as the ones mentioned above, to understand the archaeomagnetic characteristics of the samples and their potential as reference points using archaeointensity. It is expected that this project helps to cement interest in

archaeomagnetism in Colombia in order to provide data for macro-regional models and as a viable form for dating.

The first part of the document gives a background in several concepts around the magnetic properties of materials and the geomagnetic field of Earth. This with the purpose of explaining the principle of archaeomagnetic dating.

The second section will present the archaeological context. First a general description of the studies of the Muisca Chiefdoms and the interest of archaeologist to study them as complex societies is given. After will come the localization, and brief description of the archaeological interest regarding the Nueva Esperanza site, giving an emphasis on the chronological question. This will also include the geological information about the area and a background on the mineralogical studies carried out with Muisca pottery.

The third section will be dealing with the methodologies applied. It starts describing how the samples were selected and prepared according to each of the experiments carried out. These experiments were the Thellier-Thellier method, the thermomagnetic analysis and isothermal remanent magnetization (IRM). Petrographic observations and SEM-EDS analysis was also carried out by prof. Lambrini Papadopoulou from the Geology Department of the University.

The fourth section presents the results of each experiment

The fifth section will address the discussion of the results. It is divided in four subchapters. The first part will present dialogue of the rock magnetic and SEM-EDS analysis, and the implications around the Thellier-Thellier method. The second part will be a detailed description of the information available in the publications regarding archaeomagnetic studies in Colombia, giving a general overview of the data situation. The third part is similar to the previous one, but the archaeomagnetic models of areas surrounding Colombia. From the previous information and the results of the Thellier-Thellier experiment, the fourth part shows a comparison between the intensity levels with the dates associated.

Finally, we will present some general conclusions and comments from the project and future expectations.

Overview of basic magnetic concepts

- *The Earth's magnetic field*

The exact mechanisms behind the reason why the Earth's magnetic field is generated are still a matter of discussion. The consensus is that the field is associated with the outer core, a region 3000km beneath the planet's surface that is composed of molten iron and nickel slowly churning. According to this hypothesis, the field is generated because of the movement of free electrons in this layer. And due to the Earth's rotation along with gravitational and thermodynamics effects, the generated field behaves as a self-sustaining dynamo.

The magnetic field of the Earth resembles the field produced by a simple bar magnet, with two poles, located in the center of the Earth (named "geocentric axial dipole"), which is tilted nowadays by approximately 11° with respect to the rotational axis. Because of this, the positions of the Earth's magnetic poles do not coincide with its geographic poles. In present times, the north geomagnetic pole is situated in the north of Canada and the South geomagnetic pole is in Antarctica. The geomagnetic field is often visualized in terms of field lines that emanate from the south geomagnetic pole and converge at the north geomagnetic pole (Figure 1) (De Marco, 2007). Although the magnetic field at the Earth's surface is predominantly explained as an axial dipole, the actual magnetic field is more complicated. Significant deviations from a dipole field exist since there are additional, non-dipolar aspects in the geomagnetic field, but due to the limitations of the present project, this matter will not be addressed.

To understand the geomagnetic field information at a certain point of the Earth's surface, it can be represented as a vector that manifests two characteristics: direction and intensity. The direction is determined by two angles: declination (D) and inclination (I). The first one (D) is the angle between the horizontal component of the magnetic-field vector (H) and the geographic north, while the second one (I) is the angle between the horizontal plane and the total field vector (F). These direction values are dependent of the orientation of the location where the measurements are being done. The intensity (F), which is independent of the orientation factor, represents the strength of the field at a certain point, and thus, affecting the strength of magnetization that magnetic minerals will obtain (Tarling 1983; De Marco 2007). These magnitudes are often represented in cartesian coordinates, where X corresponds to the north, Y to the east, and Z is the vertical component, regarded as positive in a downward direction (Tarling 1983) (Figure 2). In geomagnetism, the most used unit in the International System of Units for the magnetic field intensity is the Tesla (T), in a scale of micro (μT) and/or mili (mT).

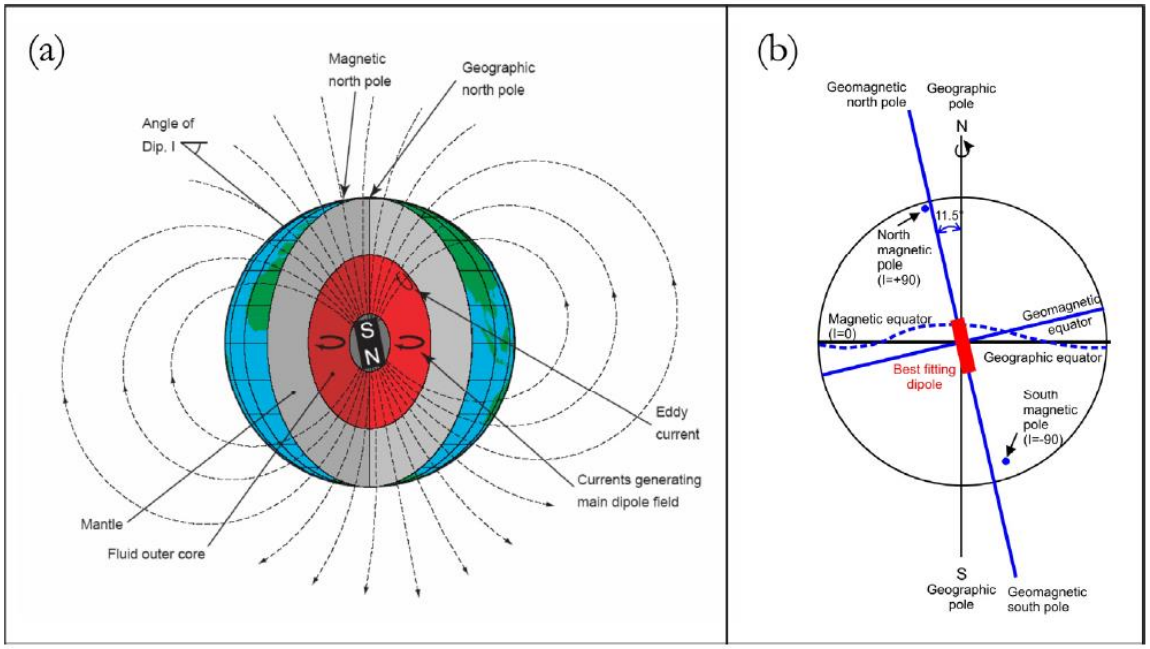

Figure 1 - (a) The Earth's main dipolar magnetic field is shown. The outer core that generates the current electric circulation is shown in red, with field lines emanating from near the south geographic pole and converging near the north geographic pole. Taken from Linford, 2004 in De Marco, 2007. (b) Inclined axial-dipolar part of the Earth's magnetic field, similar to the field that would be produced by a magnetic bar located at the Earth's center tilted by about 11.5°. Taken from Butler, 1992 in De Marco, 2007.

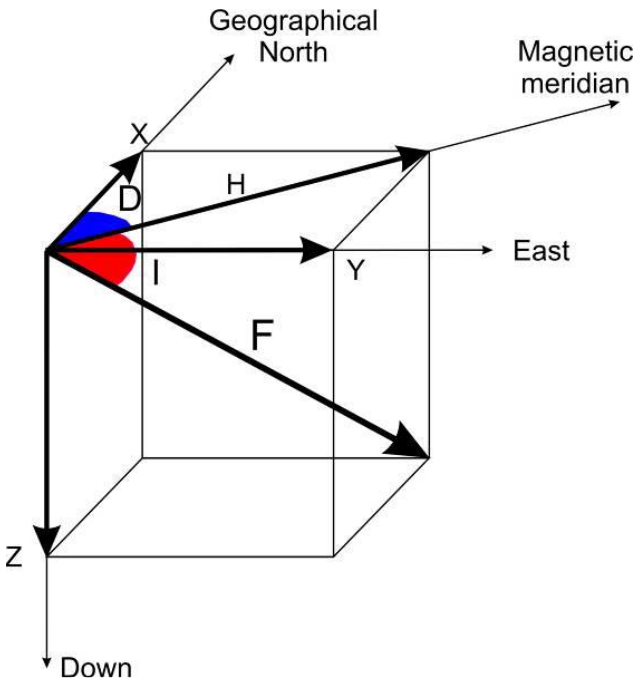

Figure 2 - Magnetic field components. Taken from De Marco, 2007.

- *Magnetic properties*

This subchapter will present a series of important concepts that help to understand magnetic properties, and that will be mentioned several times during the present project. These definitions were taken from Tarling (1983) and the glossary of De Marco (2007).

The best start is to define *magnetic moment*. This concept expresses the magnetic intensity, or strength, of a magnet. The magnetic moment can be expressed in terms of volume (A/m) or weight (Am2/kg). The effect of a magnetic moment in a material is known as *magnetization*. Only materials with iron oxides can acquire magnetization.

When a material is magnetized, there are going to be regions where the magnetic moments of the atoms are parallel, separated by walls. These regions are called *magnetic domains*. They form spontaneously to minimize the energy potential of a magnetized material. The effect of the magnetic domains can vary depending on the grain of the material. A *grain* is a macroscopic sample of a crystalline mineral that will generally consist of multiple conjoined crystals of varying shapes and sizes. Each of these crystals, within which the atoms are arranged on a single regular lattice, is termed grain. So, when an entire grain of a mineral is being magnetized in the same directions, the effect is called a *single domain behavior*. When a grain is divided into several magnetic domains, each one magnetized in a different direction, is called *multidomain behavior*.

These properties of the magnetic materials can be affected by different parameters. *Coercivity*, is one of those, which consists in the magnetic field that must be applied to a material in order to change its magnetization in the opposite direction, depending directly on the grain size and shape. Another parameter, the *magnetic anisotropy*, is when the magnetic material shows a directional variation of the magnetic properties, based on the magnetic forces applied on it. The last one we present here is the *magnetic susceptibility*, which is a value that expresses the ability of a sample to acquire a magnetization in a magnetic field. Different materials have different levels of magnetic susceptibility.

Depending on the ability of materials to get magnetized, and the behavior of the electrons at an atomic level, there are three groups. The first one, *diamagnetic materials*, consists in materials that practically lose the magnetization induced when the magnetic field is removed. This is due to their susceptibility being small, almost imperceptible. The second group, *paramagnetic materials*, are materials that at an atomic level present magnetic moments that do not interact with each other. Also, their orientation is random, so the produced magnetization is zero. When a magnetic field is applied, the magnetic moments are aligned according to the field, but as soon as the field is removed, the orientation goes back to random. In contrast with the two first groups, is the third group, the *ferromagnetic materials*, which are materials that can produce their own magnetic field in the absence of an applied one. These materials have atoms with magnetic moments, but unlike the paramagnetic case, adjacent atomic moments interact strongly. During removal of the

magnetizing field, magnetization does not return to zero but retains a record of the applied field. The recording, and keeping, of past magnetic fields is called *remanent magnetization*.

Inside the ferromagnetic materials there are other three types, based on the crystal structure which affect the spin alignment of the atoms, and therefore the behavior of the magnetic energy (Figure 3). The first category is the *ferromagnetic (sensu stricto)*, in which the atomic spins are aligned parallel to each other, resulting in a very strong external field generated even in the absence of an applied field. The second case is the *antiferromagnetic*, where the atomic spins are aligned in an anti-parallel form, making each layer cancel the other due to equivalent magnetic moments. The third case is the *ferrimagnetic*, where the spins are also aligned in an anti-parallel form but have different magnitudes so that the materials have weaker magnetization than the ferromagnetic ones, tacking the direction towards the stronger layer. Most of the important ferromagnetic minerals fall in this last category.

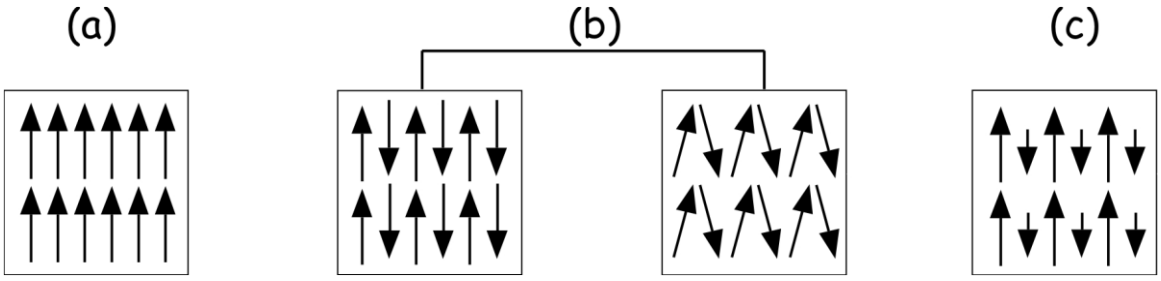

Figure 3- Spin alignment in: (a) ferromagnetism (seunsu stricto), (b) antiferromagnetism and (c) ferrimagnetism. Taken from Tauxe, 2005 in De Marco, 2007

The final concept that we decided to bring in this chapter is the *Curie temperature*. When the temperature is rising, there is a point where a material loses its ferromagnetic properties and becomes paramagnetic. On cooling, back through this temperature, magnetic moments of ferromagnetic materials become parallel. Each material has its own Curie temperature The understanding of the Curie temperature, next to the general characteristics of ferromagnetic materials and remanent magnetization, form the basis for the principles of archaeomagnetism, which will be explained further in a later chapter.

- *Magnetism and minerals of interest*

The most common ferromagnetic minerals are the iron oxides (e.g., magnetite, maghemite and haematite), the iron oxide hydroxides (e.g., goethite) and the iron sulfides (e.g., greigite and pyrrhotite) (De Marco, 2007). From these, the most important magnetic minerals subjected to archaeomagnetic studies are three iron oxides: magnetite (Fe_3O_4), maghaemite, (γ-Fe_2O_3) and haematite (a-Fe_2O_3). Their importance lies in the fact that they are found in most soils, clays and rocks used to form archaeological materials. Fine grained

iron oxides are responsible for the red color of baked clay when heated in an oxidizing atmosphere or greyblack when heated in a reducing atmosphere.

Other minerals of interest are the titanomagnetites, pyrrhotite and greigite. Of all these minerals, it is important to know the Curie temperature and Coercivity (Table 1), because these characteristics will help in the archaeomagnetic interpretation.

Mineral	Formulas	M_S (Am^2/kg)	T_C or T_N (°C)	χ (E-06 m^3/kg)	H (mT)
Magnetite	Fe_3O_4	90-92	575-585	200-1100	10-50
Ulvöspinel	Fe_2TiO_4		-153	~1*	
Ti-magnetite 60%	$xFe_3O_4(1-x)$ Fe_2TiO_4	24	150	25-120	8
Ilmenite	$FeTiO_3$		-233	1-1.13	
Haematite	α-Fe_2O_3	0.4	675	0.1-7.6	>1000
Maghaemite	γ-Fe_2O_3	70-80	~600	400-500	
Pyrrhotite	Fe_7S_8	~20	~320	0.1-300	100-500
Greigite	Fe_3S_4	~25	~333		60-100
Goethite	αFeOOH	<1	~100-120	0.26-0.28	>1000
Lepidocrocite	γFeOOH		-196		

Table 1 - Main characteristic of the most common magnetic minerals. From this table we want to highlight the Curie temperature and the Coercivity (H). Table taken from De Marco, 2007.

- *Remanent magnetization*

There are different ways that the recording, and maintaining, of past magnetic fields can happen inside ferromagnetic materials. In other words, different types of remanent magnetizations. The main one that must be understood is the *Natural remanent magnetization* (NRM), which is the in-situ remanent magnetization of a natural sample, such as rocks, baked clay, and other materials, as first measured in the laboratory (De Marco, 2007). Tarling (1983) define the NRM as the summation of all components of specimen remanence acquired by natural processes. What we can take from these definitions is that the NRM is composed of one or more magnetizations, depending on the history of the sample. Samples with a geological time span tend to have a more complex magnetization process than the archaeological samples, due to their long exposure to various magnetizing factors. It is important to remark that, to some extent, all magnetization that can affect the NRM can be replicated in laboratory conditions (Tarling,

1983). For the case of the archaeological samples, which is the interest of the present project, three types of magnetizations are of interest: the *Thermoremanent magnetization* (TRM), the *Viscous remanent magnetization* (VRM), and the *Isothermal Remanent Magnetization* (IRM).

The TRM is acquired by a sample after its cooling from a temperature higher than the Curie Temperature in an ambient magnetic field (De Marco, 2007). Tarling (1983) defines this type of remanence as the one acquired by cooling over a range of temperatures starting at or below the Curie temperatures. One crucial difference here is that Tarling refers to "temperatures" as in plural. So, when the samples reach a temperature higher than the Curie temperature, and then proceed to cool down in room temperature, they gain the Total-TRM (tTRM). The remanent magnetizations acquired from temperatures lower than the Curie temperature, are called Partial-TMR (pTRM). The understanding of the TRM is the basis to the Thellier-Thellier method for achaeointensities, which will be explained in the Methodology chapter.

The VRM is a particular case since it is considered an undesirable component of magnetization, due to instability, and that can be eliminated by thermal demagnetization processes at low-moderate temperatures, or by alternating field demagnetization at low fields (Tarling, 1983; De Marco, 2007). This instability is because the VRM is acquired spontaneously by a sample after an exposure to a weak magnetic field, meaning that the magnetic domains react at temperatures approx. to 200°C or lower, and their magnetization directions can realign at room temperature with enough time. Even if this kind of remanence can be eliminated by thermal demagnetization in laboratory processing, it is important to have account of it to avoid errors.

The IRM is acquired by a sample after the application of an increasing magnetic field and removal of the field. This field is generally strong and is applied in a few seconds. Due to the uncommon natural circumstances that the IRM can happen, this is a remanent magnetization that is considered mostly for laboratory work (Tarling, 1983; De Marco, 2007).

- *Basic principles of archaeomagnetism*

Archaeomagnetic dating is based on the constant change, both in direction and intensity, of the Earth's magnetic field. The principle of archaeomagnetism consists of the property that archaeological materials rich in iron oxides retain a stable thermoremanent magnetization (TRM), after being heated above certain elevated temperatures (the Curie temperature) and subsequently cooled (Tarling, 1983; Gómez-Paccard & Pavón Carrasco, 2018b). This magnetization creates a record in the material which preserves the direction and intensity of the geomagnetic field, of the region and the moment, when it was last heated. If the magnetization remains unchanged, it can be used to provide information about the past geomagnetic field. Using this principle, and studying material properly dated by other methods, geophysicists can establish master curves of geomagnetic field variation for a

particular region, called secular variation curves (SVC), which can then be used as a dating guide for baked archaeological materials of unknown age (Tarling, 1983; Gómez-Paccard & Pavón Carrasco, 2018; Brown, et. al., 2021).

Because iron oxides are present in most clay sources, this dating method is useful when working with ceramics or other fired clay materials such as kilns, bricks, burned walls, or similar (Tarling, 1983; Schnepp, 2018). Although this form of paleomagnetism has become useful for archaeological dating, the study of the material in this framework also allows to obtain information on the composition, provenance, and baking process of the object (Gómez-Paccard & Pavón Carrasco, 2018).

It is important to notice that the accuracy of the curves depends on the data available for the region, which means that the study of well dated materials is essential to obtain better reference curves (Schnepp, 2018; Gómez-Paccard & Pavón Carrasco, 2018b; Brown, et. al., 2021). There are three values that can be determined when doing an archaeomagnetic research (which we have previously mentioned): the angles of declination (D), inclination (I), and the intensity magnitude (F). Respectively they represent the direction of the magnetic compass relative to the geographic north, the tilt of the magnetic field line, and the field's strength (Tarling, 1983; Schnepp, 2018; Gómez-Paccard & Pavón Carrasco, 2018b; Brown, et. al., 2021).

Materials sampling protocols to obtain archaeodirection (declination and inclination) are well established in paleomagnetism laboratories (for an example see English Heritage, 2006). In order to obtain accurate information on archaeodirection, the sample must be oriented from fired clay elements that remain in situ, such as kilns. On the other hand, Gómez-Paccard & Pavón Carrasco (2018a) describe that one of the advantages of intensity studies is that they can be carried out on objects that are not taken from clay elements in situ, such as pottery fragments. The technique used to obtain intensity was developed by Emile and Odette Thellier during several decades of work (Tarling, 1983; LeGoff, et al., 2006; Brown, et. al., 2021), resulting in a demagnetization process the called Thellier-Thellier method (Thellier & Thellier 1959). This will be explained more in depth in the **Methodology** chapter.

Archaeological Context

- *Overview of the Muisca Chiefdoms as Complex Societies*

For this section, a summary of how the Muisca Chiefdoms have been studied from the archaeological perspective, trying to understand them as complex societies, will be presented. The purpose is to give a general context of the importance of the Nueva Esperanza – TCE sector site, the area where the samples are from.

The 'Muiscas' or 'Muisca Chiefdoms' are the names given to the prehispanic population that inhabited the lands of the Eastern Andean Highlands of Colombia, in a greographical region called the Cundiboyacense Plateau. For archaeological purposes, the Cundiboyacense Plateau is usually divided into two macro-regions, the southern valleys of the Sabana de Bogotá and the northern, higher, valleys of Boyacá. This idea has been used to facilitate the interpretation between the archaeological and ethnohistorical records because the Spaniards described different powerful rulers among the chiefs of the South and the North (Botiva, 1989).

The archaeological chronology stablished for these societies consider their appearance during the first millennium BC until the Spanish Conquest (XVI century) and Colony (XVII and XVIII centuries) (Boada & Cardale de Schrimpff, 2017). Even so, the exact date of appearance and the dates of changes between the prehispanic subperiods, on the different regions that conforms the Cundiboyacense Plateau, have been subjects of debate for several decades (Silva Celis, 1981; Botiva, 1989; Boada & Cardale de Schrimpff, 2017).

Although the name 'Muisca' is used to describe these societies, ethnohistoric research and archaeological record are showing that these people were different among each other, with cultural similarities but not a political union (Gamboa, 2013; Langebaek, 2019). Still, for the sake of pragmatism, this name is still used (Langebaek, 2019).

The Muisca Chiefdoms have been considered as one of the most complex and hierarchized societies that the Spaniards observed with their arrival to America. This idea was consolidated in the Spanish chronicles (Broadbent, 1964; Langebaek, 1987; Therrien, 1996; Gamboa, 2013; Langebaek, 2019) and it lasted during the formation of the Colombian nation in the 19th century and with the arrival of the first foreign archaeologists in the early decades of the 20th century (Therrien, 1996; Langebaek, 2003; Langebaek, 2019). Since then, one of the interests within the archeology of the Cundiboyacense Plateau has been to identify factors that could have influenced the social complexity of the prehispanic inhabitants of the area.

Reichel-Dolmatoff (1986), applied the concepts of 'chiefdoms' and 'early states' in the prehispanic societies of Colombia. He puts the Muiscas as an incipient state, a political conglomerate that exceeded the stage of the chiefdom but did not reach the complexity of a

state. The base of this approach are the records left by the Spaniards. Despite this, the same author also points out that the archaeological record that accounts for the social characteristics observed by the Spaniards is scarce. Years before, Sylvia Broadbent (1965) evidences the same, although she attributes it to the scarce scientific research in the area. In turn, Haury and Cubillos (1953), from one of the first excavations carried out in the Sabana de Bogotá with adequate academic rigor, raised the idea that the prehispanic inhabitants of the region did not seem to have the degree of complexity described by the Spaniards, arguing ecological reasons that prevented this.

Currently, no one considers the Muiscas as incipient states, and the concept of 'chiefdom' is not often used, in preference of speaking of complex societies, but Reichel-Dolmatoff's questions persist. Archaeological investigations have emphasized explaining the emergence of Muisca society understood as complex societies in a regional scale (Langebaek, 1995), the participation of agriculture in these processes (Boada, 2006; 2007), the dynamics of social change in different sequences of occupation together with settlement patterns and established relationships with the environment (Langebaek, et al., 2001), and the concern to identify a social hierarchy based on evidence of specific activities that would produce accumulation of wealth and prestige (Boada, 2007).

Research around the concept of prestige has suggested that some chiefs gave more importance to the celebrations than to the accumulation of wealth (Salge, 2007; Fajardo S. , 2011). Some other hypotheses deal with several subjects: the development of kinship through the sequences of occupation in prehispanic periods as the base of complexity (Romano, 2003; Boada, 2007); the control of settlement formation and construction of houses due to the great importance they had for the Muiscas, according to linguistic and ethnohistoric data (Henderson & Ostler, 2009); the access to favorable soil for cultivation, from the perspective of domestic units within a particular political group (Kruschek, 2003); the consumption and distribution of foreign ceramics (Patiño, 2005); the differentiation present in the funeral practices and their respective garments (Langebaek, 2012); the control of specific areas that could allow microverticality and contact with other societies (Argüello, 2015); or in the pattern of settlement and demographic levels according to social forces of attraction (Fajardo S. , 2016).

Several authors have highlighted the importance of addressing the domestic unit as an analytical basis to reach other data on social behavior and social complexity processes, which may not be observed in other work scales, such as the regional one (Romano, 2003; Patiño, 2005; Henderson & Ostler, 2009; Fajardo S. , 2011). At the same time, at the regional level, Boada (2013) analyzes the demographic dynamics associated with the prehispanic populations of the Sabana de Bogotá, explaining that the social trajectory that took place in this area differs from what is being evidenced for other sectors of the Cundiboyacense Plateau. She explains that this may indicate that the formation of the different prehispanic complex supralocal communities in the Cundiboyacense Plateau may have varied from base-factors. Finally, Langebaek (2019) expresses that, although sometimes the Muisca Chiefdoms do not appear too hierarchical for us, as modern

observers, the archaeological research has demonstrated that they were societies with different and deep levels of complexity and that the investigations must carry on because we only have discovered the tip of the iceberg.

This paradigm was constructed with ethnohistorical evidence, and several types of archaeological research have contributed to understanding these past societies. Regional surveys, excavations, settlement patterns, funerary contexts, kinship structure, agriculture, craftsmanship, demography and so many other subjects common in archaeological discussions have been treated in this region, nowadays supported by new techniques and methodologies such as ancient DNA, isotope analysis, biomarkers, in-depth statistical analysis, among others. However, the matter of chronology is still on debate, and thus the importance of the site.

For the Cundiboyacense Plateau, the pre-Hispanic chronology is highly debated in terms of dates, social changes related to these and the different places in which the area is subdivided (for example, differences between the Sabana de Bogotá and the northern part belonging to Boyacá), but there is an established division: Herrera (which has already been proposed with interal subdivision, see Boada & Cardale, 2017), Early Muisca and Late Muisca (Langebaek 2008: 68-71, Boada & Cardale, 2017). Chronological debates focus mostly on the time limits of the first two sequences. This complication is deepened when comparing the chronologies with the associated ceramic types, since often there is no common agreement, and also because is possible that the types had different moments of development withing the regions of the Cundiboyacense Plateau, as several authors have already begun to show (Argüello 2015: 38, Jaramillo 2015: 32-43). The challenge that archaeology faces with refining the chronology of the Sabana de Bogotá responds to the need of better understand social changes within temporary spaces in this region (Jaramillo 2015).

For the Sabana de Bogotá, the southern part of the Cundiboyacense Plateau, the latest chronological division proposed for pre-Hispanic times (Boada & Cardale, 2017) is as follows: Early Herrera (400 BC - 200 AD), Intermediate Herrera (200 AD - 700 AD), Late Herrera (700 AD - 1000 AD), Early Muisca (1000 AD - 1350 AD) and Late Muisca (1350 AD - 1600 AD). Still, the same authors express that this chronology is not exempt of any of the challenges previously mentioned. Also, there are still problems differencing the division between the Herrera sub periods, and the transition to the Early Muisca period. That is why some authors still prefer to squeeze all the Herrera subperiods in one and put the Early Muisca period earlier in the sequence, this being the case of the Nueva Esperanza site.

- *The Nueva Esperanza archaeological site*

The Nueva Esperanza site is located in the southern part of the Sabana de Bogotá, in the vicinity of the Soacha municipality -E977235 N977318 (Magna Sirgas Colombia - Bogotá)-, 2572 m.a.s.l. (Rivas, 2021) (Figure 4). Its surrounding areas are already of high

archaeological potential, due to the excavation of nearby sites during the last decades, and the presence of the Salto de Tequendama, a waterfall that according to the Spanish records, was an important landmark to the Muisca cosmology.

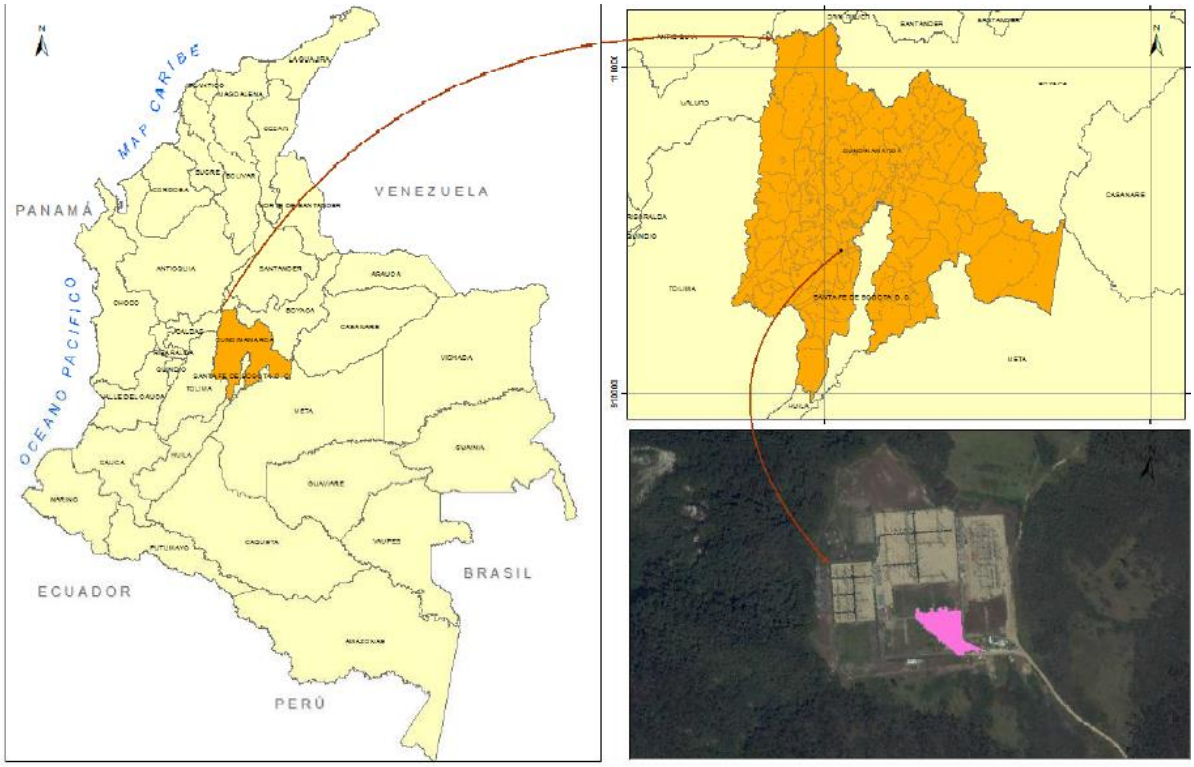

Figure 4- Localization of the Nueva Esperanza site inside the Colombian territory. The purple highlight in the satellite image is the TCE area. Taken from Rivas (2021:37)

The geological information for the site (Figure 5 and Figure 6), which will be explained next, is taken from Gonzáles (2016c), Romano (2016) and Rivas (2021). The archaeological site is located on a terrace of natural origin Coluvio - Alluvial (Qta), elongated in a North - South direction on the Guaduas geological formation (KPggu) with an inclination less than 15 °, and as part of the Guadalupe group (Ksg). The Guaduas formation (KPggu) is formed in its upper part by variegated claystone, with layers of fine-grained quartz arenite. In its lower part there is clay, siltstone, and quartz sandstone with layers of carbon. Gonzáles (2016c) mentions that due to the non-expansive fine textures of these rocks, they could be used in pottery work. The Guadalupe formation (Ksg) is subdivided into the Labor and Tierra (Kslti) formations, made up of fine to medium-grained sandstone in thick layers; the Plaeners formation (Ksp) whose composition is siliceous and chert in thin to medium layers, with intercalations of mudstones and fine quartz sandites; and lastly the Hard Sandstone formation (Ksad), basically composed of fine-grained quartz sandstone in thin to very thick layers, with intercalations of coarse siliceous siltstones.

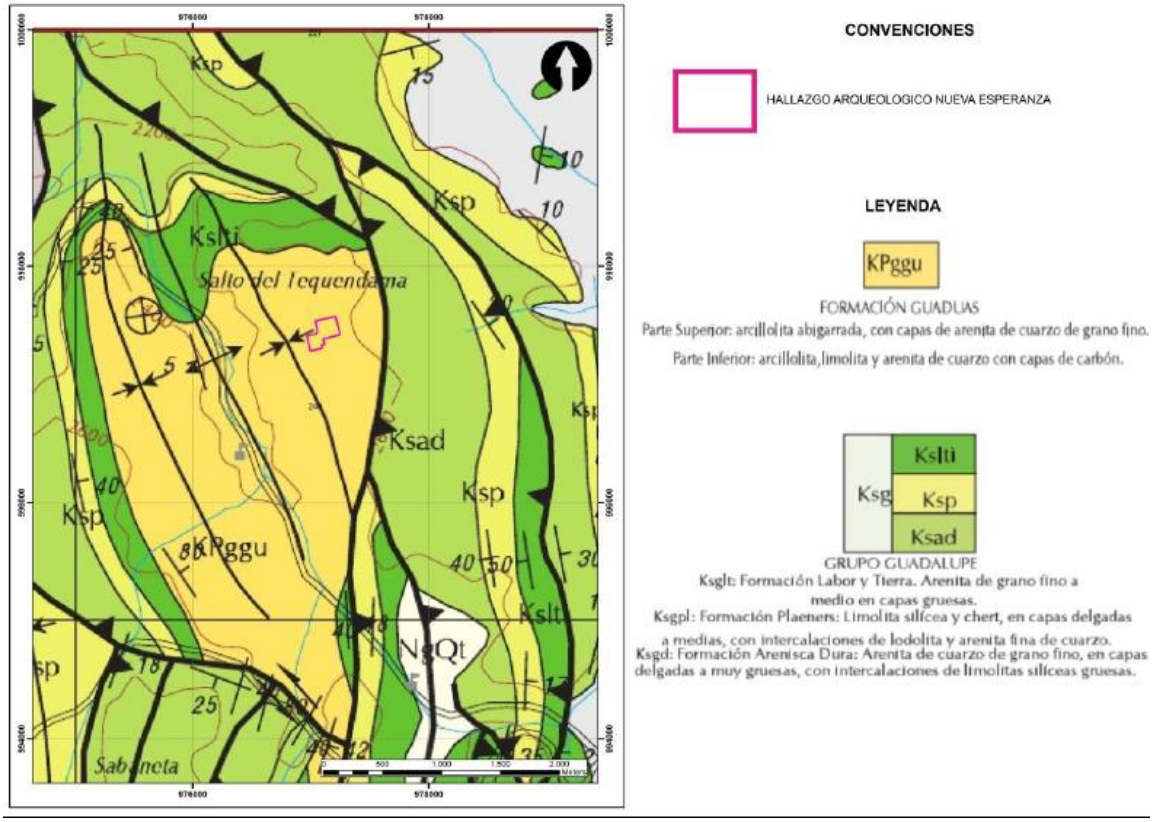

Figure 5 - Geological map of the area. Taken from González (2016c:23)

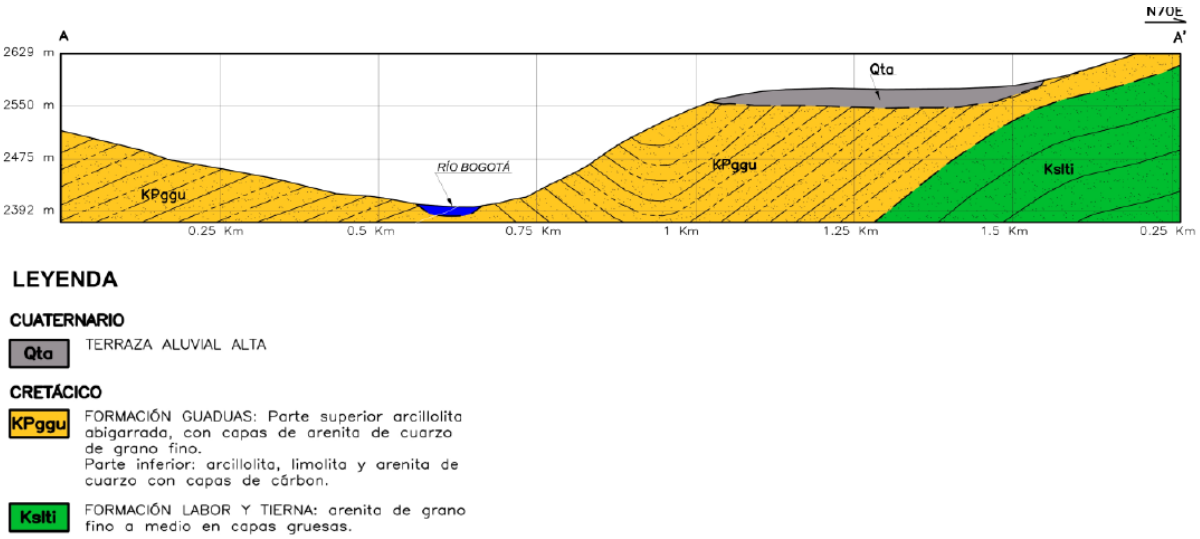

Figure 6 - Geological stratigraphy of the area. Taken from González (2016c:26)

The site has a recent and outstanding history on the archaeology of the Eastern Andes of Colombia, being the product of several years of research from different preventive archaeology projects, providing a large amount of information on a pre-Hispanic (Muisca) settlement that will keep feeding, for years to come, the discussions briefly exposed in the paragraphs above (González, 2016b; Romano, 2016; Rivas Estrada, 2021). Because this site is one, if not, the most extensive archaeological excavation made in Colombia to the date, the evidence for any kind of research is at hand. Particularly, a topic of interest for this project, are the discussions around the chronology of the site related to the dates obtained and the ceramic typologies.

The analyzes carried out in two different sectors of Nueva Esperanza (González, 2016a; Lizcano, 2016) showed that for this area of the Sabana de Bogotá there are a majority of clear typologies with respect to the Herrera Period (400 BC-200 AD). Although there are also some for the Early Muisca Period (200 AD-1000 AD) and the Late Muisca Period (1000 AD - 1600 AD), it can be observed that there is a process of change, in typological fashions mostly based on temper descriptions, among the 9th-11th centuries approximately, which is when the transition is considered. Despite this, the process is not very clear at the level of ceramic materiality, which raises doubts regarding the relative chronology (the authors speak in particular of the *Funza Cuarzo Abundante* type, which they subdivided), which means that it can be an interesting point were applying archaeomagnetic dating helps to refine chronological limits and materiality characteristics. As stated before, the Nueva Esperanza site was excavated by different companies within different preventive archaeology projects, so the ceramic group studied for this project is from the TCE sector.

- *Mineralogical information from the pottery of the area*

The studies to determine the mineralogical composition from the Muisca pottery are scarce and difficult to track, mostly because a part of them are nonpublished data. Even so, there has been some efforts that, when compared to each other, can give a general idea of the composition and even a possible provenance of certain typological groups. All studies that will be presented are based on thin section and petrographic analysis. The earliest record found is from Paepe & Cardale (1990), who try to determine if there are differences at the mineralogical level between the three typologies established for the Herrera period (at that moment) in the Sabana de Bogota. The three typologies are *Mosquera Rojo Inciso* (MRI), *Mosquera Roca Triturada* (MRT) and *Zipaquira Desgrasante Tiestos* (ZDT). For the ZDT and the MRT, the authors explain that they were made from local sources but may have different variations according to the possible manufacturing area inside the Sabana de Bogota. The MRI is a different case. Although the researchers divided the MRI into four subgroups, two of them are originating from foreigner sources. The MRI type (a) presents temper from volcanic origin, places where rocks of andesitic, dacitic, riodacitic and rhyolitic type are frequent. The type (b) presents temper from magmatic and metamorphic origin. For the first case the authors suggest that the origin could be the Magdalena River,

west to the Sabana de Bogota; and for the second case they suggest that the origin could be Central Highlands, west to the Magdalena River. These suggestions were supported with an atomic absorption spectroscopy analysis that the researchers also carried out.

The next work was the report made by Fernández (2009) about two pottery fragments. One from the typology *Funza Cuarzo Fino* (FCF) and the other one from *Tunjuelo Laminar* (TL), usually associated with the Early Muisca period. They were obtained in the municipalities of Suba and Cota, respectively. The author observed two groups of temper, one of volcanic origin composed by beta quartz (with bays and straight extinction), feldspar (zoned plagioclase or with twinning of albite, pericline or Carlsbad) rock fragments (tuff of crystals, chert and porphyritic rhyolite) and heavy minerals (hornblende and pyroxene). The other group of temper is of sedimentary origin, composed by phosphate quartz sandstone (very fine-grained, well selected), silica-cemented quartz sandstone (very fine-grained, well selected), phosphate lodolite (partially transformed into chert), quartz siltstone (phosphate-clayey), claystone, shale and chert. According to his observations, the fragment of FCF had more quantity of volcanic temper than sedimentary, while the case of the TL was the other way around. What arises from this information is that, as the previous investigation stated, the presence of volcanic rock is not common for the area of the Sabana de Bogotá.

The last information to present is by Calderón (2016). This is a very important source of information because it comes from the petrographic study on thin sections cut from Nueva Esperanza samples. The author analyzed the results of twenty samples, coming from different typologies that characterize the three main periods of the Muisca occupation (Herrera, Early Muisca and Late Muisca). His findings are quite similar to the observations made by the previous authors. The petrographic analysis identified high percentages of plagioclase in seven of the samples: sample 2 (61.4% - MRI), sample 4 (54.8% - ZDT), sample 3 (38.2% - MRI), sample 9 (22.3% - FCA), sample 8 (16% - FCA), sample 10 (16% - FCA), sample 12 (15% - FCA). The author highlights this information because it indicates that a temper of igneous origin was used, which is not common in the region. In the rest of the sample, the tempers correspond to sedimentary rocks of marine origin with preeminence in their composition of quartz, iron oxides and clay minerals, which agree with the predominant rock types in the geological formation of the area

Observing the typologies of the samples that were analyzed, together with the information from the previously exposed studies, we begin to see a possible tendency of non-local temper for certain typologies of the Herrera and Early Muisca periods.

Methodology

- *Sample preparation*

As was mentioned in the Introduction, thirty-nine (39) ceramic fragments excavated from three funerary contexts of the archaeological site of Nueva Esperanza - Sector TCE (municipality of Soacha, in the Sabana de Bogotá) were selected as follows: 10 fragments from TCE06-(B-2)-VI-R57-T21, 20 fragments from TCE14-H10-II-R6-T30 and 9 fragments from TCE04-H3-III-R13-T43. To be able to manage them and keep track during the different experiments that were realized, each fragment was renamed (Table 2).

Also, most of the equipment used required regularly shaped sub-samples called "specimens". To create them, in the context of this project, the first step was to select the most suitable fragments of pottery, in other words, the fragments with less evidence of bad baking process, or that did not show any burning after made. These needed to be cut into cubes of similar dimensions (2cm x 2cm, approx. The thickness depended on the fragment itself), that were called in alphabetic order (Figure 7). A workshop saw located in the facilities of the Aristotle University of Thessaloniki was used to cut the fragments (Figure 8).

From the original thirty-nine samples, twenty were selected to create at least three specimens per fragment. Of those twenty, five were selected to have an extra cut that were subject of the petrographic analysis done by prof. Lambrini Papadopoulou. So, for example, if a specimen is called “TC14-11a” it means it is the first cut of a FCA1 fragment that comes from the TCE14-H10-II-R6-T30 context.

Original name	**Typology**	**N fragments**	**New name**
TCE06-(B-2)-VI-R57-T21	DG	10	TC6 - (from 1 to 10)
TCE14-H10-II-R6-T30	DG	7	TC14 - (from 1 to 7)
	RT	3	TC14 - (from 8 to 10)
	FCA1	5	TC14 - (from 11 to 15)
	FCA3	5	TC14 - (from 16 to 20)
TCE04-H3-III-R13-T43	DG	5	TC4 - (from 1 to 5)
	FCA3	2	TC4 - (from 6 to 7)
	RT	1	TC4 - 8
	FCA2	1	TC4 - 9

Table 2 - Names given to the pottery fragments during the present project

Figure 7 - From the original sample to the specimens (with the cut for petrographic analysis)

Figure 8 - Workshop saw used to cut the samples into the specimens

Now, the next step is regarding the shape of the specimens. As was said before, most of the equipment used required regularly shaped, which is cylindrical. To create this, the specimens were put on a plexiglass mold with cylindrical shapes. Then, gypsum plaster was cast into the mold, covering the pottery fragment, and forming an object of the desired shape. The result was a cylinder of 2.5 cm in diameter and 2.2 cm long, approx. This new shape of the specimens was then covered by a layer of alumina cement, that would help to protect the specimen from the high temperatures of the oven during the Thellier-Thellier method. Then, a line was drawn on one of the tops and side of the cylinder, as a guide of

the Z-axis for the Thellier-Thellier method. Due to this project being focused on intensity values, these guides can be arbitrary. But is important to remark that in the case of direction values, the lines highly depend on the sampling process made on the field. The specimen's name will be written on the top (Figure 9, Figure 10).

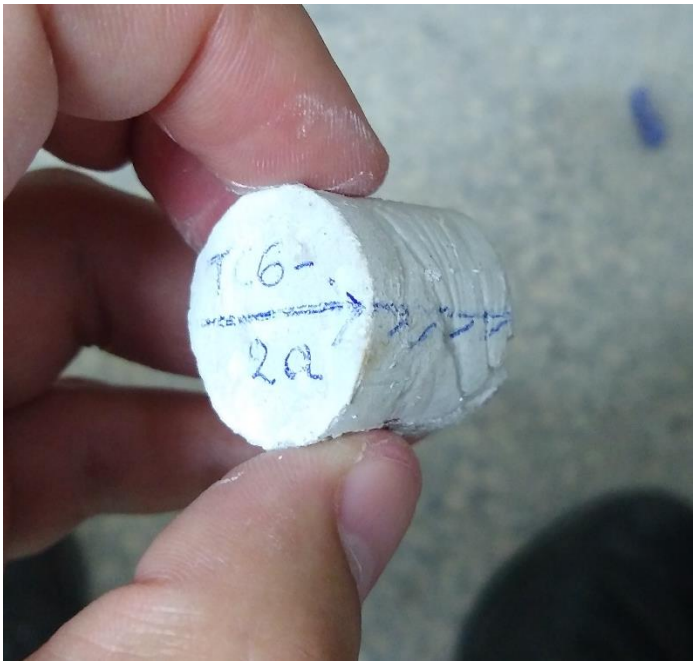

Figure 9 - Result of the specimen preparation

Figure 10 - Specimens aligned before a heating/cooling cycle of the Thellier-Thellier method. The guidelines help to maintain the same order which is important for the field applied.

Not all the specimens prepared were used in the Thellier-Thellier method. A few were used for the IRM measurements. And some were not made into the cylindrical shapes but were

grinded to be used for the thermomagnetic measurements. These decisions were made based on the initial NMR measurement, the relation between the fragments of the same contexts, and the idea that no more, and no less, of three specimens per sample were going to be used for the Thellier-Thellier method. The next table (Table 3) presents a summary of what specimen was used for each one of the experiments:

Sample	Specimen	Th-Th	IRM	TherMag	Petrography	SEM
TC6-1	a	X			X	X
	b	X				
	c	X				
	d					
	e					
	f					
TC6-2	a	X				
	b	X				
	c	X				
	d			X		
TC6-3	a	X				
	b	X				
	c	X				
	d			X		
	e					
TC6-4	a	X				
	b	X				
	c	X				
TC6-7	a	X				
	b	X				
	c	X				
TC6-8	a	X			X	
	b	X				
	c	X				
TC6-10	a					
	b					
	c		X			
TC4-1	a	X				
	b	X				
	c	X				
TC4-3	a	X			X	
	b	X				
	c	X				
TC4-5	a	X				
	b	X				
	c	X				
	d			X		

TC4-6	a	X			X	X
	b	X				
	c	X				
	d			X		
	e					
TC4-8	a	X				
	b	X				
	c	X				
TC4-9	a					
	b					
	c		X			
TC14-11	a	X				
	b	X				
	c	X				
	d			X		
TC14-12	a				X	X
	b					
	c		X			
	d					
TC14-14	a					
	b					
	c		X			
TC14-16	a	X				
	b	X				
	c	X				
TC14-6	a	X				
	b	X				
	c	X				
	d					
TC14-10	a	X				
	b	X				
	c	X				
TC14-9	a	X				
	b	X				
	c	X				
TC14-17	n/a			X		

Table 3 - Summary of samples and specimens used

- *Experimental procedures*

As mentioned before, the Thellier-Thellier method is used to obtain the intensities which will give the data for the archaeomagnetic dating, but this is not the only process made during experimental analysis on this framework. Rock magnetic measurements can identify the presence of particular ferromagnetic minerals of the sample due to their magnetic and chemical characteristics (Tarling, 1983). The importance of identifying these minerals lies in the fact that the resulting information can provide an insight on how the magnetic remanence was obtained, and also helps to build and interpret the demagnetization process, and remagnetization, which in this case is the Theller-Thellier method (Tarling, 1983; De Marco, 2007).

Also, the results of the rock magnetic measurements have been considered as a guideline to pre-select specimens that would be expected to give good quality intensity values in the Thellier-Thellier method. But as Kondopoulou, et al. (2017) demostrate, sometimes this is not the case, with specimens whose magnetic measurements were considered not good but even so gave high quality of intensity values in the Thellier-Thellier, and also the other way round. The authors explain this behaviour, among other things, due to the particular geological composition of the samples, giving an argument on why it is so important to have good knowlendge of the geology of the studied region. Because of this it is important to always make both types of measurements, to have more information available to provide a more accurate interpretation.

- *Rock magnetic measurements*

Two rock magnetic measurements were used for the present project: Thermomagnetic Measurement and Isothermal Remanent Magnetization Measurement (IRM).

- Thermomagnetic Measurements

In general, the thermomagnetic measurements have the objective to produce two curves that represent the monitoring of the magnetic susceptibility against an increasing temperature and subsequent cooling, respectively. There is a moment when, due to a certain high temperature reached, the magnetic susceptibility will decrease to near cero values. Those temperatures are the previously mentioned Curie temperatures, which are characteristic for each mineral and can be used to identify the main ferromagnetic minerals the sample contains, and which have defined the magnetic behavior (Tarling, 1983; De Marco, 2007). When the maximum temperature imparted to the sample is reached it will begin to decrease to get a reverse curve (the cooling one). If this second curve is similar to the first one, even with some minor changes, it means that there were no important

chemical changes during the heating and the sample is stable at a mineralogical level (De Marco, 2007).

As De Marco (2007) explains, archaeological burnt materials usually present single Curie temperatures and reversible heating and cooling curves. Generally, tiles, bricks and high-fired baked clays show stable susceptibility behavior. However, when both curves do not coincide, it means that irreversible chemical changes happened or that it has a complex combination of ferromagnetic minerals. This is the tendency of burnt soils or plasters.

Usually, the samples for this experiment are heated until 700°C. If the curves coincide in this case, it probably means that magnetite (or titanomagnetite) can be the dominant ferrimagnetic phase. Experiments on heating clays showed that crystallized hematite appears upon heating above 800-1100°C, therefore, the absence of hematite is a further indication that such high temperatures were not achieved (De Marco, 2007). For a pre-selection for the Thellier-Thellier method, the ideal is that the sample is as stable as possible, which means that both curves must be similar.

- Isothermal Remanent Magnetization Measurement (IRM)

When a material is exposed to a strong magnetic field, it acquires a magnetization known as Isothermal Remanent Magnetization (IRM). This ability is often used in laboratory experiments, in order to distinguish a particular mineralogy of a sample (Tarling, 1983). The difference in the magnetic susceptibility and coercivity of magnetite and hematite makes this method of analysis the most effective for distinguishing the presence of Ti-poor titanomagnetites and Ti-poor ilmenohematites (Tarling, 1983).

The usual procedure in this analysis is to induce IRM by exposing a sample to an increasing magnetizing field, then measure resulting IRM. After, repeat the procedure using a stronger magnetizing field (De Marco, 2007). According to the results, there can be three general interpretations (Tarling, 1983; De Marco, 2007): if a sample contains only soft magnetic minerals (like titanomagnetite or ferromagnetic titanohematite), the acquired IRM would be during fields of 300 mT or less, but no additional IRM would be acquired in higher field levels. If only hematite (or goethite) is present, IRM is gradually acquired in fields up to 3 T. Samples containing both titanomagnetite and hematite (or goethite) rapidly acquire IRM in fields of 300 mT or less, followed by gradual acquisition of additional IRM in stronger fields. This last possibility allows detection of small amounts of hematite (or goethite) even when coexisting with more strongly ferromagnetic titanomagnetite.

Unlike the thermomagnetic measurement, the IRM has the advantage that it does not involve any chemical changes (Tarling, 1983). For a pre-selection for the Thellier-Thellier method, the ideal is that the sample is magnetized as fast as possible, which means that the IRM resulting curve shows that the acquired magnetization happened during fields of 300 mT or less, with no additional magnetization acquired in higher fields.

- *Thellier-Thellier experiment*

The Thellier-Thellir method is the most used to obtain intensity in archaeomagnetism, with new variants that have been developed over the years, that seek to improve the quality of the information obtained (Tarling, 1983; Brown, et al, 2021). The basic idea is to replace the NRM of the sample with a laboratory induced TRM, applying an intensity field that must be as close as possible to the intensity of the geomagnetic field at the time the samples were last burnt. Therefore, any previous chronological context of the samples is important, especially with the lack of an SVC.

To achieve the objective of the experiment, the general process works with the demagnetization of the sample, which is carried out through heating and cooling cycles. The method consists of stepwise double heating, based on the law of additivity of partial thermoremanent magnetizations (pTRM). For each temperature step, two heating cycles are done, by reversing the laboratory field inside the oven. The laboratory field applied both during heating and cooling the samples along their Z axis, should be representative of the ancient intensity (Thellier & Thellier, 1959).

So, the first step is the measurement of the remanent magnetization possessed by the samples and then moving on to its replacement by the new pTRMs, produced by each cycle. The gradual increase in temperature in the first steps can be of 50°C. When moving to higher temperatures, the change is smaller, reaching 5-10°C. The point is to reach the Curie temperature of the samples, after doing the necessary temperature cycles. The mentioned "Law of Additivity" states that the sum of all independent pTRMs will result in the total TRM, which is why is important to keep control on each of the heating and cooling steps (De Marco, 2007). Other important principle that justifies the behaviour of the pTRMs is the "Law of Independence", which states that a remanence acquired by cooling between any two temperature steps are independent of those acquired between any other two temperature steps (De Marco, 2007).

Between two and three temperature steps “pTRM checks” are performed, which consist in the repetition of lower temperature pTRM steps. These checks allow to verify that the ability of the sample to acquire a pTRM has not changed due to the occurrence of chemical alteration during the previous heating (Thellier & Thellier, 1959).

The idea is to create an NRM-TRM plot (the most common to represent this is the called "Arai plot") (Figure 11) which shows the connection between the NRM component left in the sample after every heating and the pTRM acquired at each step, including the checks (Gómez-Paccard & Pavón Carrasco, 2018a). The samples characterized by a high-quality linear plot represent stability in the remanent magnetization. The idea of this replacement is based on the “Law of Reciprocity”, which assumes that the blocking and unblocking of the remanence occur at the same temperature, but, if the plot obtained is not of high-quality, means that this Law did not apply, which translate that the sample has a more complex composition that made unsuccessful the measurement (De Marco, 2007).

Finally, there are two important factor that must be considered during the experiment, in order to have a reliably record: the TRM anisotropy and the cooling rate. As stated in the first chapter, the anisotropy makes reference to the possibility that the magnetization of some materials is easier in some directions than others. Here we will talk particularly of the anisotropy caused by the thermoremanent magnetization. Now, this means that the magnetization direction recorded in such materials will tend to be distorted from its true value towards one of these more favorable directions, hence affecting the apparent intensity of the field recorded (English Heritage, 2006). To keep control of this during the experiment, when a specimen loses 70% of its magnetization it is aligned to its different axis, heated, cooled and then measured, also reversing the field (X+, X-, Y+, Y-, Z+) (Figure 12). Gómez-Paccard & Pavón Carrasco (2018a) explain that the control of the field induced in the laboratory is one of the possibilities for the TRM anisotropy check, although there are authors that have developed other methods.

For the cooling rate, it means that during the experiment, the cooling part of the cycle can affect the TRM acquisition due to fans integrated in the oven. But is important to remark that the archaeointensity of interest was obtained by the sample during past times, with an environmental cooling rate, and not an accelerated one, and the idea is to check this too measuring additional TRM acquisition steps at different cooling rates (Gómez-Paccard & Pavón Carrasco, 2018a). So, for the experimental procedure, what was done is that, when the specimens finished the demagnetization process, they were heated two last times. In the first one, they were left in the oven to cooldown slowly, which happened between 24-48 hours. In the second one, the fast cooling that was normally used was applied (fans of the oven). This way, any errors from the quick, laboratory cooling can get corrected (cooling-rate effect)

As Tarling (1983) explains, the biggest problem is that the measures needed for intensity are more numerous than those for direction, which implies more sources of error; but it is still an area worthy of research and use. In a similar way, Gómez-Paccard & Pavón Carrasco (2018a) claim that obtaining archaeointensity information is more complicated (than the case of direction) and also requires very long experimental times, thus why recent archaeointensity compilations are poorly distributed, both temporally and spatially.

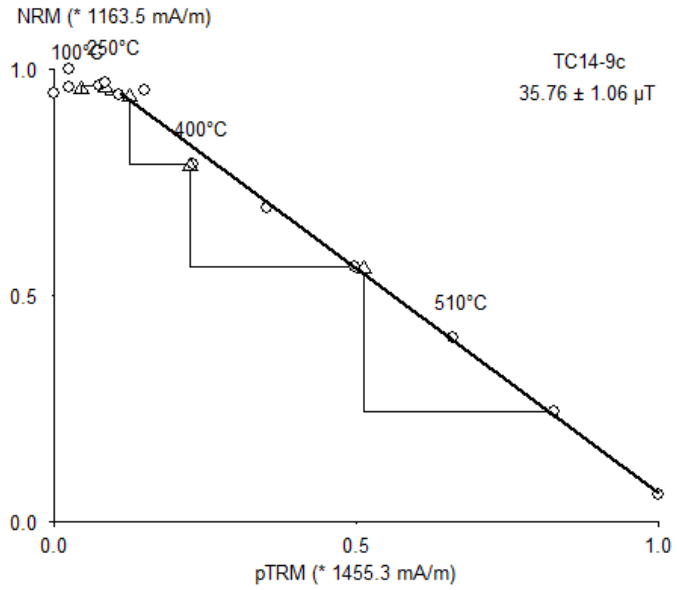

Figure 11 - Arai plot of the specimen TC14-9c, shown for the purpose to demonstrate the linear plot described

Figure 12 - Alignment of the specimens on their X axis (top) and Y axis (bottom). They are heated and then cooled in this position, in contrast to the main Z axis.

- *Petrographic observations and SEM-EDS analysis*

Archaeological ceramics are artefacts created from heated clay that were fabricated and used by past societies. The development of ceramic technology by past humans to create objects of a desired shape that could endure is considered as a crucial step in development of ancient technology (Quinn, 2013). Regarding the field of materials science, archaeological ceramics can be studied on many levels using different techniques, with the aim to understand the characteristics of the raw materials from which they were formed. These techniques are not only directed to understand the clay, but also any other material that was used to decorate the artefact, like pigments (Noll & Heimann, 2016).

The techniques used can go from the simple visual observations of the form and surface decoration to the scientific characterization of their components and microscopic structures using specialized analytical equipment. This can be generally subdivided into geochemical and mineralogical approaches, depending on the focus of the technique, being also complementary (Quinn, 2013; Noll & Heimann, 2016). The data obtained from this kind of analysis are generally used to interpret their place of manufacture (also called provenance), thus providing evidence for archaeological discussions via processes such as trade and exchange, distribution and migration; or also to bring up information regarding the technological development that helped to create the artefact (Quinn, 2013; Noll & Heimann, 2016; Tite, 2016).

The focus of the present project is to understand the archaeomagnetic characteristics of the samples and their potential as reference points using archaeointensity, and besides the experiments previously described, it was decided to apply petrographic observations and SEM-EDS analysis to understand more of the geochemical and mineral components of the sample, that could characterize their magnetic properties. Although these techniques were not the main objective of the project, we decided to briefly explain them.

Thin section petrography and scanning electron microscopy (SEM) can be used to detect compositional and microstructural characteristics of the ceramics, but at a different scale. Quinn (2013) describes the thin sections as 30 μm thick slices of an artefact fixed onto a glass microscope slide, which are analyzed using a polarizing light microscope or petrographic microscope, producing optical effects that can be used for the identification of rocks and minerals. Using thin sections is mostly to examine the composition of the main paste of ceramic artefacts, decoration, or deterioration (Quinn, 2013). In comparison to the optical microscopy process of the thin sections, a scanning electron microscope (SEM) provides more in-depth information mainly for two reasons: SEM provides a higher magnification of the specimen and when equipped with an X-Ray energy dispersive spectrometer (EDS), it gives quantitative information regarding the chemical composition of the different phases or components present in the sample (Tite, 2016). Even so, this does not mean that SEM is a replacement of the optical petrographic technique but is more a complementary approach between both studies.

Besides being able to determine the composition by energy-dispersive X-ray microanalysis, the SEM is also able to create an image of the object. As Noll and Heimann (2016) explain, the SEM's function is based on the production of an electron beam that can be focused down to a diameter of 1μm, and depending on the readings, the equipment can generate a high-resolution image of the surface (secondary electrons) or an image that gives semi-qualitative elemental information (backscattered electrons). So, in overall, the SEM-EDS can give information regarding its chemical composition, supported by an image that gives a morphological approach (Figure 13).

Even so, SEM suffers from some limitations. Samples have to be conductive in order to be studied and for this reason, nonconductive samples are coated with a thin gold or carbon film to prevent surface charging by the impinging primary electron beam, and this can affect the quality of the produced image (Noll & Heimann, 2016).

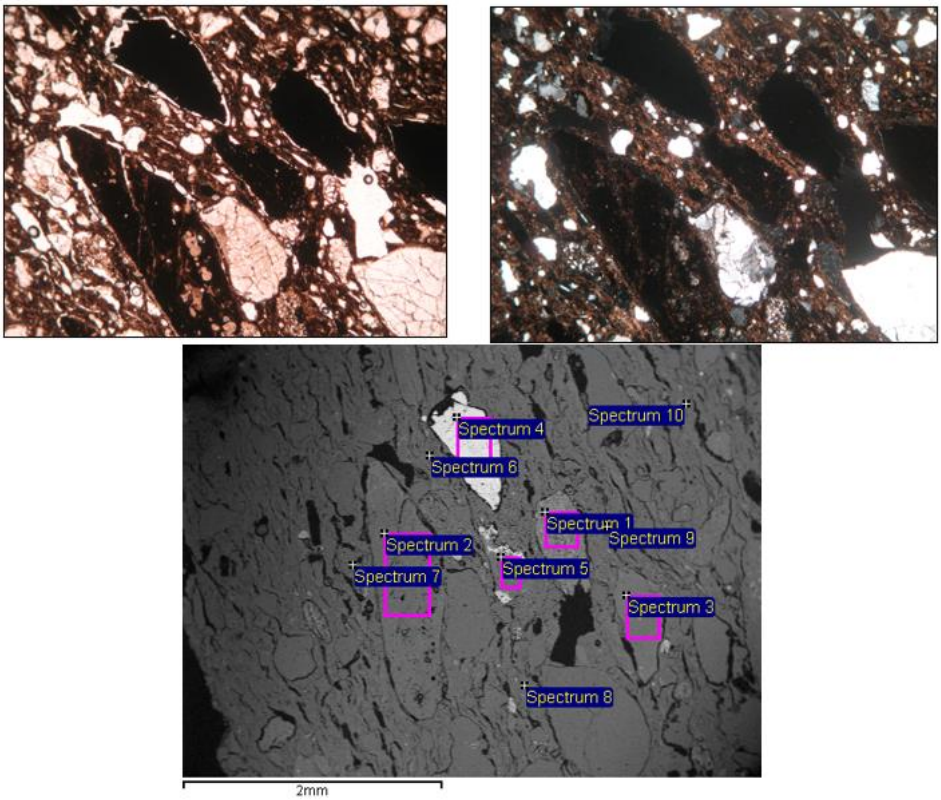

Figure 13 - Top images are thin sections under the petrographic microscope. Left under plain polarized light (PPL) and right under crossed polarized light (XPL). Bottom is the backscattered SEM from the same area. The points are the places where x-ray spectrometry was applied. From sample TC6-1

Results

- *Rock magnetic measurements*

  - Thermomagnetic Measurements

As was said before, the thermomagnetic measurements have the objective to produce two curves that represent the monitoring of the magnetic susceptibility against an increasing temperature and subsequent cooling. The objective of this curves is to determine approximately the Curie temperature of the sample, and to see if there were any chemical changes induced. As Table 3 shows, the thermomagnetic experiment was carried out on six samples, two from each context studied.

The instrument temperature applied in this experiment was from 50°C to 700°C and backwards. The results can be seen in Figure 14. What the graphics indicate is that the six samples generally show a good reversibility of the heating and cooling curves, giving evidence that no significant mineralogical changes occur during heating. For the case of the Curie temperature, the ones of TC14 and TC6 appear to be a bit before reaching 600°C. On the other hand, both cases of the TC4 appear a bit after 600°C. This means that the samples have a majority of magnetite minerals, with the possibility of very few other harder components.

For the thermomagnetic measurements, the instruments used were the MS2WFP models of Furnace and Power Supply Unix, located in the Laboratory of Geophysics of the Aristotle University of Thessaloniki (Figure 15).

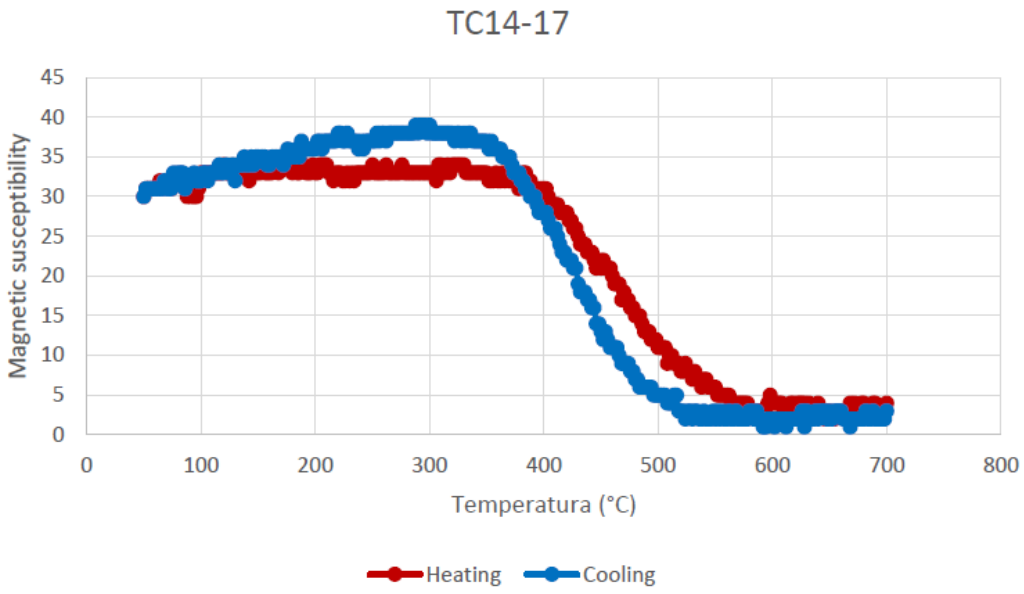
TC14-17
Magnetic susceptibility
45
40
35
30
25
20
15
10
5
0
0
100
200
300
400
500
600
700
800
Temperatura (°C)
Heating
Cooling

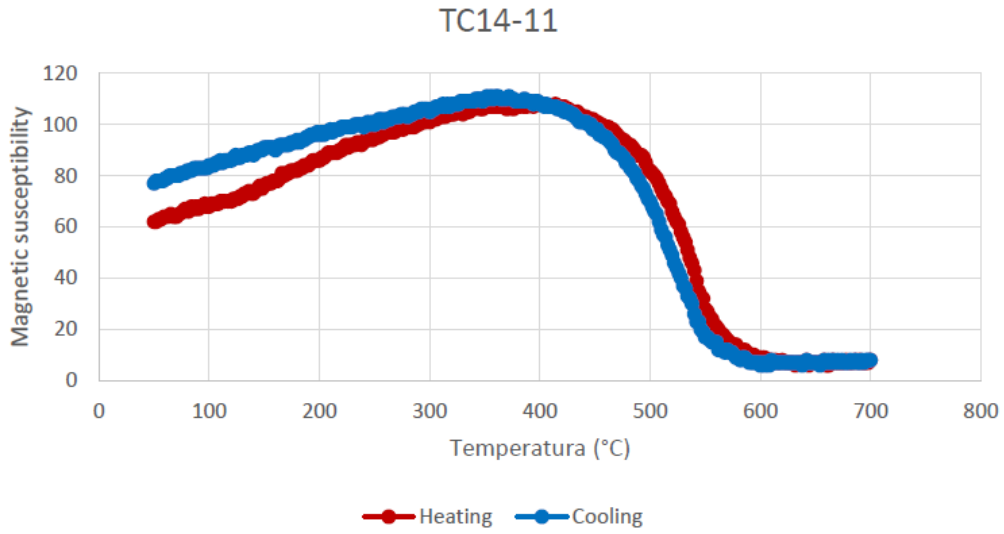
TC14-11
Magnetic susceptibility
120
100
80
60
40
20
0
0
100
200
300
400
500
600
700
800
Temperatura (°C)
Heating
Cooling

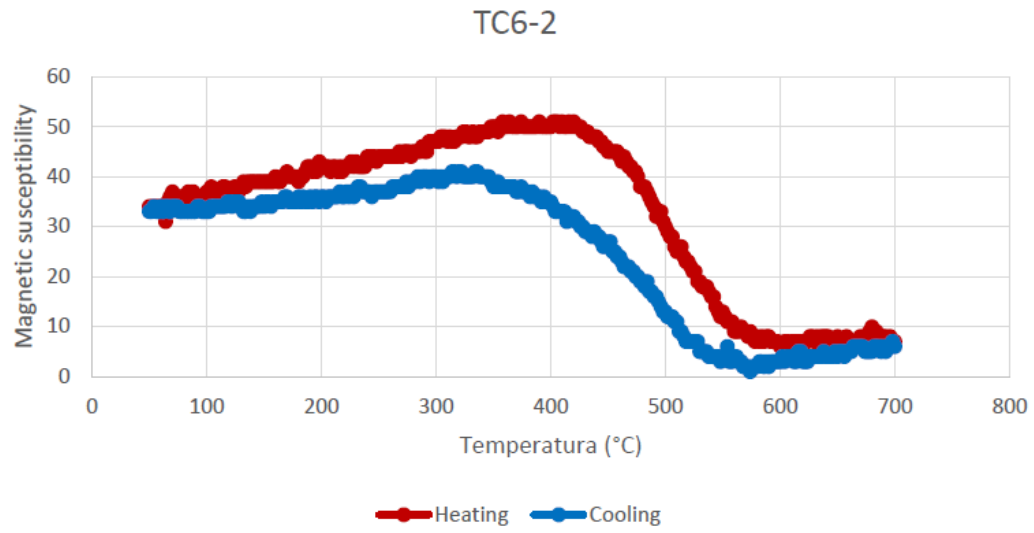
TC6-2
Magnetic susceptibility
60
50
40
30
20
10
0
0
100
200
300
400
500
600
700
800
Temperatura (°C)
Heating
Cooling

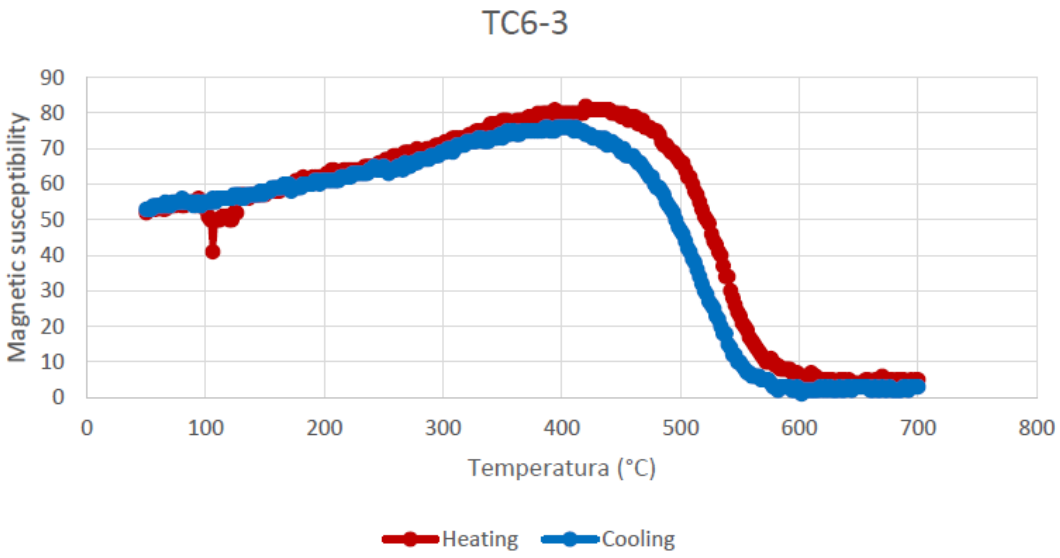
TC6-3
Magnetic susceptibility
90
80
70
60
50
40
30
20
10
0
0
100
200
300
400
500
600
700
800
Temperatura (°C)
Heating
Cooling

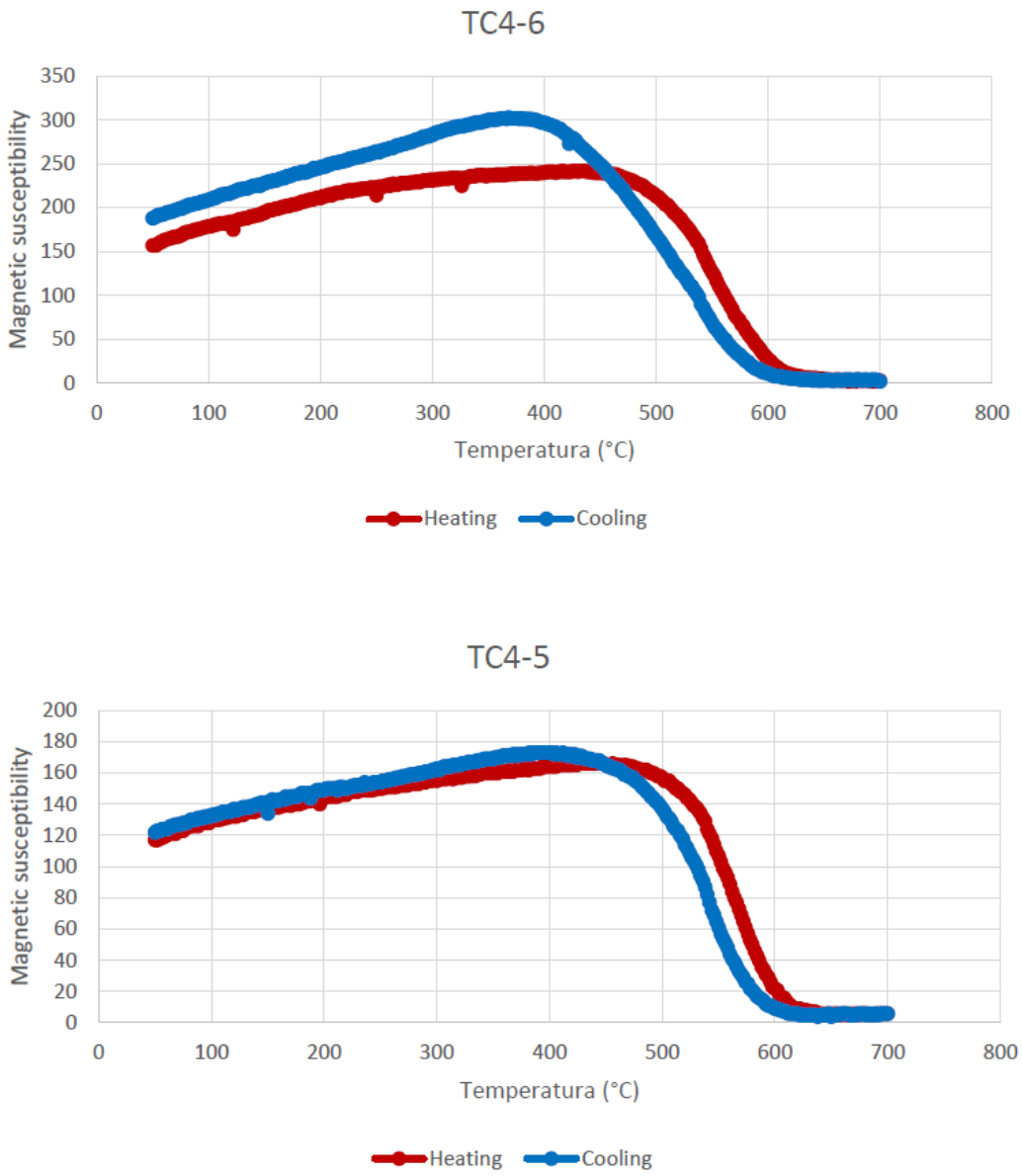

Figure 14 - Thermomagnetic curves of the samples analyzed

Figure 15 - Models MS2WFP of Furnace (left) and Power Supply Unix (right), by Bartington Instruments

- Isothermal Remanent Magnetization Measurement (IRM)

As was said before, when a material is exposed to a strong increasing magnetic field, it acquires a magnetization known as Isothermal Remanent Magnetization (IRM). This ability is often used in laboratory experiments, in order to distinguish a particular mineralogy of a sample (Tarling, 1983). As Table 3 shows, four specimens were selected for this experiment. One from the TC6 context, one from the TC4 context and two from the TC14 context.

The specimens were measured in their initial state (NRM), and for fourteen magnetic fields applied, ranging from 30 to 1205 mT. The result can be seen in the Figure 16.

According to the graphic, all the specimens acquired saturation between 200 and 300 mT. But still there is a gradual incrementation on the stronger fields, although small. This indicates that there is a dominance of soft magnetic minerals, like titanomagnetite or maghemite, but with a small presence of other harder minerals.

For the IRM measurements, the instrument used was the ASC Scientific, model IM-10-30 Impulse Magnetizer, located in the Laboratory of Geophysics of the Aristotle University of Thessaloniki (Figure 17).

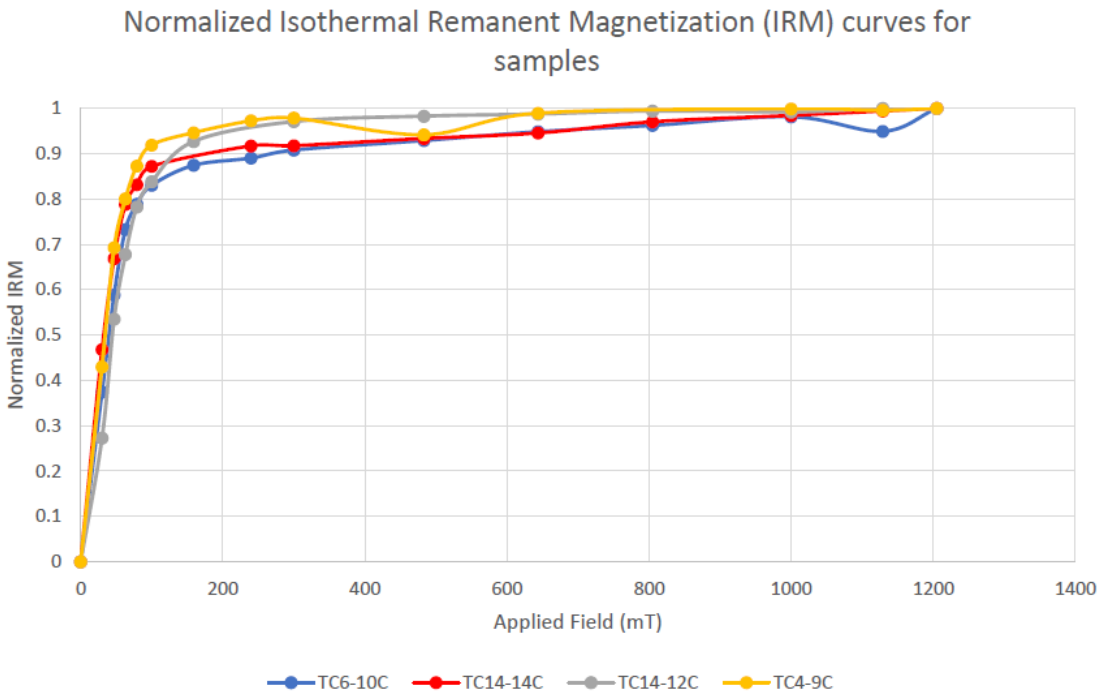

Figure 16 - IRM acquisition of the specimens analyzed

Figure 17 - ASC Scientific IM-10-30 Impulse Magnetizer, Bartington Instruments

- *Thellier-Thellier experiment*

As explained in the previous chapter, there are three main moments for a Thellier-Thellier experiment: the stepwise increment of temperature for each cycle, the TRM anisotropy measurements done when the specimens lost 70% of their magnetization, and the cooling rate correction measurement that is done when the specimens are nearly totally demagnetized.

The first and lowest temperature in which the samples were heated was 100°C, while the highest temperature most specimens reached was 570°C. At the beginning, the temperature was raised by a step of 50°C for each heating, until it reached the 400°C. After the step difference dropped to 40°C, and then to 30°C. Every two temperatures, a check measurement was taken (pTRM check). There were two moments where the samples lost 70% or more of their magnetization, and thus the TRM anisotropy measurements were taken. These temperatures were 480°C and 510°C. The cooling rate measurement were set at 570°C, doing one at a slow cooling rate and other one with the normal faster process with the fans of the oven. This process is summarized in the Table 5.

The laboratory magnetic field used for an experiment must be close to the expected archaeointensity value. After checking the information from the previous studies in the region, it was decided that the magnetic field used in this experiment would be of 45μT.

The oven used for the experiment was the Magnetic Measurements Thermal Demagnetiser (Serial Number 142), distributed by Magnetic Measurements. It worked with the TTi L301 power supply, by Thurlby Thandar Instruments, providing the steady magnetic field for the whole experiment as the samples were burnt and cooled down (Figure 18). The measurements of the magnetization of the samples were done with the Molspin Limited spinner (Figure 19). Both instruments located in the Laboratory of Geophysics of the Aristotle University of Thessaloniki.

°C	**Field direction**
100	+
100	-
150	+
150	-
100	pTRM check
250	+
250	-
300	+
300	-
200	pTRM check
350	+
350	-
400	+
400	-
300	pTRM check
440	+
440	-
480	+
480	-
400	pTRM check
First batch anisotropy test	
510	+
510	-
Second batch anisotropy test	
540	+
540	-
480	pTRM check
570	+
570	-
570 slow	+
570 fast	-

Table 4 - Heating/cooling steps done during the Thellier-Thellier experiment

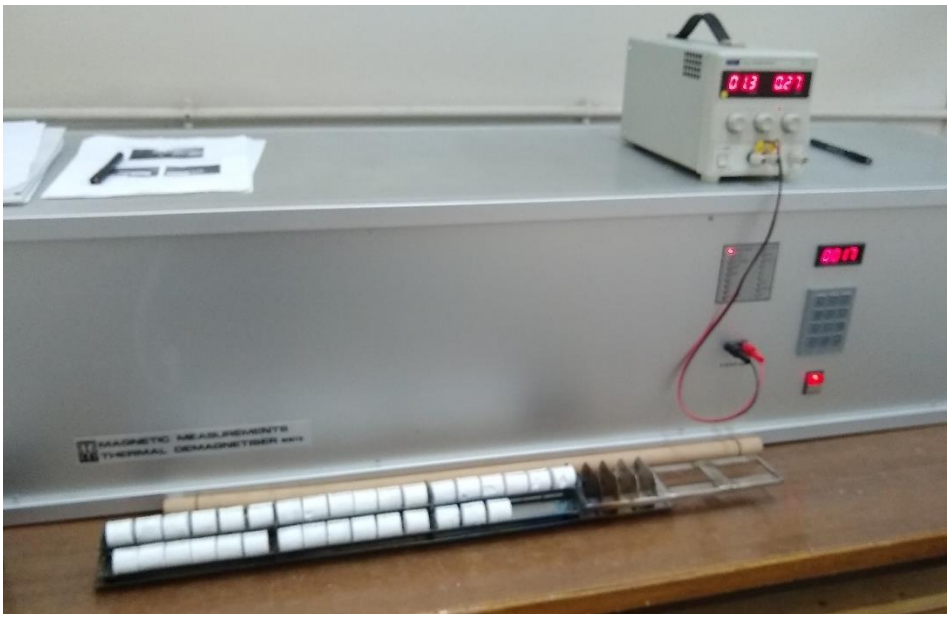

Figure 18 - Magnetic Measurements Thermal Demagnetiser (below) with the TTi L301 power supply (top)

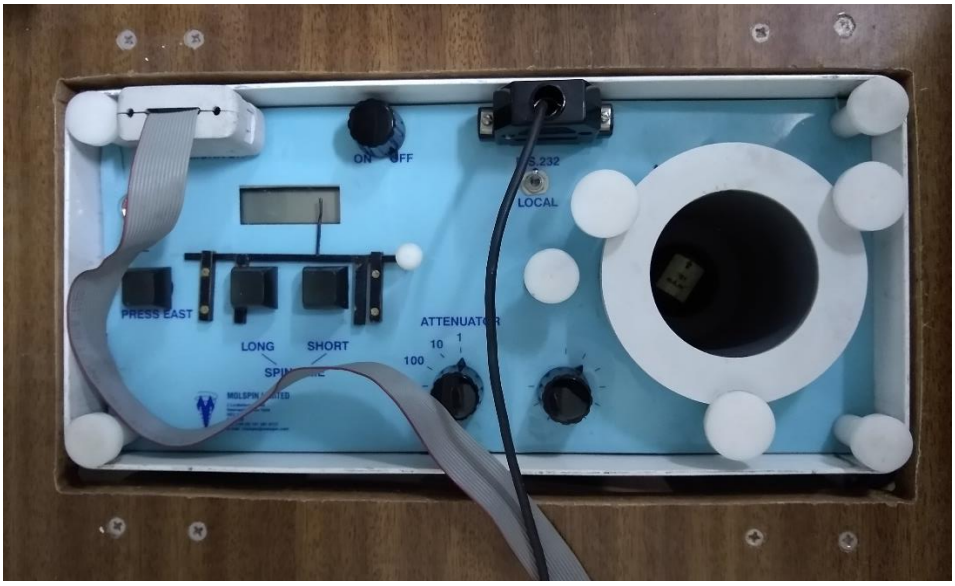

Figure 19 - Molspin Limited spinner

After each step, the measurements were checked using the software ThellierTool 4.2. This software helped to maintain control of the specimen's demagnetization process with Arai Zijdelverd, and decay plots. Those specimens that began to show a highly non-linear pattern were discarded along the process (Figure 20). From the 48 specimens that were originally selected for the Thellier-Thellier, 34 finished all the cycles. By the end of this experiment, the data of these 34 specimens were analyzed using the RenArMag_v3511 software, applying the TRM anisotropy correction. After this, several were discarded, and at the end only 24 were completely analyzed with the cooling-rate corrections, which gives a 50% of success rate.

Table 5 presents the summary of the results obtained from the RenArMag_v3511 software. The criteria stablished to determine what specimen was discarded before the corrections was based on the guidelines presented by Gómez-Paccard (2006), along with the parameters suggested by the ThellierTool 4.2. software and the final plots obtained.

In general, the specimens of the three contexts behave in a similar way. There were only two TRM anisotropy steps, and those two temperatures were close between them (480°C and 510°C). Also, the temperature of saturation was the same of all the samples, except for two (TC6-2a and TC6-2b) that reached saturation one step before. During the first steps, the specimens didn't show a very linear pattern, but this tends to normalize between 300°C-400°C. Even so, in most of the samples, this lineal patter was not the best, but decent enough. Figure 21, Figure 22 and Figure 23 show two cases of each context. All the plots of the analyzed specimens are present in the Appendices.

It is important to remark two aspects that happened during the experiment: the first one is that the context TC14 was the one that got more specimens rejected, and the second one is that during the 480°C step several specimens presented an erroneous data, which affected the interpretation of said specimens. The problem with this situation was that because some of the specimens had the TRM anisotropy test at 480°C and a pTRM-check, we had to be careful of how to manage this erroneous data. Therefore, for some of the specimens this step was deleted if it did not interfere with the TRM anisotropy test. In the Appendices section is possible to see the plots of some of these cases, like the specimens TC6-7a, b, c.

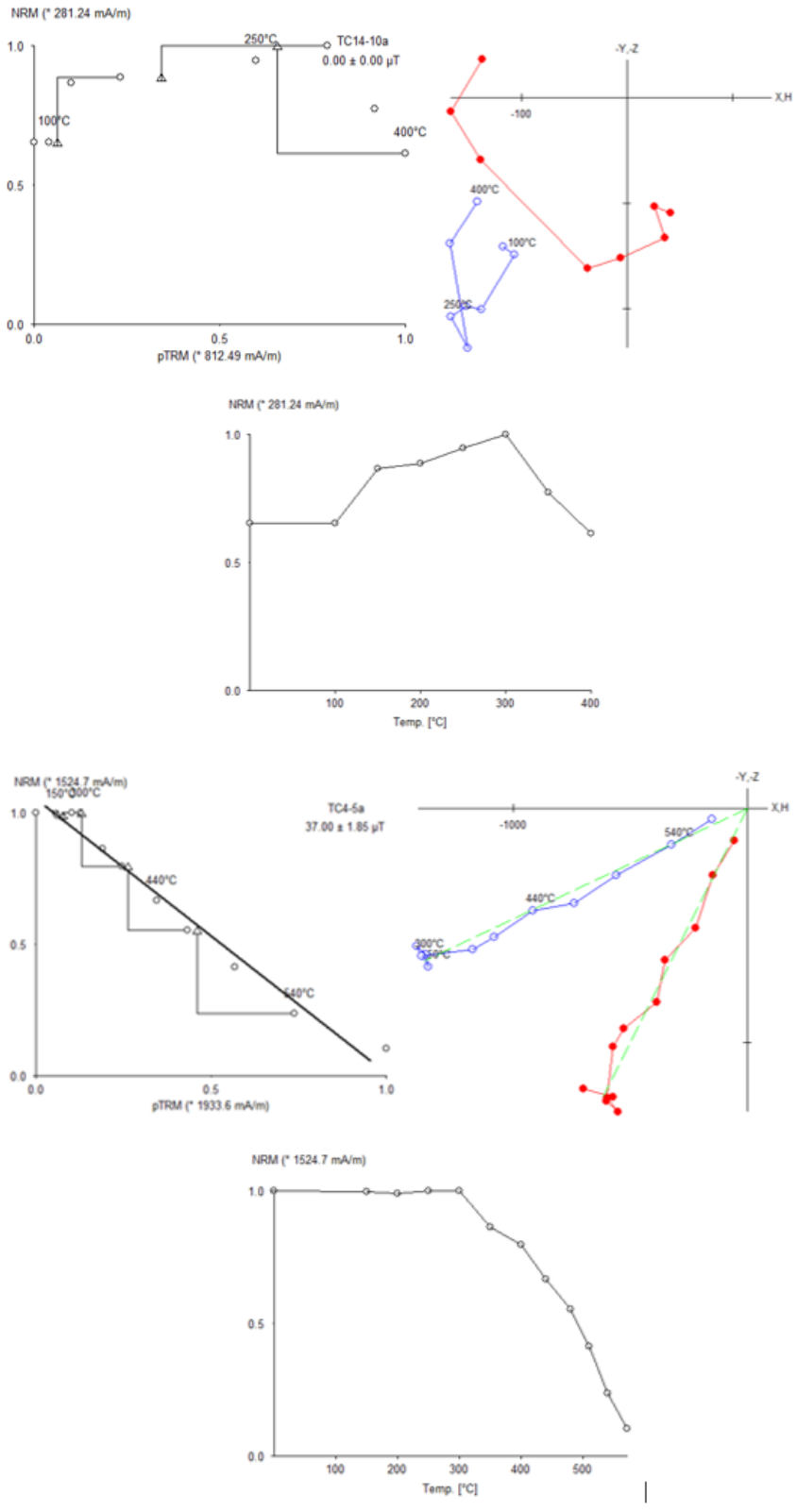

Figure 20 - Arai, Zijdelverd, and decay plots (clockwise order) of two specimens. TC14-10a (top) was discarded after the 400°C, in comparison to the results of TC4-6a (bottom) which endured the full experiment with success.

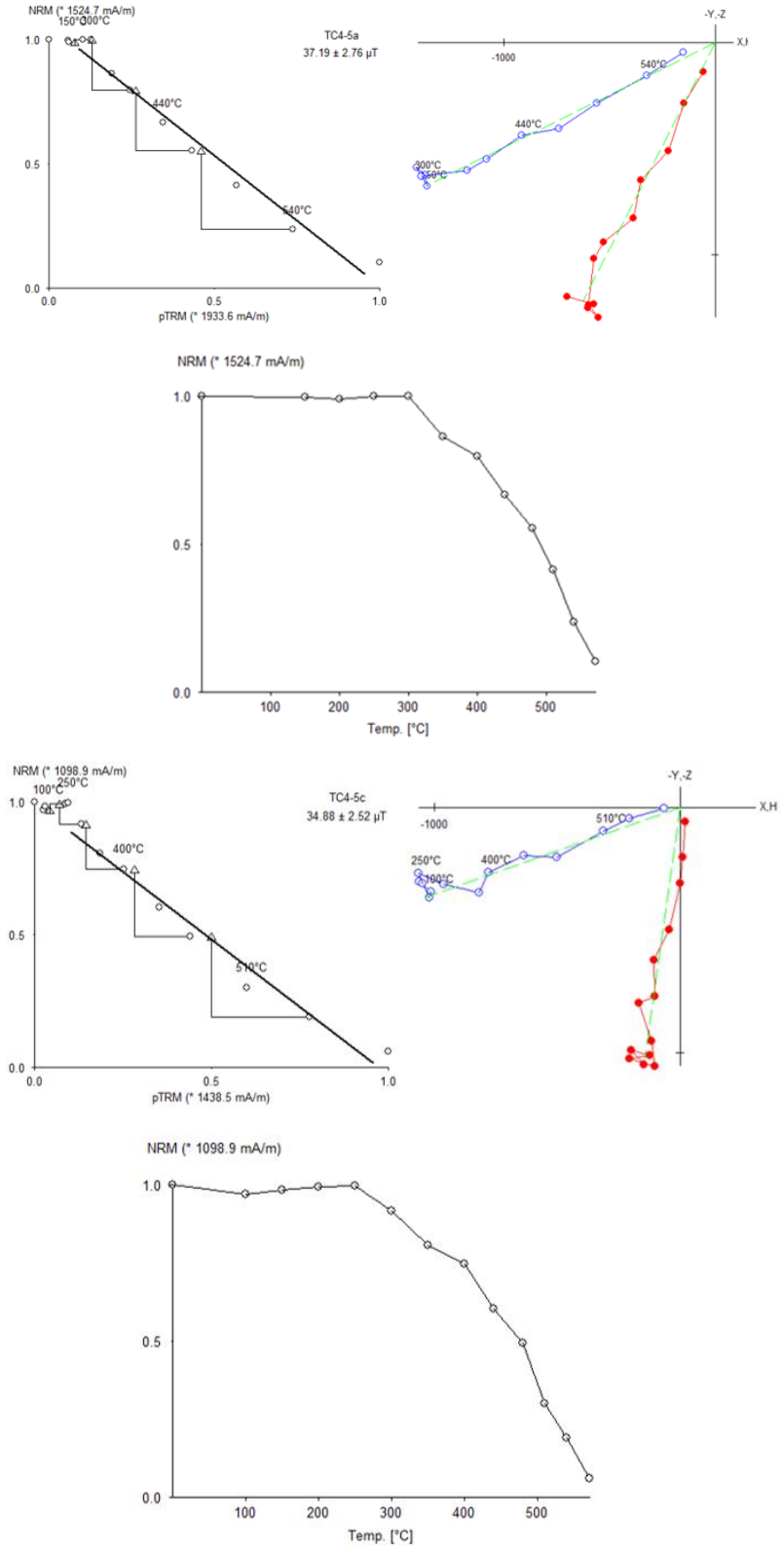

Figure 21 - Arai, Zijdelverd, and decay plots (clockwise order) of two specimens from the TC4 context and same sample, TC4-5a (top) and TC4-5c (bottom)

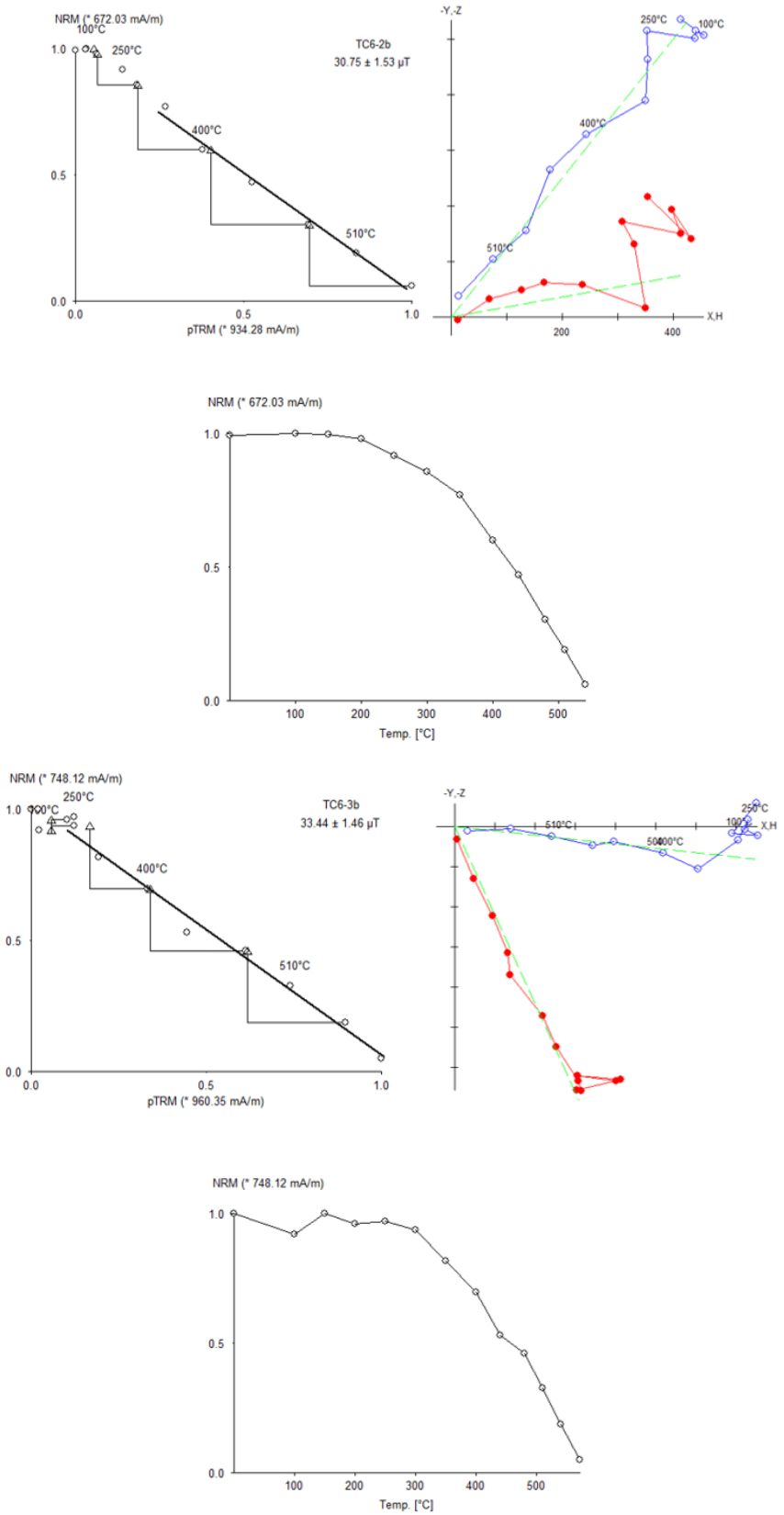

Figure 22 - Arai, Zijdelverd, and decay plots (clockwise order) of two specimens from the TC6 context, TC6-2b (top) and TC6-3b (bottom)

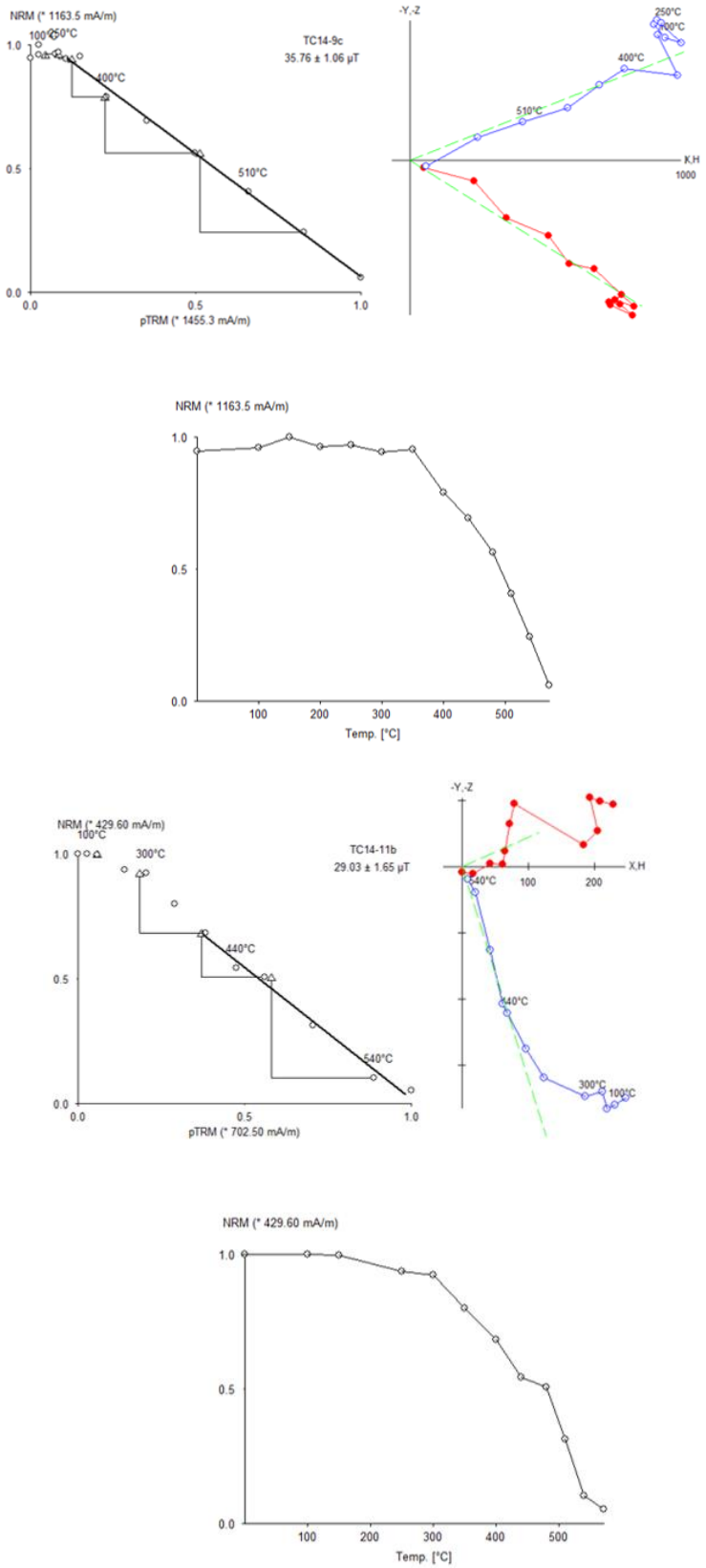

Figure 23 - Arai, Zijdelverd, and decay plots (clockwise order) of two specimens from the TC14 context, TC14-9c (top) and TC14-11b (bottom)

Table 5 - The results and values for each specimen of each sampled

Sample	F lab	Tmin-Tmax (°C)	n	f	g	q	Mad (°)	Dang (°)	F (μT)	SD	F@ (μT)	SD	F@_ave_sample	SD	F@_ave_ctx	SD	Fcorr (μT)	Fcorr_ave_sample	SD	Fcorr_ave_ctx	SD
TC4-1b	45	150-440	7	0.473	0.786	3.153	18.79	13.9	20.82	2.45	27.7	3.04									
TC4-1c	45	440-570	5	0.63	0.741	5.255	10.84	10.12	12.8	1.14	17.38	1.73									
TC4-3a	45	100-540	11	0.728	0.848	25.488	8.84	166.48	25.81	0.62	52.74	2.39									
TC4-5a	45	300-570	8	0.857	0.84	9.689	5.23	0.9	37.19	2.76	45	3.34					42.35104				
TC4-5b	45	100-570	11	0.951	0.876	14.282	9.55	1.92	24.98	1.46	24.96	1.42	36.5833	10.398			23.18178	34.038694	9.8347		
TC4-5c	45	300-570	8	0.878	0.84	10.202	6.26	3.83	34.88	2.53	39.79	3.02			39.68667	4.389	36.58326			36.2044	3.063
TC4-8a	45	250-540	7	0.79	0.747	8.388	14.52	1.11	41.29	5.69	42.36	5.89	42.79	0.6081			37.9204	38.370154	0.636		
TC4-8c	45	250-540	7	0.762	0.763	6.446	6.66	6.01	32.86	2.97	43.22	4.01					38.81991				
TC6-1a	45	300-570	7	0.86	0.76	20.034	11.79	5.02	30.31	1.71	33.84	1.85					32.65153				
TC6-1b	45	250-540	7	0.823	0.727	12.927	9.12	3.94	31.57	2.76	35.44	2.08	37.29	4.6591			34.72513	36.210828	4.4904		
TC6-1c	45	250-570	9	0.843	0.839	18.326	10.27	4.65	38.21	1.48	42.59	1.54					41.25582				
TC6-2a	45	0-480	10	0.614	0.823	17.964	9.29	13.08	34.16	0.96	46.97	1.29					36.91786				
TC6-2b	45	350-540	6	0.714	0.799	11.485	10.01	4.58	30.76	1.53	35.41	2.02	41.19	8.1742			28.15165	32.534755	6.1987		
TC6-2c	45	100-440	8	0.553	0.783	7.98	23.27	2.65	32.34	1.76	53.59	3.41									
TC6-3a	45	350-540	6	0.678	0.799	15.93	6.97	9.36	36.43	1.23	35.66	1.22					33.29785				
TC6-3b	45	300-570	0	0.847	0.855	16.561	6.27	2.09	33.42	1.46	36.64	1.87	36.15	0.693			33.98626	33.642053	0.4868		
TC6-4a	45	0-480	10	0.711	0.833	7.306	12.88	11.41	27	2.19	27.33	2.73			34.32083	7.321				31.0346	6.343
TC6-4b	45	350-570	7	0.807	0.81	18.924	11.53	2.95	15.9	0.55	18.5	0.75					17.02915				
TC6-4c	45	200-540	8	0.875	0.766	8.981	12.08	11.93	21.87	1.72	23.57	1.77	21.035	3.585			21.97016	19.499654	3.4938		
TC6-7a	45	250-570	8	0.838	0.804	14.773	7.26	5.25	28	1.28	26.05	1.24					23.40889				
TC6-7b	45	200-510	7	0.571	0.731	6.549	12.39	11.43	33.44	2.13	40.54	3.98	31.2033	8.1003			36.92816	28.305627	7.4902		
TC6-7c	45	100-510	9	0.639	0.776	5.665	12.83	11.44	31.49	2.76	27.02	1.16					24.57984				
TC6-8a	45	250-570	8	0.788	0.799	23.672	7.89	2.85	31.05	0.83	41.13	1.11					37.95302				
TC6-8b	45	300-570	7	0.814	0.799	18.054	9.25	1.93	29.88	1.08	37.87	2.4	39.0567	1.8018			35.70671	36.014946	1.8038		
TC6-8c	45	200-570	9	0.887	0.85	21.353	13.07	3.37	32.21	2.81	38.17	2.97					34.3851				
TC14-9a	45	250-570	9	0.892	0.852	15.302	11.75	3.33	36.64	1.82	41.81	1.92					38.32609				
TC14-9b	45	300-570	8	0.791	0.829	22.332	9.85	2.54	36.08	1.06	41.96	1.5	41.1167	1.3329			39.20614	38.41689	0.748		
TC14-9c	45	300-570	8	0.836	0.834	23.563	8.46	4.06	35.77	1.06	39.58	1.1			35.99333	7.245	37.71844			33.2043	7.372
TC14-11a	45	300-540	7	0.782	0.763	7.558	11.81	175.07	23.62	1.74	23.24	1.76									
TC14-11b	45	400-570	6	0.597	0.767	8.08	8.24	5.72	29.04	1.64	30.87	1.53	30.87	1.53			27.99164	27.991635	1.53		
TC14-11c	45	440-570	5	0.553	0.673	2.638	13.17	7.95	11.13	1.57	11.13	1.57									
TC14-16a	45	200-400	5	0.502	0.717	3.745	15.26	8.32	56.23	5.38	52.87	5.74									
TC14-16b	45	150-440	7	0.588	0.809	19.482	16.21	19.1	35.56	0.87	35.06	1.64									
TC14-16c	45	0-400	8	0.444	0.788	3.72	30.58	19.88	36.95	4.89	37.49	6.73									

The yellow lines indicate samples that got rejected, after the anisotropy correction, because they would not meet the required criteria. Sample: Sample's Code Name | F lab: Magnetic Field use in Laboratory | Tmin-Tmax: Minimun and Maximun Temperatures of Successive Points in Linear Segment | n: Number of Successive Points in Linear Segment | f: : Fraction of NRM | g: Gap Factor | q: Quality Factor | Mad: Maximum Angle of Deviation | Dang: Deviation Angle | F: Initial Intensity Measured | SD: Standard Deviation | F@: Intensity after adding the Anisotropy | F@_ave_sample: average value of Intensity per sample, after adding Anisotropy | F@_ave_ctx: average value of Intensity per context, after adding Anisotropy | Fcorr: Intensity after Adding the Cooling Measurement | Fcorr_ave_sample: average value of Intensity per sample, after adding Cooling Measurement | Fcorr_ave_ctx: average value of Intensity per context, after adding Cooling Measurement

- *Petrographic observations and SEM-EDS analysis*

Before starting this section, we must clarify that these experiments were not done by the author of the present project but were a collaboration with Prof. Lambrini Papadopoulou from the Geology Department of the Aristotle University of Thessaloniki. Prof. Papadopoulou made the thin sections, then communicated the petrographic observations to the author. Based on these observations, the SEM-EDS analyses were done on a few selected sections, and then again, the results were given to the author and discussed with Prof. L.Papadopoulou. For more details, Table 3 shows which sample was used for what. First, we are going to present the summary of the petrographic observations from the thin sections, and then the information of interest obtained from the SEM-EDS analysis.

Five samples were selected for the petrographic observations: TC4-3, TC4-6 ,TC6-1,TC6-8, and TC14-12. The first three samples belonged to the same ceramic typology *Desgrasante Gris* (DG), while the fourth one was classified as *Funza Cuarzo Abundante 3* (FCA3) and the fifth one as *Funza Cuarzo Abundante 1* (FCA1). In general, all the samples presented quartz and feldspar in a notable amount, but there are very small differences between the five samples. The first three samples, the ones that belong to the DG typology, tend to present more shards that looked like metallic minerals. Also, the second, third and fourth sample present particles with more homogeneous shape, which could mean a different source location or different technology. All samples, except the fifth one, present a notable amount of pottery shards in their compositions. Even with these differences, all particles observed can be obtained in the region, because they correspond to the local geology, and it is possible that local sand was used as temper for the ceramic fabrication.

Three representative samples, among the previous five, were selected for the SEM-EDS analysis: TC4-6, TC6-1, and TC14-12. For a better understanding, and based on the petrographic observations, the results are divided in what was analyzed: clay, shards (either pottery shards or metallic minerals), and others (feldspars, quartz clusters, among other particles). For each thin section, two circles were marked. In each circle some images were taken, and for each image different spots were analyzed. So, the results will be presented by sample, then by circle (C1 or C2). The images for each circle are named with a number and letter ‘a’ (1a, 2a, and so on), and the spots analyzed only by consecutive numbers.

The complete results and photographs from the petrographic observations can be seen in the Appendices. Here we will present tables that summarize the compound percentage of the points analyzed (Table 6, Table 7, Table 8) making emphasis on the magnetic ones, and the images taken with the SEM-EDS (Figure 24, Figure 25, Figure 27, Figure 26, Figure 28, Figure 29).

For the TC4-6 sample the clay has a high silica composition with SiO_2 ranging from 60.42 to 88.64 wt% while Al_2O_3 shows a larger variation from 7.33 to 26.61 wt%. Other oxides that are present are FeO (1.29-3.75 wt%), TiO_2 (0.05-6.01 wt%), CaO (0.9-1.74 wt%), MgO (0.35-1.16 wt%), K_2O (1.03-4.51 wt%) and Na_2O (0.34-1.18 wt%). Most of the

shards showed a concentration of 1-7.92 wt% of FeO, with <1% of TiO_2. Shard C1-2a has a high concentration of FeO while shard C2-2a has high concentrations of FeO and TiO2 probably due to iron and titanium oxides which are evidenced by the bright color in the SEM backscattered image. In general, the most common compound present was SiO_2, followed by Al_2O_3. This information shows that indeed most of the particles observed before were pottery shards, with some concentrations of iron oxides and a few presences of titanium oxides, which are magnetic minerals. In the case of other particles, several quartz grains were observed, a feldspar, and a zircon.

For the TC6-1 sample, the clay has a high silica composition with SiO_2 ranging from 59.65 to 96.73 wt% while Al_2O_3 shows a larger variation from 2.97 to 29.19 wt%. Other oxides that are present are FeO (0.11-5.63 wt%), TiO_2 (0.01-1.49 wt%), CaO (0.03-1.61 wt%), MgO (0.19-0.93 wt%), K_2O (0.07-2.71 wt%) and Na_2O (0.07-0.54 wt%). Most of the shards showed a concentration of 1-5% of FeO, with <1% of TiO2. But three spots detected high concentrations of FeO, one of 45.07% (C1-2a-1), other of 22.35% (C2-1a-1) and other of 90.64% (C2-1a-4). From these three, the first two also presented a level of 1% of TiO2. Thanks to the SEM backscattered image we can confirm that C2-1a-4 is actually an iron oxide. This information shows that indeed most of the particles observed before were pottery shards, with some concentrations of iron oxides and a few presences of titanium oxides, which are magnetic minerals. In this sample, clusters of quartz were also observed.

For the TC14-12 sample, the clay has a high silica composition with SiO_2 ranging from 61.29 to 77.4 wt% while Al_2O_3 shows a larger variation from 19.39 to 25.76 wt%. Other oxides that are present are FeO (3.16-5.66 wt%), TiO_2 (0.41-0.81 wt%), CaO (0.76-1.62 wt%), MgO (0.53-0.96 wt%), K_2O (0.97-3.13 wt%), Na_2O (0.19-0.62 wt%) and MnO (0.22 wt%). Only one shard was found and analyzed, showing the lack of pottery fragments, something already detected from the petrographic analysis. This shard contained quartz in an aluminosilicate matrix. In the case of the particles, several quartz grains, feldspar and also amphiboles were observed.

shards													
	C1							C2					
	1a			2a		3a		1a		2a			
	1	2	3	1	2	5	6	1	2	2	3	4	5
Na2O	0.19	0.99		1.02	0.63	0.53	0.79	0.53	0.62	1.05		0.95	2.75
MgO	0.95			1.19	0.98	0.76	1.1	0.7	0.87	1.92		0.86	0.27
Al2O3	26.45	19.87	27.4	24.87	30.84	20.2	24.23	29.54	28.68	17.63	1.08	24.27	38.3
SiO2	63.32	72.95	58.15	49.68	57.4	70.6	62.83	60.98	60.18	22.92	1.36	46.78	50.86
K2O	4.27	2.58	4.11	5.18	5.43	2.85	4.56	4.39	4.24	1.74	0.21	4.16	4.94
CaO	0.98	0.53	1.17	0.74	0.9	0.91	0.66	0.66	0.99	2.21	0.52	0.52	0.62
TiO2		0.81	1.24	0.86	0.78	0.85	1.28	1.53	0.81	0.55	96.23	0.78	
FeO	3.85	1.53	7.92	16.43	3.09	3.22	4.56	1.77	3.81	51.86	0.83	21.61	2.43

clay									
	C1						C2		
	1a			2a			1a		
	4	5	6	3	4	5	3	4	5
Na2O		0.92	0.7	0.73	0.97	0.77	0.34	0.83	1.18
MgO			0.76	0.89	0.85	0.76	0.35	0.8	1.16
Al2O3	22.45	19.85	22.73	16.38	14.44	21.74	7.33	21.67	26.61
SiO2	69.09	73	69.22	75.62	76.56	69	88.64	63.58	60.42
K2O	3.45	2.41	2.96	2.48	2.92	3.46	1.03	3.84	4.51
CaO	1.26	1.37	1.18	1.22	0.96	1.36	0.9	1.34	1.74
TiO2			0.28	0.57	0.62	0.27	0.05	6.01	0.89
FeO	3.75	2.44	2.16	2.12	2.67	2.43	1.29	1.94	3.35

fel	
	C1
	1a
	8
Na2O	6.96
Al2O3	24.15
SiO2	62.76
K2O	0.49
CaO	5.35
FeO	0.18
BaO	0.13

qtz					
C1				C2	C2
1a	2a	3a		1a	2a
7	6	1		6	1
9	7	2			zir
		3			
		4			

Table 6 - Summary of the percentage of each compound detected with the SEM-EDS on the sample TC4-6

shard										
	C1					C2				
	1a		2a			1a				
	1	2	1	2	3	1	2	3	4	5
Na2O	0.19	0.02	0.11	0.29	0.4	0.1	0.19	0.42	0.26	0.22
MgO	0.84	0.79	1.1	0.5	0.97	0.56	0.48	0.77		0.82
Al2O3	26.08	19.83	16.46	20.61	27.88	24.38	24.93	26.84	2.8	18.86
SiO2	65.27	72.28	34.28	72.38	62.36	47.66	70.01	65.25	6.66	71.01
K2O	3.04	1.86	1.46	1.97	3.37	3.13	1.62	2.33		3.26
CaO	0.63	0.9	0.38	0.46	0.46	0.68	0.81	0.22	0.09	0.29
TiO2	0.58	0.66	1.04	0.63	0.89	1.07	0.8	0.52		0.62
FeO	3.36	3.62	45.07	3.07	3.8	22.35	1.14	3.72	90.64	4.79

cluster		
	C1	C1
	1a	1a
	4	3
Na2O	0.14	qtz
Al2O3	1.16	
SiO2	98.22	
K2O	0.37	
CaO	0.13	
FeO	0.08	

clay													
	C1								C2				
	1a				2a				1a				
	5	6	7	8	4	5	6	7	6	7	8	9	10
Na2O	0.2	0.07	0.54	0.23	0.14	0.38	0.11	0.11	0.19		0.1		
MgO	0.86	0.69	0.41	0.21	0.72	0.52	0.58	0.93	0.62	0.19	0.22		0.03
Al2O3	21.46	23.17	20.61	18.21	22.05	28.8	14.23	29.19	26.53	11.92	5.86	2.97	3.18
SiO2	68.17	66.33	70.46	74.03	69.64	59.29	80.31	59.65	63.1	85.83	92.72	96.73	95.19
K2O	1.62	2.18	1.89	1.34	1.71	2.71	0.94	1.84	2.53	1.15	0.28	0.07	0.05
CaO	1.25	1.44	1.61	0.79	0.78	1.01	0.46	0.81	0.88	0.56	0.15	0.03	0.21
TiO2	1.04	1.15	0.54	1.35	0.56	1.49	0.42	1.7	1.11		0.01	0.15	
FeO	5.34	4.72	3.83	3.76	4.3	5.56	2.81	5.63	4.84	0.52	0.5	0.11	1.42

Table 7 - Summary of the percentage of each compound detected with the SEM-EDS on the sample TC6-1

shard	
	C1
	3a
	2
Na2O	0.13
MgO	0.78
Al2O3	20.58
SiO2	64.03
K2O	1.01
CaO	0.53
TiO2	0.46
Cr2O3	
MnO	
FeO	12.59

clay						
	C1				C1	
	1a				2a	
	5	6	7	8	3	4
Na2O	0.19	0.2	0.39	0.2	0.22	0.62
MgO	0.96	0.53	0.92	0.57	0.92	0.85
Al2O3	25.76	15.81	23.35	19.39	20.94	20
SiO2	61.29	77.4	67.39	72.7	70.39	70.58
K2O	3.13	0.97	1.41	1.41	2.11	1.96
CaO	1.62	1.12	1.58	1.03	0.76	1.32
TiO2	0.8	0.71	0.7	0.41	0.67	0.81
FeO	5.66	3.16	4.1	4.24	3.92	3.98
MnO					0.22	

fel			
	C1		
	1a		2a
	3	4	5
Na2O	7.23	2.1	8.43
Al2O3	23.36	18.15	21.72
SiO2	63.6	64.61	65.07
K2O	0.22	11.87	0.61
CaO	5.39	0.29	4.1
FeO	0.16	0.42	0.12
BaO	0.04	2.57	

qtz				
C1		C1		
1a		2a		3a
1	2	6		1

amph		
	C1	
	2a	
	1	2
Na2O	1.75	1.69
MgO	11.18	14.29
Al2O3	10.7	9.06
SiO2	48.6	48.07
K2O	0.52	0.39
CaO	11.05	10.54
TiO2	1.05	1.45
Cr2O3	0.2	0.16
MnO		1.08
FeO	14.99	13.21

Table 8 - Summary of the percentage of each compound detected with the SEM-EDS on the sample TC14-12

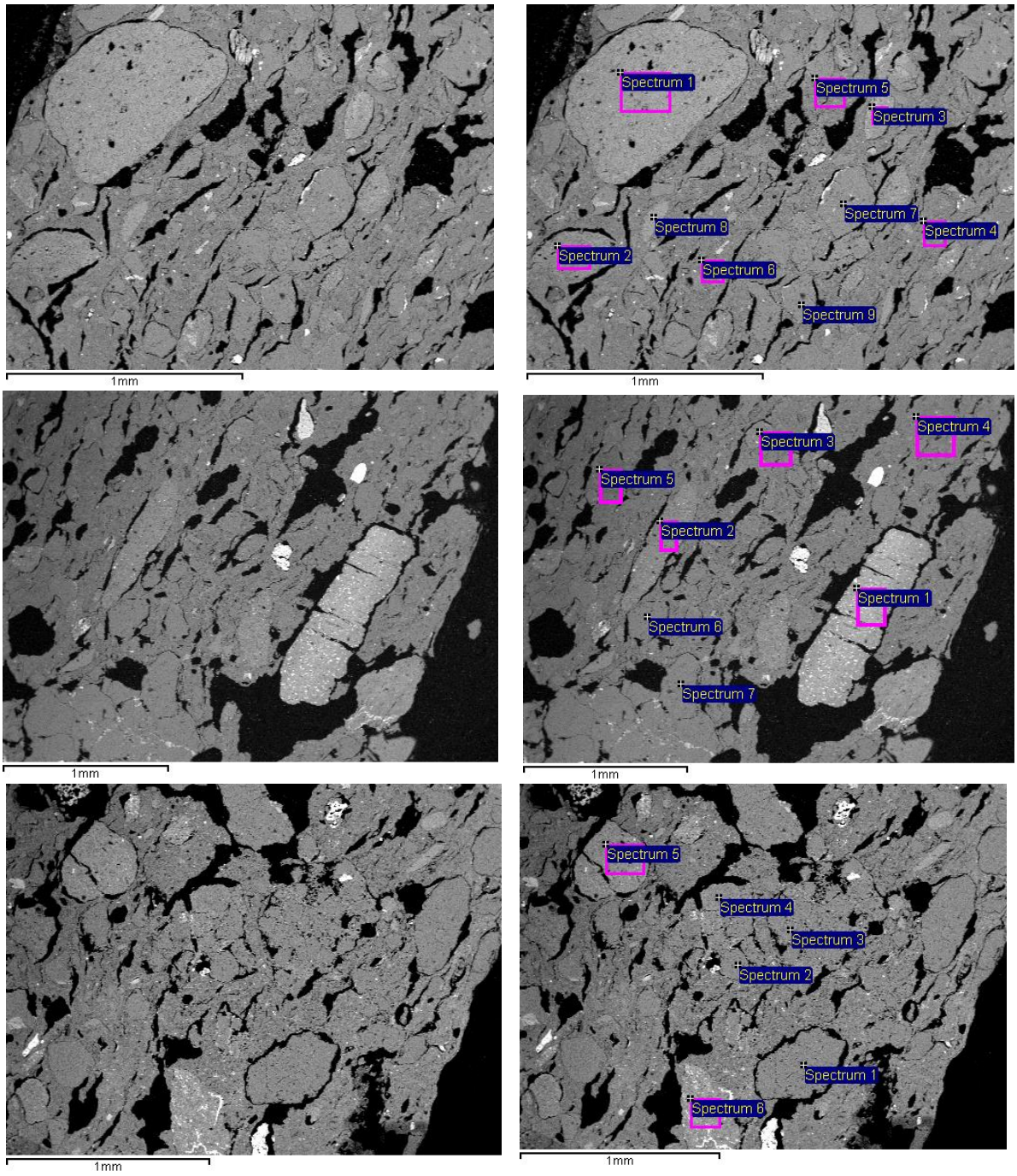

Figure 24 - SEM-EDS images from sample TC4-6. C1. From top to bottom: 1a, 2a, 3a. Left is the clean image, right shows the spots of analysis

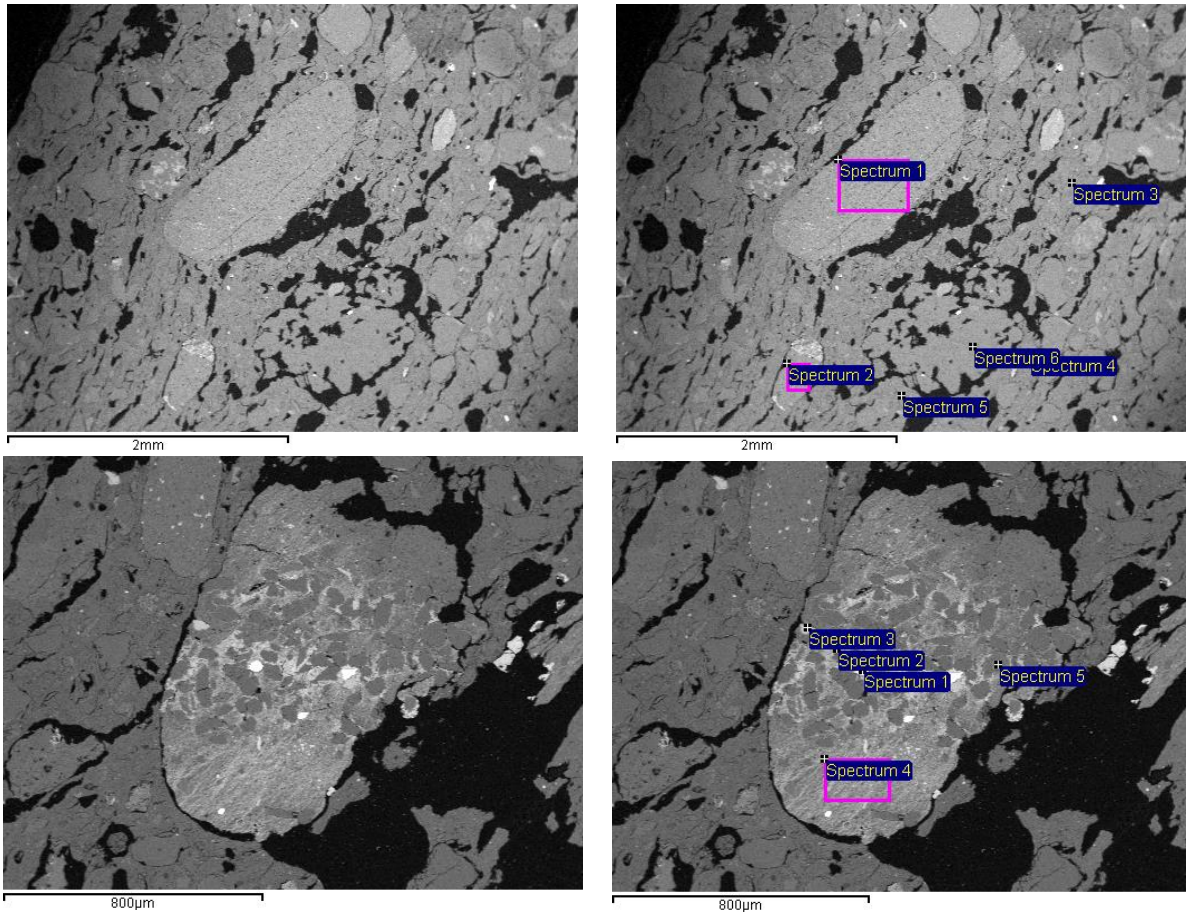

Figure 25 - SEM-EDS images from sample TC4-6. C2. From top to bottom: 1a, 2a. Left is the clean image, right shows the spots of analysis

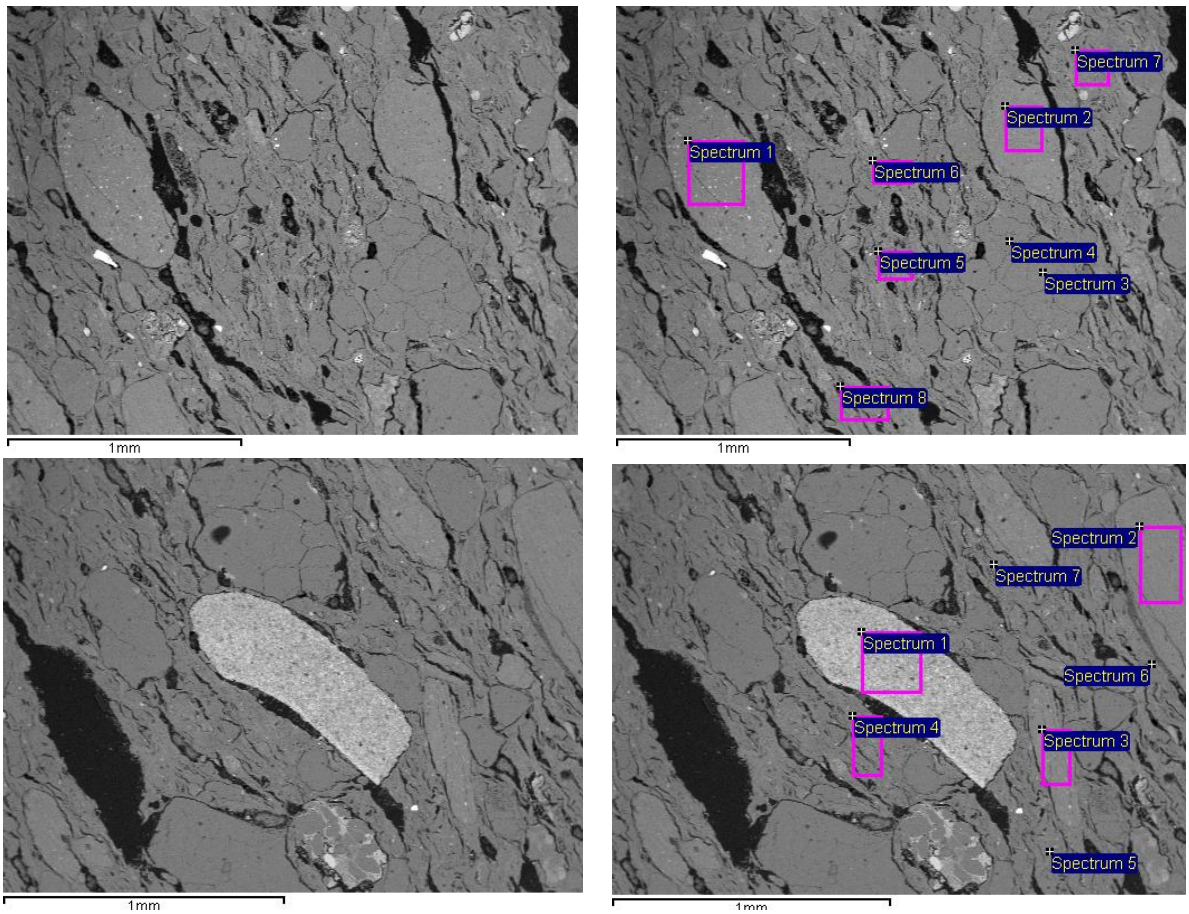

Figure 27 - SEM-EDS images from sample TC6-1. C1. From top to bottom: 1a, 2a. Left is the clean image, right shows the spots of analysis

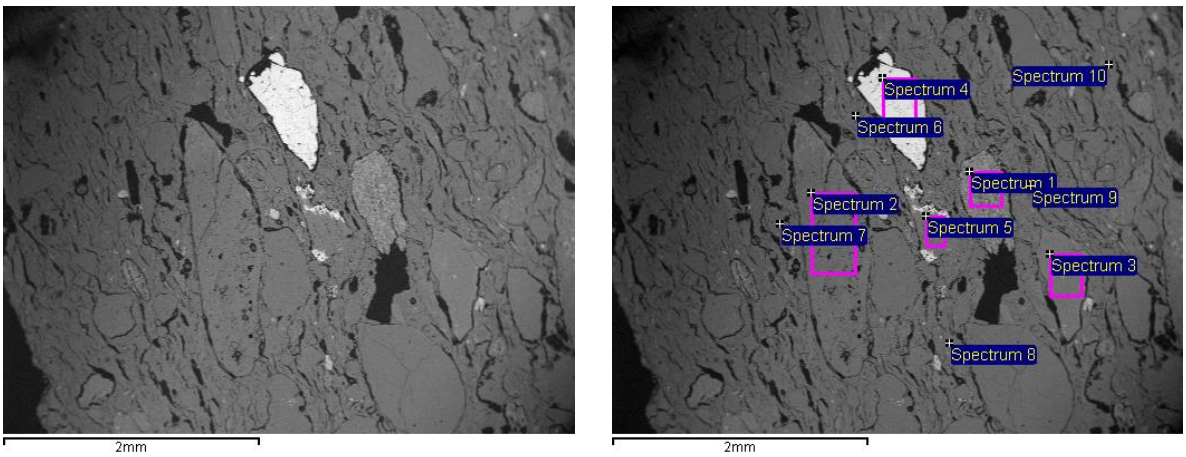

Figure 26 - SEM-EDS images from sample TC6-1. C2. 1a. Left is the clean image, right shows the spots of analysis

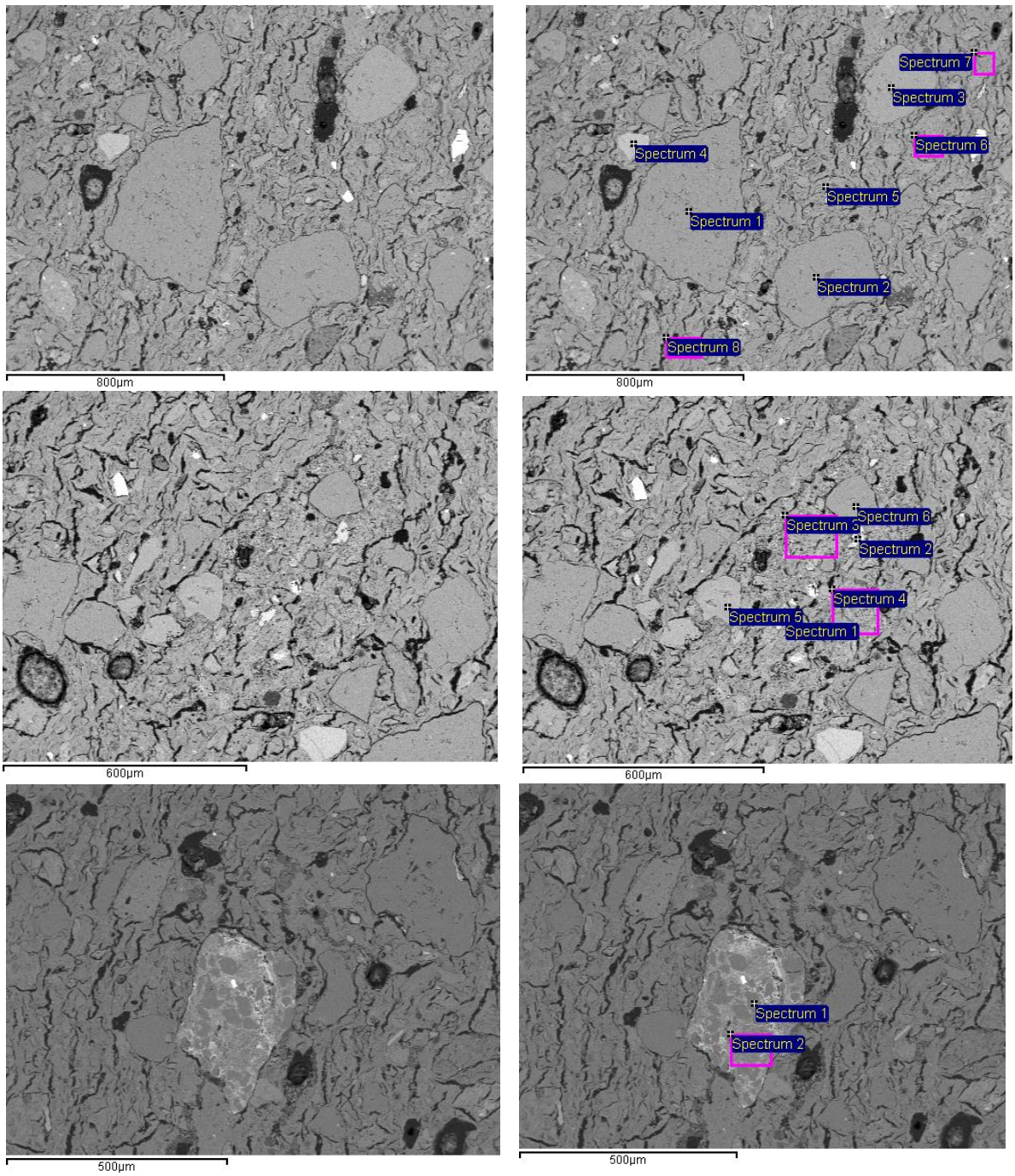

Figure 28 - SEM-EDS images from sample TC14-12. C1. From top to bottom: 1a, 2a, 3a. Left is the clean image, right shows the spots of analysis

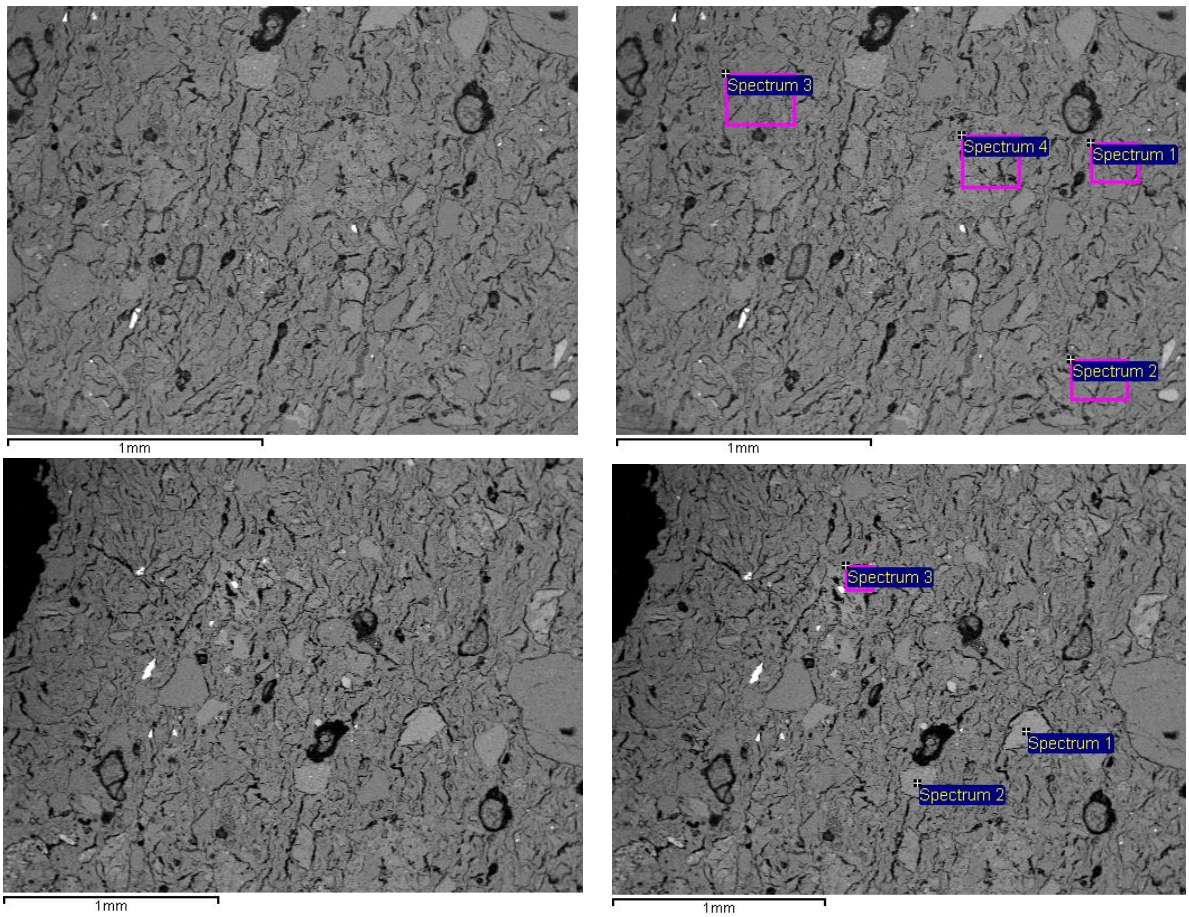

Figure 29 - SEM-EDS images from sample TC14-12. C2. From top to bottom: 1a, 2a. Left is the clean image, right shows the spots of analysis

Discussion

The discussion will be divided in four parts. The first one will be about the results from the rock magnetic experiments and the SEM-EDS analysis, to check if the geochemical and mineralogical information obtained can give certain degree of context to the behavior of the specimens during the Thellier-Thellier experiment. The second one will be a contextualization of the previous archaeomagnetic studies in Colombia. This is tied with the third part, which gives the contextualization of the archaemagnetic models of areas surrounding Colombia, because with these two, the idea is to explain the situation in which the data obtained from this project are going to be integrated. Finally, the last subchapter will be a comparison from all the published data from the area of interested, with the new intensity measurements being accordingly relocated to Bogotá.

- *Implications from the rock magnetic experiments and the SEM-EDS analysis*

An important information acquired through the thermomagnetic measurements is the Curie point of a sample, this helps in the process of understanding a sample's consistency and allows to observe possible mineralogical transformations resulting from the heating-cooling process. We must remember two things: first, if the second curve (the cooling one) overlaps the first one, even with some minor deflections it means that there were no important chemical changes during the heating and the sample is stable at a mineralogical level (De Marco, 2007); second, if both curves do not coincide and the cooling is above the heating one it means that irreversible chemical changes happened

Now, if the curves coincide in a heating done until 700°C, this probably means that magnetite, titanomagnetite or maghemite can be the dominant ferrimagnetic phase. The results that we obtained show that the six samples generally show a good reversibility of the heating and cooling curves, giving evidence that no significant mineralogical changes occur during heating. The cases of TC14 and TC6 appear to lose magnetization a little before reaching 600°C. On the other hand, both cases of the TC4 appear to be a bit after 600°C. According to the Table 1, the magnetite has a Curie Temperature around 575-585 °C, while the maghemite has one of around 600°C. Thus, at least from the thermomagnetic perspective, it is possible that there is a majority of magnetite in the cases of TC14 and TC6, while in the cases of TC4 possibly maghemite is dominant.

Parallel to this experiment, are the IRM results, which show the magnetic acquisition of saturation. The important aspect here is to check at what field level does the sample acquired most of the IRM. The results obtained showed that all the specimens acquired high level of saturation between 200 and 300 mT, but still with a gradual incrementation on

the stronger fields. This indicates the dominance of soft magnetic minerals, like magnetite, titanomagnetite or maghemite, but with a small presence of other harder minerals.

When we compare the results of both rock magnetic experiments, we see a similar behavior. Both experiments show that, even if the results are promising, there are some small amounts of other minerals that can affect the quality. Minerals like magnetite or maghemite are, apparently, the rule, but still is not the perfect scenario.

Keeping this information and comparing it with the results of the SEM-EDS analysis, we see a congruency. The TC4-6 and TC6-1 samples showed constant (and sometimes high) levels of FeO, and from the magnetic results, we can assume that they consist from magnetite and maghemite. These samples also show low levels of TiO2. The difference starts when we look to the results of the TC14-12 sample, where we see the participation of more compounds besides the FeO. Also, it is important to notice that this last sample did not present a notable amount of pottery shards. It is important to remind that the archaeologist have observed that for this area, some typologies have pottery sherds as temper (Boada & Cardale, 2017)

When we bring together the results of the three experiments and check them against the percentage of success from the Thellier-Thellier method, some observations rise. But before, we remind that at the end of the Thellier-Thellier (Table 5) method most of the TC14 specimens were discarded, followed by the specimens from TC4. This happened also with the specimens discarded during the experiment. So, the question is what could have happened.

In the case of the samples analyzed from the TC14 group, the magnetic experiments were considered successful, but the SEM-EDS analysis did show different information at an elemental and particle level. It is possible that the lack, or presence, of the pottery shards on the specimen could affect the results from the Thellier-Thellier method, these shards being also firing events. Depending on the temperature to which they were fired and if this is higher than the new ceramic product, they can affect seriously the outcome of the Thellier experiment. Another possibility falls on the other elements present in the sample, which for the TC14 appears to be very different.

Even so, this creates some contrast with the sample TC4-6. This sample is a very particular one because it was considered successful in the Thellier-Thellier experiment, and the thermomagnetic experiment (check Table 3). In the case of the SEM, the data did not show anything out of order, but if we look closely to the thermomagnetic curves, the cooling line is above the heating line during the first 450°C, and the three specimens from this sample used in the Thellier-Thellier were discarded after the 400°C measurements.

Although some of these results could explain the behavior during the Thellier-Thellier method, it is hard to generalize for all the context, only from some few samples. Even so, although most of the successful specimens came from samples belonging to the DG ceramic typology, it would be difficult to explain with the evidence at hand. Which is why

it is important to keep going with these kinds of studies on the archaeological material from Colombia, and that this data help as some first steps.

Finally, comparing the results of the SEM-EDS analysis against the information mentioned in the subchapter "Mineralogical information from the pottery of the area", we see that the samples studied in the present project may have been fabricated with local materials, some already mentioned by Calderón (2016). The only exception detected was the amphibole present in the TC14-12 sample. And as we said before, observing the typologies of the samples that were analyzed, together with the information from the previously exposed studies, we begin to see a possible tendency of non-local temper for certain typologies of the Herrera and Early Muisca periods. But even with this, we keep an open question mark, and an encouragement for more petrographic studies and a proper provenance project.

- *Previous archaeomagnetic studies in Colombia*

As mentioned in the introduction, very few archaeomagnetic data have been published for Colombia, all of them on intensities due to the archaeological characteristics of the country, which provides a big number of ceramic fragments and not so many fired features in situ for pre-Hispanic times. An “intensity” measurement refers to the intensity of the magnetic field (represented with micro-Tesla (μT)), one of the three previously mentioned characteristics that define the orientation (Declination, Inclination) and the magnitude F of the geomagnetic vector on a place on Earth’s surface, and so, used for archaeomagnetic analysis.

It is important to note that the results presented by these investigations are the expected in a region with no prior archaeomagnetic studies, which means that the intensity data obtained were compared with global models to see the possibility of a correlation, due to the lack of a regional secular variation curve. Also, these first investigations started from comparing the information with other forms of dating in order to understand the local archaeomagnetic characteristics, and then discuss the efforts to build the reference curves. Therefore, the published results that will be shown in this chapter, as well as those of the present project, start from contexts previously dated by radiocarbon (or thermoluminescence in the case of the Piedras Blancas site). At the end there will be a map with the location of the Colombian archaeological sites with archaeomagnetic data (Figure 30).

Another important aspect to clarify is the definition of the global models. It is common that the researchers compare their results with global models to give a more concise discussion around their data according to global datasets. The following models are those that the authors who published Colombian data have used.

1. The **ARCH3K.1** model is defined by the webpage GEOMAGIA (2021) as “Constructed using available archaeomagnetic data up to 2009. It covers the past 3 ka. Data are strongly biased towards the Northern Hemisphere and Europe in

particular. The model gives reasonable field values for the Northern Hemisphere but should not be used for global studies or Southern Hemisphere field predictions.".

2. The same webpage defines th*e* **CALS10K.1b** model as one that "Covers the past 10 ka and incorporates the largest number of data to date. It is based on sediment, lava, and archeological data available up to 2011. The data compilation is dominated by sediment data. The final model is an average obtained from bootstrap sampling (the 'b' in the model's name denoting bootstrap sampling) to account for uncertainties in palaeomagnetic and chronological data".

3. **SED3k**, also defined by GEOMAGIA, is "Constructed using available sediment data up to 2009. It covers the past 3 ka. Data have a better global distribution (less biased towards the Northern Hemisphere) than ARCH3k.1 and can be used for prediction in the Southern Hemisphere. The model output is smoothed in time as a result of the sedimentary recording process and the methods of sub-sampling employed".

4. Finally, the **SHA.DIF.14 K**, proposed for the Holocene by Pavón-Carrasco et.al. (2014), is a model based on archaeomagnetic and lava flow data, avoiding the use of lake sediment data. Particularly the authors cover with the model the last 14000 years, from the 12000 BC to the 1900 AD.

The first published data for Colombia were from Berkovich, et al. (2017) for two sites in the Middle Magdalena Valley: La Sonrisa (Honda, Tolima) and La Salada (Puerto Bogotá, Cundinamarca). For La Sonrisa, the authors report three radiocarbon dates (all cal. BP) associated with different moments of the human occupation identified: L2-1 is 749 ± 37, L2-3 is 789 ± 74 and L1-3 is 348 ± 93. For La Salada, only one radiocarbon date (also cal. BP) was reported: 1714 ± 56. These results were the point of comparison for the archaeointensity results. For the L2-3 occupation the total mean value of the corrected intensity was 34.0 ± 0.9μT, for L2-1 it was 33.2 ± 2.5μT, for L1-3 28.2 ± 0.9μT, and for La Salada 39.2 ± 2.7μT. The authors compared these data with two global models, ARCH3K.1 and CALS10K.1b, but did not find a tendency between both sources, encouraging future research to create the regional intensity curve.

The second dataset was presented by Cejudo, et al. (2019) for the archaeological site Portalegre, in the municipality of Soacha (Cundinamarca), in the Sabana de Bogotá (Eastern Colombian Andes). The results showed good quality data for thirty-seven specimens cut from two potsherds, each potsherd associated to one radiocarbon dating (presented in AD years): for Soacha 6 it is 1230 ± 110 and for Soacha 7 1035 ± 115 (Cejudo, et al., 2019). For Soacha 6 the total mean value of the corrected intensity was 33.2 ± 2.89μT and for Soacha 7 this was 45.31 ± 3.17μT. The authors compared these results with the global geomagnetic model SHA.DIF.14 K, but the patterns observed disagree with the radiocarbon information. In response to this, they propose a regional variation curve for Southern Mexico and the Caribbean. The result is a reference curve that goes from 3000BC

to 2000AD, and they compare it with the curve from Central Mexico and the Southern USA (CMSUS) (Goguitchaichvili, et al., 2018), as well as the one from South America (Goguitchaichvili, et al., 2019). Some similarities between the Caribbean and the CMSUS were observed, but a very distinctive behavior of these two with the South American one was noticed. Finally, the authors suggest that the Caribbean curve "should be considered as the most reliable dating tool in Colombia and surrounding regions" (Cejudo, et al., 2019).

The same year Obregón, et al. (2019) presented the data from samples taken from the archaeological site of Piedras Blancas (Medellín, Colombia) located on the Northwestern Colombian Andes. In a different target than the other articles, the objective of this one is to compare thermoluminescence dating previously done to the artifacts, with archaeomagnetic one. After the experiments, two specimens were considered with high quality information: UIA167PS5D and UIA167CII2AN4. The thermoluminescence date of the first one is 1505 ± 24 AD, but in the second case the thermoluminescence information was from two associated sherds and not from that specimen. The ages of those sherds are 1574 ± 32 AD and 1632 ± 63 AD. For the first specimen, the archaeointensity value was 37.3 ± 2.4μT, and for the second one 34.5 ± 2.6μT. The results show that thermoluminescence provides a more exact dating, but there is a reason behind this. The authors explain that due to the lack of a regional register of archaeomagnetic values, they needed to compare the results of this dating with the global data model SHA.DIF.14k, which presented a big range of errors and even several time spans of chronologic provenance. Finally, they concluded that the thermoluminescence technique gives a better dating, complementing the information from the typological chronology, but they also call for data to create a reliable archaeomagnetic record for the past two millennia of the Colombian territory.

Finally, the last publication on the subject was by Rojas, et al. (2020), for the San Pedro archaeological site, located in the Momposina Depression, in the northern part of Colombia. Although the authors said that nine fragments were selected for the archaeointensity experiment, they only report eight results with their corresponding radiocarbon dating. For a better understanding, next will be presented the specimen's name, with the radiocarbon dating (BP) associated and the total mean value of the corrected intensity:

SP-8854; 1450 ± 30; 26.87 ± 1.59μT	SP-8857; 1450 ± 30; 21.52 ± 2.25μT
SP-6537; 1410 ± 30; 28.32 ± 3.74μT	SP-6423; 1410 ± 30; 26.18 ± 3.42μT
SP-6574; 1410 ± 30; 23.89 ± 2.22μT	SP-7582; 1400 ± 30; 20.96 ± 2.94μT
SP-18546; 70 ± 30; 29.62 ± 3.07μT	SP-27008; 1260 ± 30; 24.85 ± 2.96μT

Table 9 - Summary of the archaeointensity results reported by Rojas, et al. (2020). The first number is the specimen's name, then the radiocarbon dating (BP) and then the total mean value of the corrected intensity

The authors compared the data obtained with three different global models, SHA.DIF.14k, ARCH3k and SED3k. The first two reported unsatisfactory analysis, but with the third one they found some similarities. Even so they explain that the SED3k model is based on

sediment information, which is not the ideal for this cause. Hence, the authors keep calling for an effort to construct a secular variation curve for Colombia and continue obtaining more data.

From all the above information on published archaeomagnetic data from Colombia, we can draw a general comment: though these data were obtained following the adequate protocols and in certified laboratories, their number is quite low. For example, Berkovich, et al. (2017) presents results of seven pottery fragments, each one with six specimens analyzed, reporting the mean intensity depending on the context. Cejudo et al (2019) started with seventy-two specimens belonging to six pottery fragments, but after the study, only two potsherds which provided thirty-seven specimens gave valuable information. Obregon et al (2019) provide archaeointensity results from only two specimens associated to two different sherds. Finally, Rojas et al., (2020) present results from 8 pottery fragments, each one with six specimens analyzed, giving a total of forty-eight measurements. The authors report the mean intensity for each fragment. This study is filling better the quality criteria concerning the number of fragments/specimens.

This information is important because, if we take into account the fact that every pottery fragment-or sherd- corresponds to a firing event, then it is more than clear that these numbers cannot be representative for a whole period. Moreover, several studies conducted on the thermal properties of ceramics and pottery have proved that these can vary not only between pots of the same firing but also within the same pot. (Gosselain, 1992; Livingstone Smith, 2001)

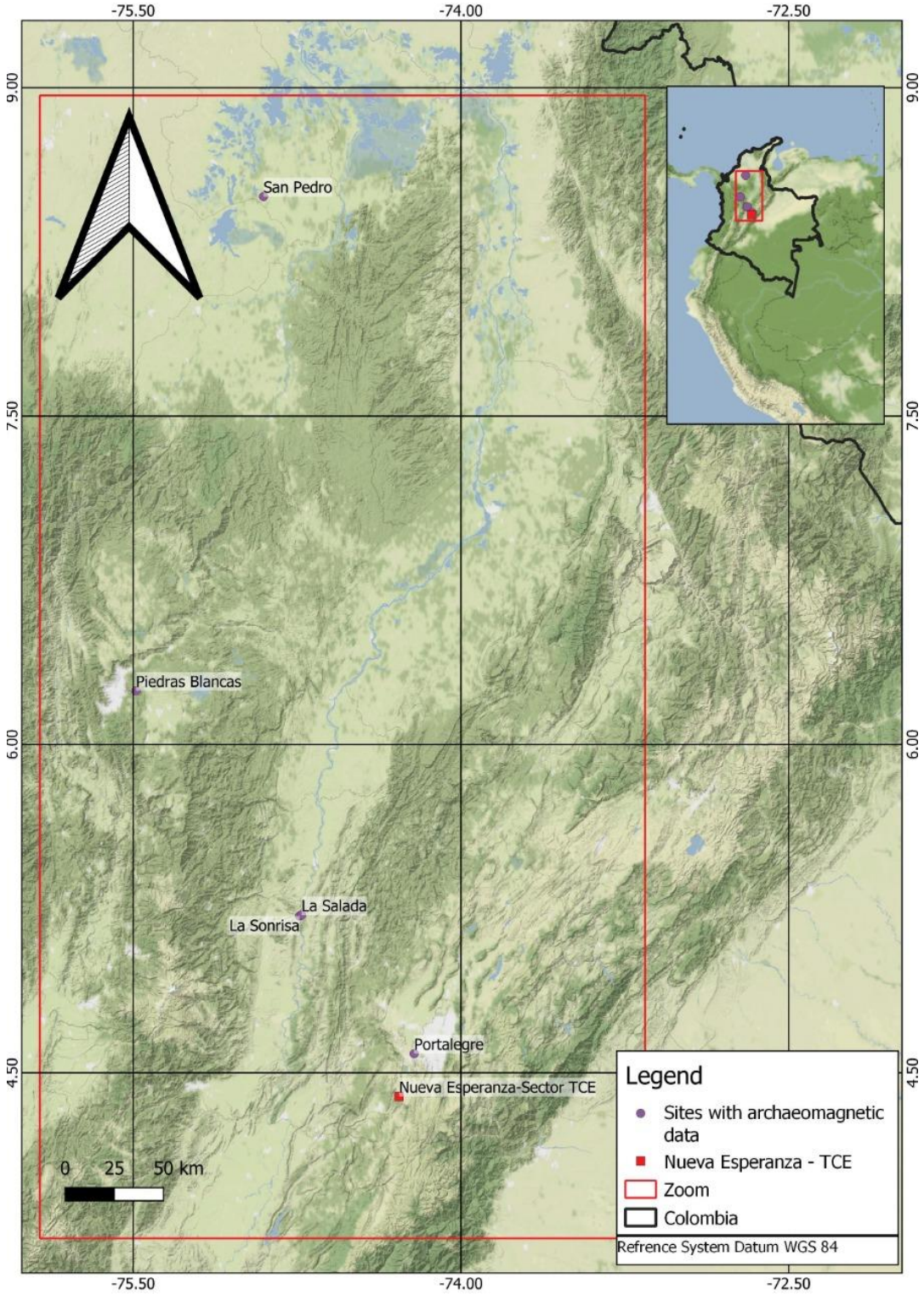

Figure 30 - Map showing archaeological sites with archaeomagnetic data in Colombia. Drawn by archaeologist Carlos Reina by request of the author.

- *Considerations of archaeomagnetic models used in areas surrounding Colombia*

Because Colombia does not have a local secular variation curve (SCV), the archaeomagnetic studies made on its territory with the aim of dating must be compared with other models. In the past, the researchers made this comparison with global models without a satisfactory conclusion. So, to try to solve this for the present project, it was decided to bring into discussion what could be another possibility among the archaeomagnetic models of the neighboring areas. This decision was made based on the explanation by Cejudo, et al. (2019), regarding the curves of other parts of the continent.

Geographically speaking, Colombia is considered as part of the South American continent, but this is not the case for the GMF. As explained by Cejudo, et al. (2019), the archaeomagnetic data from Colombia do not appear to have similarities with the southern areas of the continent. This is probably due to the South American Anomaly, also called the South Atlantic Anomaly (SAA), which consists in the emergence of an area of low field intensity spanning the southern Atlantic Ocean, Africa and South America, that is corelated to the decay of the dipole moment (Campuzano, et al., 2019). Indeed, studies carried out mainly in Argentina, showed that the data for this area are influenced by the South American Magnetic Anomaly , so the SVC for intensities that the researchers were able to build with these data work for Peru, Brazil, Argentina, Chile, and Bolivia, for a timespan of two millennia (Goguitchaichvili, et al., 2015; Goguitchaichvili, et al., 2019).

The other possibility are the curves proposed in Mesoamerica, as shown by Cejudo, et al. (2019), where for their comparisons they used the one proposed by Goguitchaichvili, et al. (2018). This intensity SVC covers the last three millenia for Mesoamerica and also the southern USA. The authors propose that this curve may potentially be used as dating tool of burned archaeomagnetic artifacts carrying thermoremanent magnetization. The work by Goguitchaichvili, et al. (2018) was the starting point for a discussion regarding the quality of the data available for Mesoamerica. After that proposal, Hervé, et al (2019), while presenting thirteen new intensity data acquired on potteries from Chalcatzingo in Mexico, made a critical analysis of the intensity measurements of Central America. The authors explain that, although the large number of intensities available for the last thousands of years in the region may show that the curve is well established, much of this information had experimental errors. Thus, the above researchers suggest that what can be considered as high-quality data is actually a minority in the dataset, which leads them to propose a curve that presents several differences with the one of Goguitchaichvili et al. (2018). They conclude by mentioning that the analysis made of the Central America dataset drastically highlights the need of new high-quality data with precise dating for almost all periods. The authors also point to the fact that the dating information can be very uncertain as the probability of no contemporaneous cooling is high for two reasons: either sherds came from different archaeological layers or from a single layer associated to a long-lived settlement.

The same year, a third curve was proposed. Mahgoub, et al, (2019a) who worked with data taken from volcanoes in Mexico for an SVC for the past 44000 years. They compared the later years of the data with the curve of Goguitchaichvili, et al., (2018), reporting some differences, possibly due to the selection of the data to build each curve and the area that they decided to work with (which from Goguitchaichvili, et al. contains information from southern USA), and also the quality of the data, in a similar fashion of the critique by Hervé, et al (2019). Shortly after, Mahgoub, et al, (2019b) present the reports of 41 intensity data covering the past 3600 years which, together with 38 previously published data of similar quality, are used to construct an intensity SCV for Central Mexico. They performed this study, based on the comments explained in the previous publication, to provide new high-quality intensity data dated between 1550 BCE to 1798 CE. The authors present this new model as they believe it to better describe the GMF evolution in Mexico, because it relies on a larger new data set with strict selection criteria.

One of the aspects that both groups, Hervé, et al. (2019) and Mahgoub, et al. (2019a, 2019b) were critical regarding the curve of Goguitchaichvili, et al. (2018) was the incorporation of the data from the southern USA, explaining that this extension would induce more error on the SVC. Now, while in Mexico there was a general discussion regarding the quality of the data, the same concern appeared in the southwest USA (Jones, et al. ,2020). Although they do not mention the work by Goguitchaichvili, et al. (2018), the data the authors discuss belong geographically to that area, explaining that some of the measurements lack standard quality controls (e.g., cooling rate correction), showing a similar problem of what has been described for Mexico.

After this, Garcia, et al. (2021) propose a fourth curve, that could be considered as an upgrade of the one by Goguitchaichvili, et al. (2018). The starting point are the discrepancies found with the previous studies, so they perform a new, critical re-evaluation of both available data and model construction techniques paying special attention to values retrieved from unpublished thesis, and other sources like historical records for the later centuries (Goguitchaichvili, et al., 2020). They claim that the selected data, which are distributed throughout the last 3600 years in Mexico, allowed the development of a reliable SVC. Also, they decided to separate the curves of Mexico and Southern USA, but they compared them, noticing that they still have similarities.

To finish this detailed discussion regarding the Mesoamerican curves, we present a case study. Alva Valdivia, et al. (2021) performed an archaeointensity dating to pottery samples from the Chihuaha area, in Northern Mexico. These samples come from the Casas Grandes cultural area, specifically from the Paquimé site. They worked on two archaeological typologies, Mimbres and Ramos, which have an age period between 900 and 1450 CE. Also, they do not have associated datings, like radiocarbon or thermoluminescence. The curve they decided to use was the one developed by Mahgoub, et al. (2019a, 2019b), giving an absolute age range of 960–1100 CE for Mimbres type, and of 1300–1600 CE for Ramos samples. This information was considered as satisfactory and accurate by the authors. In a part of the discussion presented, they explain that they decided not to use the curve by

Garcia, et al. (2021) because this one was built with data not considered as high quality by other studies, quoting Hervé, et al (2019) and Mahgoub, et al. (2019a, 2019b).

It is important to note that all the studies quoted in the Mesoamerican discussion also compared their results with several global models, always founding big differences, and thus discarding the possibility of using them for the moment.

The other curve that Cejudo, et al. (2019) used, besides Mesoamerica and South America, was the one they called Southern Mexico and the Caribbean, which could be the one of major interest for the present project. The issue is that to this date, we have not found any other research that has used this curve, but still, this does not discard the possibility of us to use it.

In order to give a bigger context to this application, the archaeomagnetic information in neighboring countries to Colombia (that were not part of the aforementioned anomaly) was consulted. For Ecuador, Herrero Bervera, et al. (2020) describe a case similar to the situation observed in Colombia. The authors begin by explaining that indeed for these latitudes there is a lack of archaeomagnetic data, for which there is no reference curve, and they doubt the usefulness of global models since the information on which they were built is mainly based on the northern hemisphere. With this argument, they go on to present a set of absolute archaeointensity determinations from pottery collections recovered from three dated (with C14) archaeological sites located at the highlands of north central Ecuador: Atuntaqui, Otavalo and La Chimba. The Atuntaqui and the Otavalo sites belong to the prehistoric Late Period (1250–1505/1525 AD), while the age of the La Chimba site is much earlier, belonging to the early ceramic period (700 BC- 250 AD). The point of interest from this research is that the authors, due to the lack of a reference curve, decided to compare the values obtained with sites from Colombia and Peru. In the Colombian case, they compared with the intensity values obtained by Berkovich, et. al. (2017), observing that, the values obtained in the lower charcoal lens of the Otavalo site were similar to those from La Sonrisa site (specifically L2-1 and L2-3). Also, thanks to the C14 dating information from both sites, part of the realization was that they were also similar at a chronological level, putting the contexts around the XIII century. Herrero Bervera, et al. (2020) also mention that there are few other archaeomagnetic data from Ecuador, but they come from earlier periods, and they are so scattered, that it is difficult to make any comparison.

For Venezuela it looks like there is not much information. Rada, et al. (2011), in their research to characterize different manufacturing techniques from several archaeological sites located on islands in the northern coast, made rock magnetic analysis but did not work on archaeomagnetic data. Even so, they quoted an article by Brandt and Costanzo-Álvarez (1999 in Rada, et al. (2011)) which is presented as a preliminary archaeomagnetic study of prehispanic Venezuelan pottery. Sadly, at the time this document was written, the article could not be located in digital media. For Panama, and other countries from Central America relatively close to Colombia, it was not possible to locate some information.

The above compilation, from the Colombian data and the models from surrounding regions, clearly demonstrates the following points. *First*, the existing dataset for Colombia is very small regarding the number of reliable data and therefore the need to complete it with new, accurate ones gives an additional value to the present project. *Second*, the composite curve for the Caribbean of Cejudo et al. (2019) is the closest possibility for comparison with our data, and although the data from Colombia is few, we will use the curve in the next discussion. And *third*, another comparison could be done with the curves for Mexico but only regarding their trend, not for detailed conclusions.

So, for the next part of the Discussion we will plot all Colombian published data, plus the data reported by Herrero-Bervera et al. (2020) that is contemporary to the Colombian data, based on relevant ages, and accordingly relocated to Bogotá, in order to visualize our new data in a broader context.

- *Archaeointensity data from Colombia and Northern Ecuador relocated to Bogotá*

For the relocation exercise we followed the process made by Cejudo et al. (2019), which consisted in a relocation for Bogotá and for Costa Rica. The relocation procedure is important when several intensity values from different areas are going to be integrated to be analyzed as a whole. The idea is to apply the following equation to transform the intensity values, standardizing them for one location (hence the name relocation). As Cejudo et al. (2019) explain, Hs are the original archaeointensities, HR are the relocated archaeointensities, θs are the geographical colatitudes and θR is the colatitude of relocation point. The coordinates considered for Bogota were Lat 4.61°, Lon −74.08°.

$$H_R = H_S \sqrt{\frac{(1 + 3\cos\theta_R{}^2)}{(1 + 3\cos\theta_S{}^2)}}$$

Cejudo et al. applied the relocation process to try to create a reference curve for Central America and the Caribbean area, as previously explained. But in our case, we want to compare the available data and see if there is and early evidence of a pattern. As we can see in the Figure 30 the sites of Nueva Esperanza, Portalegre, La Sonrisa and La Salada are close to the center of Colombia, where Bogotá es located, so their intensity value was not relocated. On the other hand, Piedras Blancas, San Pedro, and the Ecuatorian sites of Atuntaqui, Otavalo Mound (Lower charcoal lens) and Otavalo Mound (Upper charcoal lens) were relocated. This data is express in the Table 10.

Authors	Site	Coord X (wgs84)	Coord Y (wgs84)	Data presentation	Archaeological period	BP	CE	Error	Intensity (μT)	Error	Relocated
Berkovich, et al. (2017)	La Sonrisa	74°44'18.20"W	5°12'55.98"N	L2-1	Late (XII to XVI CE)	749	1201	37	33.2	2.5	
				L2-3	Late (XII to XVI CE)	789	1161	74	34	0.9	
				L1-3	Late (XII to XVI CE)	348	1602	93	28.2	0.9	
	La Salada	74°43'45.42"W	5°13'11.66"N	La Salada	Intermediate (around II CE)	1714	236	56	39.2	2.7	
Cejudo, et al. (2019)	Portalegre	74°12'44.99"W	4°34'36.60"N	Soacha 6	Early Muisca to Late Muisca (IX to XVI CE)	720	1230	110	33.2	2.89	
				Soacha 7	Early Muisca to Late Muisca (IX to XVI CE)	915	1035	115	45.31	3.17	
Obregón, et al. (2019)	Piedras Blancas	75°29'13" W	6°14'40" N	UIA167PS5D	Late (XII to XVI A.D.)	445	1505	24	37.3	2.4	37.01
				UIA167CII2AN4	Late (XII to XVI A.D.)	376	1574	32	34.5	2.6	34.23
						318	1632	63			
Rojas, et al. (2020)	San Pedro	74°5'41.164" W	8°30'10.734" N	SP-8854	no mention	1450	560-650	30	26.87	1.59	26.28
				SP-8857	no mention	1450	560-650	30	21.52	2.25	21.05
				SP-6537	no mention	1410	600-660	30	28.32	3.74	27.70
				SP-6423	no mention	1410	600-660	30	26.18	3.42	25.61
				SP-6574	no mention	1410	600-660	30	23.89	2.22	23.37
				SP-7582	no mention	1400	605-665	30	20.96	2.94	20.50
				SP-18546	no mention	70	1810-1924	30	29.62	3.07	28.97
				SP-27008	no mention	1260	690	30	24.85	2.96	24.31
Herrero Bervera, et al. (2020)	Atuntaqui	78°12'0.00" W	0°20'24.00"N	Atuntaqui	Late Period (1250–1505/1525 CE)	519	1309–1450	46	43.57	1.274	43.99
	Otavalo Mound	78°17'60.00" W	0°14'24.00"N	Lower charcoal lens	Late Period (1250–1505/1525 CE)	730	1209–1390	50	34.19	1.37	34.52
	Otavalo Mound			Upper charcoal lens	Late Period (1250–1505/1525 CE)	680	1263–1394	40	39.49	1.4	39.87
Present project	Nueva Esperanza - Sector TCE	74°16'58.20"W	4°34'18.93"N	TC4	Late Muisca (XI to XVI CE)	-	-	-	36.20	3.06	
				TC6	Early Muisca (III to X CE)	-	-	-	31.03	6.34	
				TC14	Late Muisca (XI to XVI CE)	960	990	30	33.20	7.37	
				TC4-5	Late Muisca (XI to XVI CE)	-	-	-	34.04	9.83	
				TC4-8	Late Muisca (XI to XVI CE)	-	-	-	38.37	0.64	
				TC6-1	Early Muisca (III to X CE)	-	-	-	36.21	4.49	
				TC6-2	Early Muisca (III to X CE)	-	-	-	32.53	6.20	
				TC6-3	Early Muisca (III to X CE)	-	-	-	33.64	0.49	
				TC6-4	Early Muisca (III to X CE)	-	-	-	19.50	3.49	
				TC6-7	Early Muisca (III to X CE)	-	-	-	28.31	7.49	
				TC6-8	Early Muisca (III to X CE)	-	-	-	36.01	1.80	
				TC14-9	Late Muisca (XI to XVI CE)	960	990	30	38.42	0.75	
				TC14-11	Late Muisca (XI to XVI CE)	960	990	30	27.99	1.53	

IMPORTANT NOTE: for an area with few archaeomagnetic data, it is important to have reference of dating methods related to the archaeological context. On this table, the dates that are in light-blue are the ones reported on the respective article. An importan aspect is that the CE dates from Rojas et al., and Herrero Bervera et al., are calibrated. Meanwhile the BP dates presented by Berkovich et al. are also calibrated. Cejudo et al. does not clarify, but is possible that are not calibrated. Regarding Obregón et al., those dates are from thermoluminiscence. Due to this situation, we decided to use the BP information of all, calibrated and non calibrated, for the sake of the comparision. We recommend reading the discussion present in the document for more information.

Table 10 - Intensity values from the different sites of Colombia and northern Ecuador. Also, relocation values of some of them

As we stated before, for an area with few archaeomagnetic data, it is important to have reference of other dating methods related to the archaeological context. On the table, the

dates that are in light blue are the ones reported on the respective article. An important aspect is that the CE dates from Rojas et al., and Herrero Bervera et al., are calibrated. Herrero Bervera et al. mentions that the calibration was done with CALIB Rev. 6.0.1. Meanwhile the BP dates presented by Berkovich et al. are also calibrated. They mention using OxCal 4.2.4 with the reference curve IntCal13. Cejudo et al. does not clarify but is possible that are not calibrated. Regarding Obregón et al., those dates are from thermoluminescence. For the present project, the date was calibrated using OxCal 4.4.2 with the reference curve IntCal20. Initially, we wanted to track down all the conventional dates from the original reports and make our own calibration using the same settings of the Nueva Esperaza dating, so we had a standardized data (at least for the radiocarbon dating), and hence try to correlate in a more correct way with the intensity levels. But this was not possible because of lack of time and logistical difficulties. Due to this situation, we decided to use the BP information of all, calibrated and non-calibrated, for the sake of the comparison. We expect that in a future publication, we can correct this situation and keeping the original idea. The result of the comparison of the intensity values against the date provided is the following:

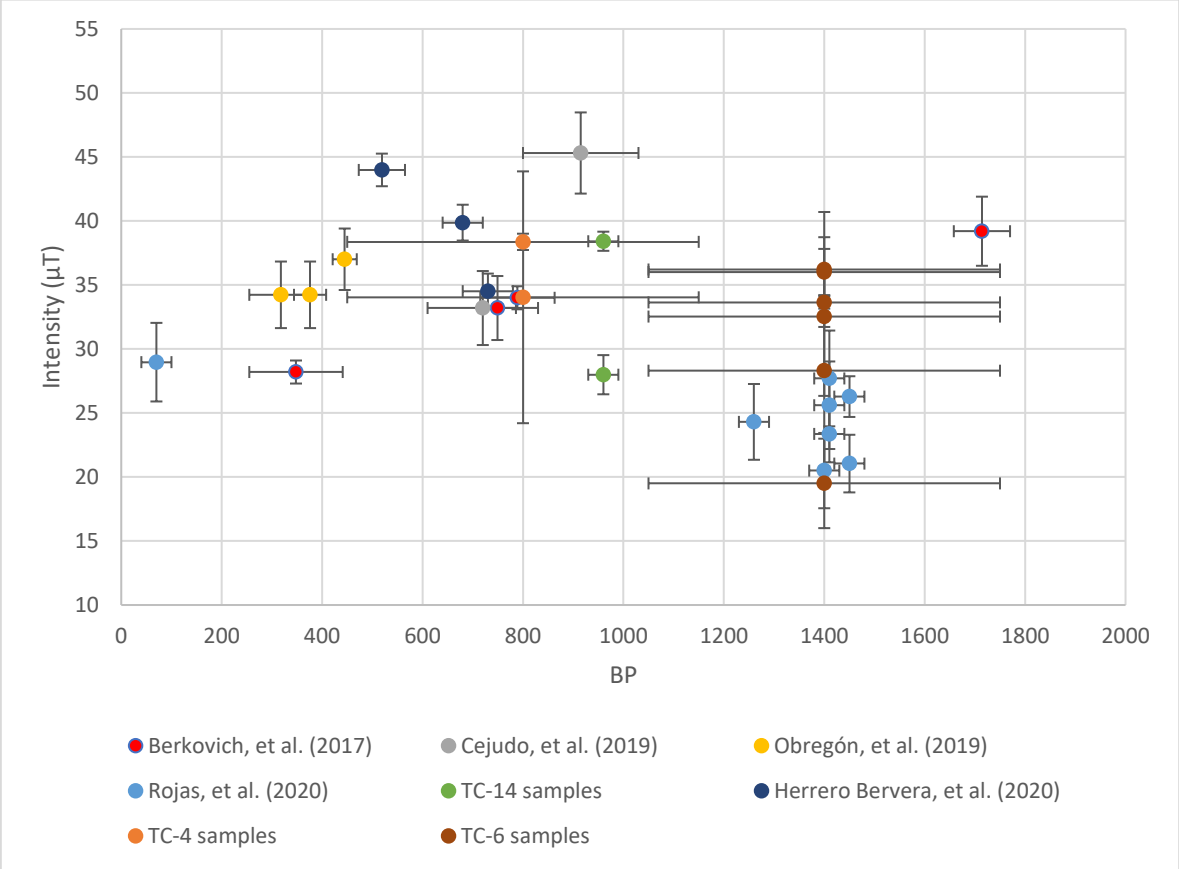

Figure 31 - Comparison of the intensity values, against the date (BP), from several sites of Colombia and northern Ecuador.

For this graphic, the data are shown according to the respective publication. In the case of the present project, the data plotted are the mean value per sample, not context. Although in

Table 10 we also presented the mean value per context, we preferred to use the one per sample to avoid the interference of possible outliers. Also, we must consider that, as mentioned before, each fragment of pottery is a heating event in itself, so grouping several intensity levels could be misleading. Sadly, two contexts used for the present project did not have direct carbon dating associated (TC6 and TC4), hence that data shown on the X axis are based on the archaeological period presented in Table 10. Although this is a" time-uncertain" based solution, it is the best possible with the available information, to give the intensity values some chronological approach. This can be seen in the high error levels. Originally the idea was to use three preselected contexts with associated carbon dating, but because of logistical difficulties during the COVID pandemic at the moment of selecting the samples to study, we had to work with what was at hand.

Although the data are few, it is possible to mention some patterns that could lead us to future hypotheses and discussions. *First,* there is a possible trend of the early dates, around 1000BP and older, showing intensity levels of less than 30μT. *Second,* most of the recent dates, earlier than 1000BP, have intensity levels between 30μT to 40μT. If we try to associate the intensity values from the samples of TC6 and TC4, even with the dating problem they presented, they actually show to fit to each trend, which makes sense according to the associated archaeological period. The TC-6 samples, being from the Early Muisca period, are part of the trend of the older dates; while the TC-6 samples, being from the Late Muisca period, are from the early dates. One of the difficulties is that the time span of these trends is, by minimum, 400 hundred years, which is difficult for creating a reference curve. The other difficulty is the outliers present, for which we cannot be sure if they are effectively outliers, or just invalid information due to the lack of data.

To try to solve this, we will compare this information with the Caribbean curve of Cejudo, et al (2019). We remind that these researchers presented two curves, one with relocation to Bogotá and another with relocation to Costa Rica, preferring the latter, but even so, they stated that the most notorious difference between the two curves is between 1000BC to 0. So, we decided to apply the curve relocated to Bogotá. The results are shown in Figure 32.

We remark that for Figure 32, the X axis is in Common Era, not BP like Figure 31. After placing the results on the Caribbean curve, they seem to agree only in the years between 1100 and 1500 CE. The earlier and later intensity values fall outside of the curve. Although this is a first iteration of the curve and requires future work with bigger datasets, we can make the archaeomagnetic dating exercise of the TC4 samples, which fall inside the curve's range of error. According to the intensity values and the curve, both samples of this context date of around 1100-1200 CE, which coincides with the archaeological chronology.

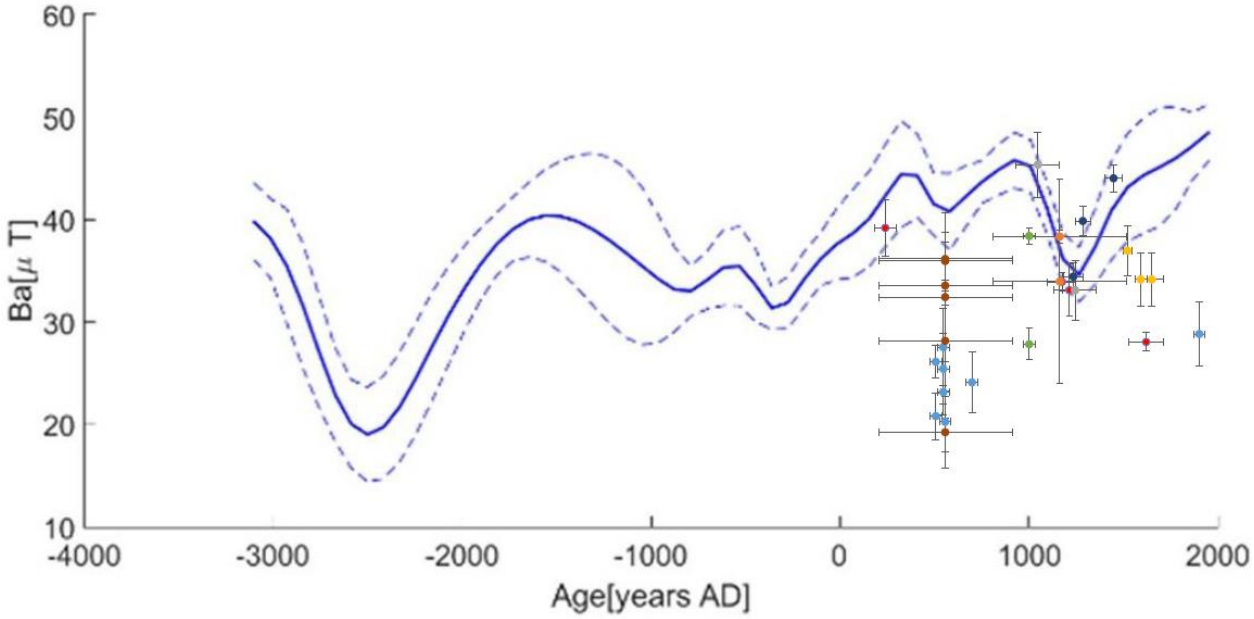

Figure 32 - Data of Colombia and Northern Ecuador compared against the Caribbean curve proposed by Cejudo et al. (2019)

Conclusion

The general objective of this research was focused to understand the archaeomagnetic characteristics of the samples and their potential as reference points using archaeointensity. The mineralogical information provided by the rock magnetic experiments and the SEM-EDS analysis gave us some reasons behind the Thellier-Thellier success rate. At the same time, these results show us the importance to start developing a proper provenance study for the archaeological ceramic of the area, providing some early evidence of possible trace elements and a possible difference of raw materials between the earlier and late periods.

The Thellier-Thellier experiment itself gave us intensity values, and with the application of the respective corrections, is something always welcomed in areas with few data of this kind. With an overview of the published archaeomagnetic information of Colombia and northern Ecuador, and of the debate regarding the models and curves proposed to the surrounding areas, we could create a context for the intensity values obtained and comment regarding the situation of the archaeomagnetic studies in the region. Indeed, as was expected, the data were so few that comparing to other models or being one on its own was not possible. But, by comparing them, we proposed several possibilities that should be checked when more data is available. We remark that these kinds of studies are the important first steps to culminate in an SVC. As happened in other parts of the world, the archaemagnetic studies in order to create a reliable dating method takes time and several research projects.

Bibliography

Alva Valdivia, L., Rodríguez Trejo, A., Cruz Antillón, R., Hervé, G., Perrin, M., Salgado Saito, M., & Mahgoub, A. (2021). Archaeomagnetic dating and magnetic characterization of ceramics from the Paquimé, Casas Grandes region, Chihuahua, Mexico. *Journal of Archaeological Science: Reports. 37*. doi:10.1016/j.jasrep.2021.103040

Argüello, P. (2015). *Subsistence Economy and the chiefdom emergence in the muisca area. A study of the Valle de Tena.* Pittsburgh: University of Pittsburgh.

Ben-Yosef, E., Millman, M., Shaar, R., Tauxe, L., & Lipschits, O. (2017). Six centuries of geomagnetic intensity variations recorded by royal Judean stamped jar handles. *Proc. Natl. Acad. Sci. 114 (9)*, 2160–2165.

Berkovich, C., Goguitchaichvili, A., Peña, G., & Morales, J. (2017). Primeros resultados de arqueointensidades de Colombia: Sitios prehispánicos en el Valle del Río Magdalena (Honda-Tolima y Puerto Bogotá-Cundinamarca). *Arqueología Iberoamericana 33*, 10-17.

Boada, A. M. (2006). *Patrones de asentamiento regional y sistemas de agricultura intensiva en Cota y Suba, Sabana de Bogota (Colombia).* Bogotá: Fundación de Investigaciones Arqueológicas Nacionales, Banco de la República.

Boada, A. M. (2007). *La evolución de Jerarquía Social en un Cacicazgo Muisca de los Andes Septentrionales de Colombia.* . Pittsburg: University of Pittsburg.

Boada, A. M. (2007). *Patrones de asentamiento regional y sistemas de agricultura intensiva en Cota, Suba y Chía (Sabana de Bogotá, Colombia).* Bogotá: Informe sin publicar.

Boada, A. M. (2013). From Small Household Clusters to the Central Place of the Bogotá Chiefdom, Colombia. En S. Palumbo, A. M. Boada, W. Locascio, & A. Menzies, *Multiscalar Approaches to Studying Social Organization and Change in the Isthmo-Colombian Area* (págs. 39-70). Pittsburgh: University of Pittsburgh, Universidad de los Andes y Universidad de Costa Rica.

Boada, A. M., & Cardale de Schrimpff, M. (2017). *Cronología de la Sabana de Bogotá.* Pittsburgh: University of Pittsburgh.

Botiva, Á. (1989). La Altiplanicie Cundiboyacense. In Á. Botiva, G. Cadavid, L. Herrera, A. M. Groot de Mahecha, & S. Mora, *Colombia Prehispánica: Regiones Arqueológicas* (pp. 87-147). Bogotá: Colcultura.

Broadbent, S. (1964). *Los Chibchas. Organización Socio-política.* Bogotá: Facultad de Sociología. Universidad Nacional de Colombia.

Broadbent, S. (1965). *Investigaciones arqueológicas en el territorio chibcha.* Bogotá: Universidad de los Andes.

Brown, M., Hervé, G., Korte, M., & Genevey, A. (2021). Global archaeomagnetic data: the state of the art and future challenges. *Physics of the Earth and Planetary Interiors*. doi:https://doi.org/10.1016/j.pepi.2021.106766

Cai, S., Doctor, R., Tauxe, L., Hendrickson, M., Hua, Q., Leroy, S., & Phon, K. (2021). Archaeomagnetic results from Cambodia in Southeast Asia: evidence for possible low-latitude flux expulsion. *Proc. Natl. Acad. Sci. 118 (11).*

Cai, S., Tauxe, L., Wang, W., Deng, C., Pan, Y., Yang, L., & Qin, H. (2020). High-fidelity archeointensity results for the late Neolithic period from Central China. *Geophys. Res. Lett. 47* .

Calderón, G. (2016). Reporte Cerámica. In J. González, *Informe Final de Propuesta de Implementación de Plan de Manejo Arqueológico Subestación Nueva Esperanza. Soacha, Cundinamarca. TOMO II* (pp. 24-30). Bogotá: INGETEC - EPM.

Campuzano, S. A., Gómez Paccard, M., Pavón Carrasco, F. J., & Osete, M. L. (2019). Emergence and evolution of the South Atlantic Anomaly revealed by the new paleomagnetic reconstruction SHAWQ2k. *Earth and Planetary Science Letters, 512*, 17-26.

Cejudo, R., Goguitchaichvili, A., Montejo, F., García Ruiz, R., Botiva, A., & Morales, J. (2019). First archaeomagnetic results from Colombia (the Bogotá Savanna Pre-Hispanic sites): Implications for the Caribbean absolute geomagnetic intensity variation curve. *Journal of Archaeological Science: Reports 26*, 1-8.

De Marco, E. (2007). *Complete magnetic and archaeomagnetic measurements in archaeological sites: contribution to the construction of the secular variation curves for Greece.* Thessaloniki: PhD Thesis.

Di Chiara, A. (2020). Palaeosecular variations of the geomagnetic field in Africa during the Holocene: a review. *Geol. Soc. Lond., Spec. Publ. 497*, 127–141.

English Heritage. (2006). *Archaeomagnetic Dating. Guidelines on producing and interpreting archaeomagnetic dates.* English Heritage Publishing.

Fajardo, S. (2011). *Jerarquía social de una comunidad en el valle de Leiva: unidades domésticas y agencia entre los siglos XI y XVII.* Bogotá: Instituto Colombiano de Antropología e Historia.

Fajardo, S. (2016). *Prehispanic and Colonial settlement patterns of the Sogamoso Valley.* Pittburgh: University of Pittsburgh.

Fernández, M. O. (2009). *Descripción Petrográfica de Cuatro Muestras: Dos de Cerámica (Te-09-2009-I-01 y Te-10-2009-I-01), Una de Roca (Te-09-2009-I-02) y una de Arcilla (Te-09-2009-I-03), del Piso Cultural de Sociedades del Arcaico y Muisca de*

la Sabana de Bogotá (Municipios de . Bogotá: Laboratorio de Ciencias Naturales, Facultad de Estudios de Patrimonio Cultural, Universidad Externado de Colombia. Manuscrito sin publicar.

Gallet, Y., Molist, M., Genevey, A., Clop Garcia, X., Thébault, E., Gómez Bach, A., & Le. (2015). New late Neolithic (c. 7000–5000 BC) archeointensity data from Syria. Reconstructing 9000 years of archeomagnetic field intensity variations in the Middle East. *Phys. Earth planet. Inter. 238*, 89–103.

Gamboa, J. A. (2013). *El cacicazgo muisca en los años posteriores a la Conquista: del psihipqua al cacique colonial, 1537-1575.* Bogotá D.C.: Instituto Colombiano de Antropología e Historia -ICANH-.

García, R., Pérez-Rodríguez, N., Goguitchaichvili, A., Rodríguez Ceja, M., & Morales, J. (2021). On the absolute geomagnetic intensity fluctuations in Mexico over the last three millennia. *South American Earth Sciences, 106*. doi:https://doi.org/10.1016/j.jsames.2020.102927

GEOMAGIA50. (2021, January 22). *GEOMAGIA50 database*. Retrieved August 1, 2021, from GEOMAGIA50 database: https://geomagia.gfz-potsdam.de/models.php

Goguitchaichvili, A., Greco, C., Garcia Ruiz, R., Pereyra Domingorena, L., Cejudo, R., Morales, J., . . . Tarragó, M. (2019). First archaeointensity reference paleosecular variation curve for South America and its implications for geomagnetism. *Quaternary Research 92*, 81–97.

Goguitchaichvili, A., Hernandez, E., Garcia, R., Cejudo, R., Cifuentes, G., & Cervantes, M. (2020). Fluctuation of the Earth's magnetic field elements in Mexico revealed by archive documents since 1587. *Physics of the Earth and Planetary Interiors, 300*. doi:doi:10.1016/j.pepi.2020.106433

Goguitchaichvili, A., Morales, J., Schavelzon, D., Vásquez, C., Gogorza, C. S., Loponte, D., & Rapalini, A. (2015). Variation of the Earth's magnetic field strength in South America during the last two millennia: New results from historical buildings of Buenos Aires and re-evaluation of regional data. *Physics of the Earth and Planetary Interiors, 245*, 15–25. doi:doi:10.1016/j.pepi.2015.05.006

Goguitchaichvili, A., Ruiz, R. G., Pavón-Carrasco, F. J., Contreras, J. J., Arechalde, A. M., & Urrutia-Fucugauchi, J. (2018). Last three millennia Earth's Magnetic field strength in Mesoamerica and southern United States: Implications in geomagnetism and archaeology. *Physics of the Earth and Planetary Interiors, 279*, 79–91. doi:doi:10.1016/j.pepi.2018.04.003

Gómez-Paccard, M., & Pavón Carrasco, F. (2018a). Archaeointensity. In S. López Varela, *The Encyclopedia of Archaeological Sciences* (pp. 1-4). Wiley-Blackwell.

Gómez-Paccard, M., & Pavón Carrasco, F. (2018b). Archaeomagnetism. In S. López Varela, *The Encyclopedia of Archaeological Sciences* (pp. 78-82). Wiley-Blackwell.

Gomez-Paccard, M., Chauvin, A., Lanos, P., Thiriot, J., & Jiménez-Castillo, P. (2006). Archeomagnetic study of seven contemporaneous kilns from Murcia (Spain). *Physics of the Earth and Planetary Interiors 157*, 16–32.

González, J. (2016a). Cronología del sitio Nueva Esperanza. En J. González, *Informe Final de Propuesta de Implementación de Plan de Manejo Arqueológico Subestación Nueva Esperanza. Soacha, Cundinamarca. TOMO II* (págs. 3-22). Bogotá: INGETEC - EPM.

González, J. (2016b). *Informe Final de Propuesta de Implementación de Plan de Manejo Arqueológico Subestación Nueva Esperanza. Soacha, Cundinamarca. TOMO II.* Bogotá: INGETEC - EPM.

González, J. (2016c). *Informe Final de Propuesta de Implementación de Plan de Manejo Arqueológico Subestación Nueva Esperanza. Soacha, Cundinamarca. TOMO I.* Bogotá: INGETEC - EPM.

Gosselain, O. P. (1992). Bonfire of the enquiries. Pottery firing temperatures in archaeology: What for? *Journal of Archaeological Science, 19(3)*, 243–259.

Haury, E., & Cubillos, J. (1953). nvestigaciones arqueológicas en la Sabana de Bogotá, Colombia (cultura chibcha). *Social Science Bulletin No. 22.*, 5-104.

Henderson, H., & Ostler, N. (2009). Organización de asentamiento muisca y autoridad cacical en Suta, valle de Leyva, Colombia: una evaluación crítica de los conceptos nativos sobre la casa para el estudio de sociedades complejas. En C. Sánchez, *Economía, prestigio y poder: perspectivas desde la arqueología* (págs. 74-146). Bogotá: Instituto Colombiano de Antropología e Historia.

Herrero Bervera, E., Athens, S., Tema, E., Alva Valdivia, L. M., Camps, P., & Trejo, A. R. (2020). First archaeointensity results from Ecuador with rock magnetic analyses and 14C dates to constrain the geomagnetic field evolution in South America: Enhancing the knowledge of geomagnetic field intensity. *Journal of South American Earth Sciences 103 (2020)*, 1-18. doi:https://doi.org/10.1016/j.jsames.2020.102733

Hervé, G., Perrin, M., Alva-Valdivia, L., Madingou Tchibinda, B., Rodríguez-Trejo, A., . . . Meza Rodríguez, C. (2019). Critical analysis of the Holocene palaeointensity database in Central America: Impact on geomagnetic modellin. *Physics of the Earth and Planetary Interiors 289*, 1-10.

Jones, S. A., Tauxe, L., Blinman, E., & Genevey, A. (2020). Archeointensity of the four corners region of the American southwest. *Geochemistry, Geophysics, Geosystems, 21*. doi:https://doi.org/10.1029/2018GC007509

Kondopoulou, D., Gómez-Paccard, M., Aidona, E., Rathossi, C. C., Tema, E., Efthimiadis, K., & Polymeris, G. (2017). Investigating the archaeointensity determination success of prehistoric ceramics through a multidisciplinary approach: new and re-

evaluated data from Greek collections. *Geophysical Journal International 210*, 1450–1471.

Kruschek, M. (2003). *The evolution of the Bogotá chiefdom: a household view.* Pittsburgh: University of Pittsburgh.

Langebaek, C. (1987). *Mercados, poblamiento e integración étnica entre los Muiscas: siglo XVI.* Bogotá D.C.: Banco de la República.

Langebaek, C. (1995). *Arqueología Regional en el Territorio Muisca. Estudio de los Valles de Fúquene y Susa.* Pittsburgh: University of Pittsburgh.

Langebaek, C. (2003). *Arqueología colombiana: Ciencia, pasado y exclusión.* Bogotá: Instituto colombiano para el desarrollo de la Ciencia y la Tecnología Francisco José de Caldas.

Langebaek, C. (2012). *Vivir y morir en Tibanica: reflexiones sobre el poder político en una comunidad muisca de la Sabana de Bogotá.* Bogotá: Compilación sin editar.

Langebaek, C. (2019). *Los Muiscas. La historia milenaria de un pueblo chibcha.* Bogotá D.C.: Penguin Random House.

Langebaek, C., Cuellas, A., Dever, A., Barragan, A., Salamanca, M., Álvarez, J., & García, E. (2001). *Arqueología regional en el Valle de Leiva: ocupación humana en una región de los Andes Orientales de Colombia.* Bogotá: Informes Arqueológicos del Instituto Colombiano de Antropología e Historia.

LeGoff, M., Daly, L., Dunlop, D., & Papusoi, C. (2006). Emile Thellier (1904-1987), a pioneer in studiesof the "fossil" Earth's magnetic field. *Historical events and people in aeronomy, geomagnetism and solar-terrestrial physics*, 98-112.

Livingstone Smith, A. (2001). Bonfire II: The Return of Pottery Firing Temperatures. *Journal of Archaeological Science, 28(9)*, 991–1003.

Lizcano, L. (2016). Análisis de los materiales cerámicos. En F. Romano, *Estudio Arqueológico y de Internvención de los Bienes Culturales para realizar el rescate en el sitio de terreno dónde se ubicarán las futuras bahías y banco de reactores* (págs. 45-71). Bogotá: INGETEC - EEB.

Mahgoub, A. N., Juárez-Arriaga, E., Böhnel, H., Manzanilla, L. R., & Cyphers, A. (2019b). Refined 3600 years palaeointensity curve for Mexico. *Physics of the Earth and Planetary Interiors 296*, 1-16. doi:doi:10.1016/j.pepi.2019.106328

Mahgoub, A., Juárez, E., Böhnel, H., Siebe, C., & Pavón-Carrasco, F. (2019a). Late-Quaternary secular variation data from Mexican volcanoes. *Earth and Planetary Science Letters 519*, 28-39. doi:https://doi.org/10.1016/j.epsl.2019.05.001

Noll, W., & Heimann, R. (2016). *Ancient Old World Pottery. Materials, Technology and Decoration* . Stuttgart: Schweizerbart Science Publisher.

Obregón, M., Ramírez Luna, A., Goguitchaichvili, A., Cejudo, R., Morales, J., Cervantes Solano, M., & Greco, C. (2019). Termoluminiscencia VS. Arqueomagnetismo: Datación absoluta de fragmentos cerámicos prehispánicos de los Andes Noroccidentales (Piedras Blancas, Medellín, Colombia). *Arqueología Iberoamericana 42*, 42-49.

Paepe, P., & Cardale, M. (1990). Resultados de un estudio petrológico de cerámicas del período Herrera, provenientes de la Sabana de Bogotá y sus implicaciones arqueológicas. *Boletín Museo del Oro (27)*, 99-119.

Patiño, A. (2005). *Intercambios de cerámica foránea entre los grupos muiscas de la Sabana de Bogotá: el caso de Chía.* Bogotá: Investigación sin editar.

Pavón-Carrasco, F. J., Osete, M. L., Torta, J. M., & De Santis, A. (2014). A geomagnetic field model for the Holocene based on archaeomagnetic and lava flow data. *Earth and Planetary Science Letters, 388*, 98–109. doi:doi:10.1016/j.epsl.2013.11.046

Portilla-Mendoza, K., Pinzón-Núñez, D., Moreno-González, L., Mier-Umaña, R., Ríos-Reyes, C., & Henao-Martínez, J. (2020). Archaeometry study of the mineral and chemical composition of pre-Hispanic pottery from "Los Teres", Mesa de Los Santos (Colombia). *Memorias: Revista Digital de Historia y Arqueología desde el Caribe colombiano (septiembre - diciembre)*, 7-43.

Quinn, P. S. (2013). *Ceramic Petrography. The Interpretation of Archaeological Pottery & Related Artifacts in Thin Sections.* Oxford: Archaeopress.

Rada, M., Contanzo-Álvarez, V., Aldana, M., Suárez, N., Campos, C., Mackowiak-Antczak, M., & Brandt, M. (2011). Rock magnetic, petrographic and dielectric characterization of prehistoric Amerindian potsherds from Venezuela. *Studia Geophysica et Geodaetica, 55*, 717-736.

Reichel-Dolmatoff, G. (1986). *Arqueología de Colombia. Un texto introductorio.* Bogotá: Biblioteca Familiar. Presidencia de la República.

Rivas Estrada, S. (2021). *Implementación de plan de manejo arqueológico para el rescate y monitoreo del sitio subestación Nueva Esperanza en el marco del proyecto segundo refuerzo de red del área oriental línea de transmisión La Virginia, Nueva Esperanza a 500 Kv.* Bogotá: Transmisora Colombiana de Energía S.A.S E.S.P.

Rojas, S., Cejudo, R., Marín, M., Hernández-Bernal, M., Goguitchaichvili, A., Morales, J., . . . Bautista, F. (2020). Estudio magnético y geoquímico de la cerámica prehispánica de la Depresión Momposina: Análisis arqueométricos en el Norte de Sudamérica. *Arqueología Iberoamericana 46*, 11-30.

Romano, F. (2003). *San Carlos: documento trayectorias evolutivas de la organización social de unidades domesticas en un cacicazgo de la Sabana de Bogotá, (Funza, Cundinamarca).* Bogotá: Boletín de Arqueología FIAN (18). Fondo de Investigaciones Arqueológicas Nacionales.

Romano, F. (2016). *Estudio Arqueológico y de Internvención de los Bienes Culturales para realizar el rescate en el sitio de terreno dónde se ubicarán las futuras bahías y banco de reactores.* Bogotá: INGETEC - EEB.

Salge, M. (2007). *Festejos muiscas en El Infiernito, valle de Leiva. Consolidación del poder social.* Bogotá: Universidad de los Andes.

Schnepp, E. (2018). Archaeomagnetic Dating of Baked Clay Features. En S. López Varela, *The Encyclopedia of Archaeological Sciences* (págs. 1-4). Wiley-Blackwell.

Shaar, R., Tauxe, L., Ron, H., Ebert, Y., Zuckerman, S., Finkelstein, I., & Agnon, A. (2016). Large geomagnetic field anomalies revealed in bronze to Iron age archeomagnetic data from Tel Megiddo and Tel Hazor. Israel. *Earth Planet. Sci. Lett. 442*, 173–185.

Silva Celis, E. (1981). Investigaciones arqueológicas en Villa de Leiva. *Boletín del Museo del Oro (10)*, 1-18.

Tarling, D. (1983). *Palaeomagnetism. Principles and Applications in Geology, Geophysics and Archaeology.* London: Chapman and Hall Ltd.

Thellier, E., & Thellier, O. (1959). Sur I'intensite du champ magnetique terrestre dans la passe historique et geologique. *Ann. Geophys., 15*, 285-376.

Therrien, M. (1996). Naciones, imperios y territories: historiografía arqueológica de la Sabana de Bogotá. En M. Therrien, & B. Enciso, *Compilación bibliográfica e informativa de datos arqueológicos de la Sabana de Bogotá: siglos VIII al XVI d.C.* (págs. 23-44). Bogotá: Instituto Colombiano de Antropología e Historia.

Tite, M. (2016). History of Scientific Research. In A. Hunt, *The Oxford Handbook of Archaeological Ceramic Analysis* (pp. 41-52). Oxford: Oxford University Press.

Turner, G., Kinger, R., McFadgen, B., & Gevers, M. (2020). The first archaeointensity records from New Zealand: evidence for a fifteenth century AD archaeomagnetic ‘spike’ in the SW Pacific region. *Geol. Soc. Lond., Spec. Publ. 497*, 47–72.

Appendices

- *Thellier-Thellier results from the specimens*

It is important to remark that the intensity shown in the Arai plot do not correspond to the final result. This is because this intensity is previous to the analysis and corrections. Even so, we present the graphs to show the linear behavior of the 24 specimens. For the final intensity, and the temperature range applied, check Table 5. The graphs were done with the ThellierTools 4.2 software.

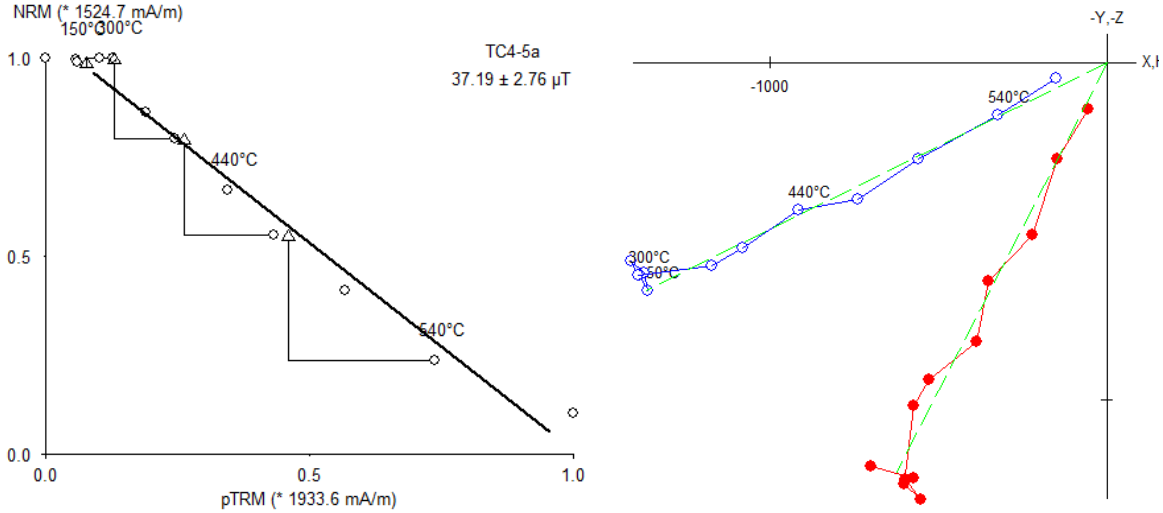

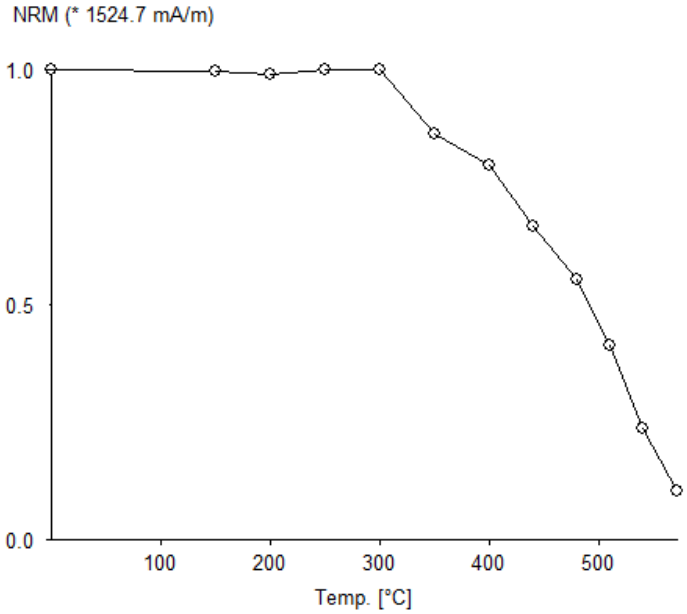

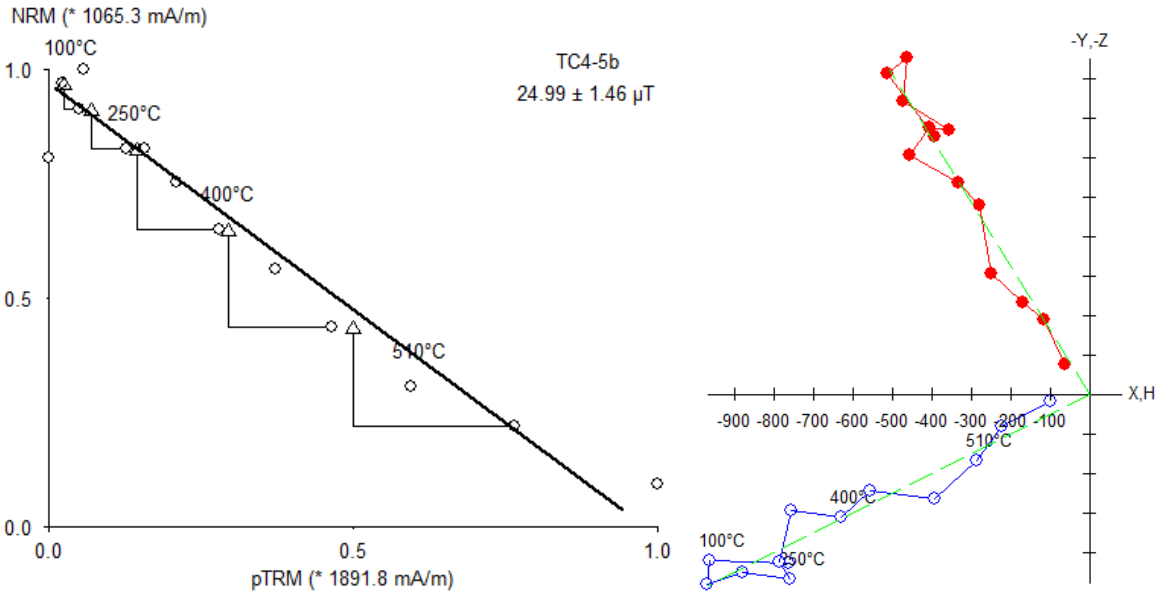
NRM (* 1065.3 mA/m)
100°C
250°C
400°C
510°C
1.0
0.5
0.0
0.0
0.5
1.0
pTRM (* 1891.8 mA/m)
TC4-5b
24.99 ± 1.46 µT
-Y,-Z
X,H
-900 -800 -700 -600 -500 -400 -300 -200 -100
510°C
400°C
100°C
250°C

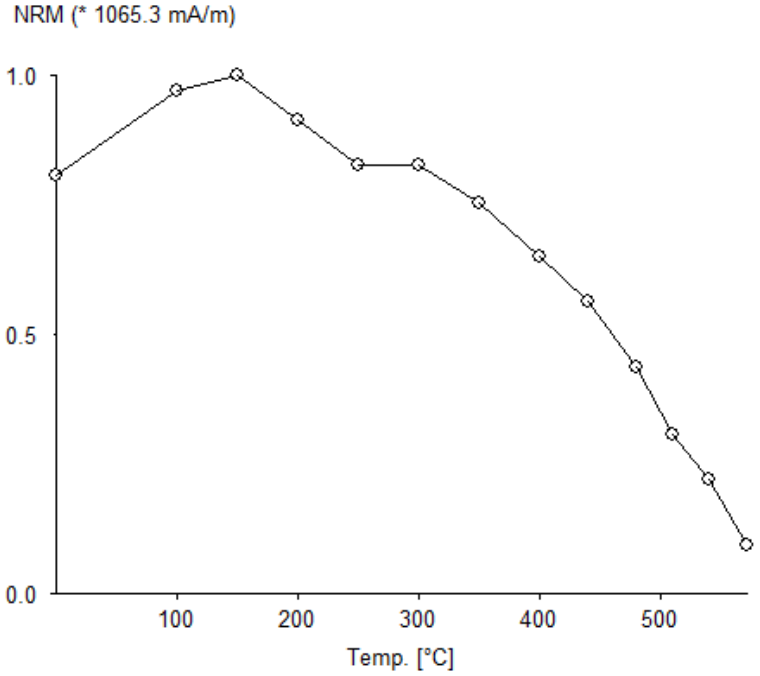
NRM (* 1065.3 mA/m)
1.0
0.5
0.0
100
200
300
400
500
Temp. [°C]

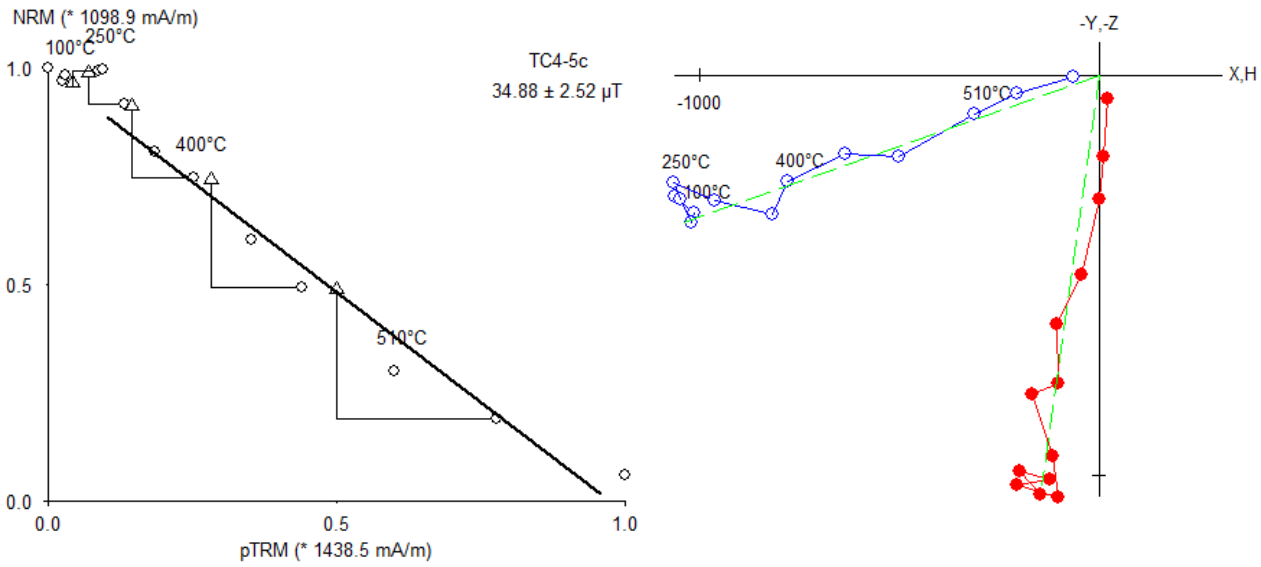
NRM (* 1098.9 mA/m)
100°C
250°C
400°C
510°C
1.0
0.5
0.0
0.0
0.5
1.0
pTRM (* 1438.5 mA/m)
TC4-5c
34.88 ± 2.52 µT
-Y,-Z
X,H
-1000
510°C
250°C
400°C
100°C

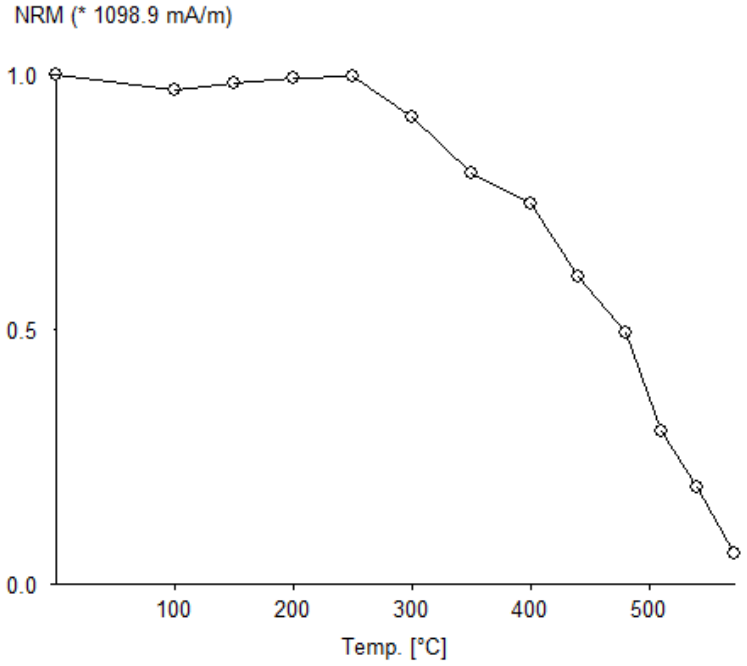
NRM (* 1098.9 mA/m)
1.0
0.5
0.0
100
200
300
400
500
Temp. [°C]

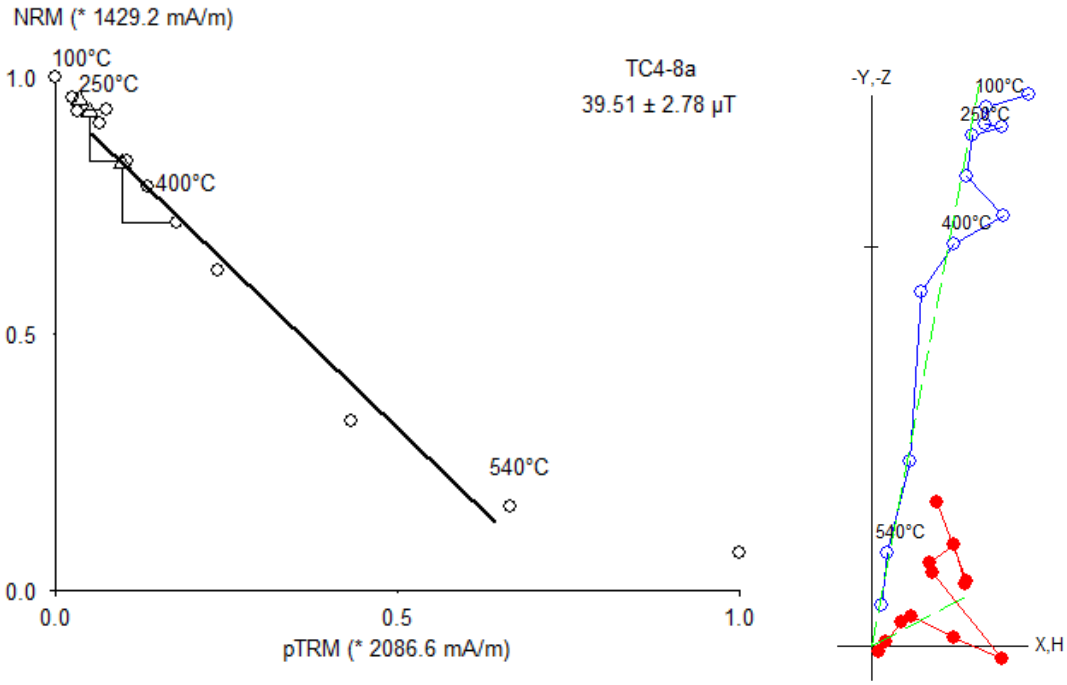
NRM (* 1429.2 mA/m)
100°C
250°C
400°C
540°C
1.0
0.5
0.0
0.0
0.5
1.0
pTRM (* 2086.6 mA/m)
TC4-8a
39.51 ± 2.78 µT
-Y,-Z
100°C
250°C
400°C
540°C
X,H

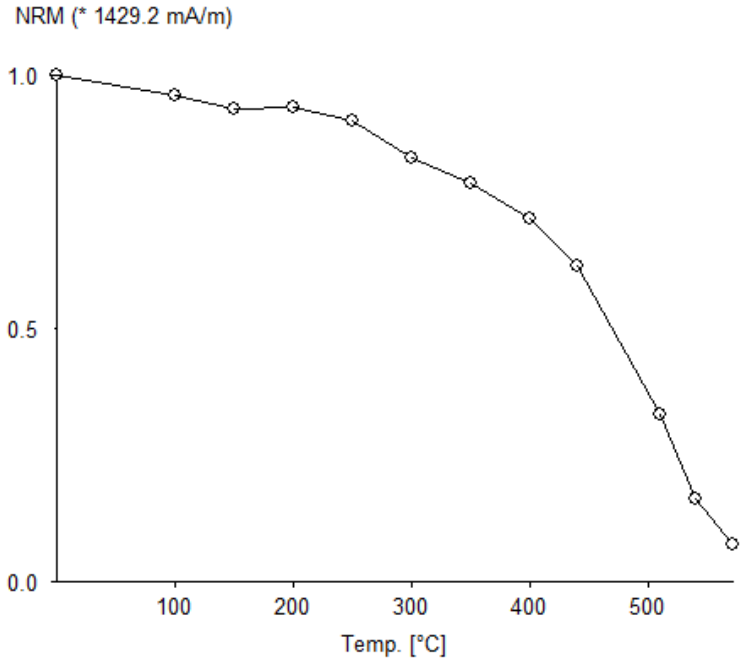
NRM (* 1429.2 mA/m)
1.0
0.5
0.0
100
200
300
400
500
Temp. [°C]

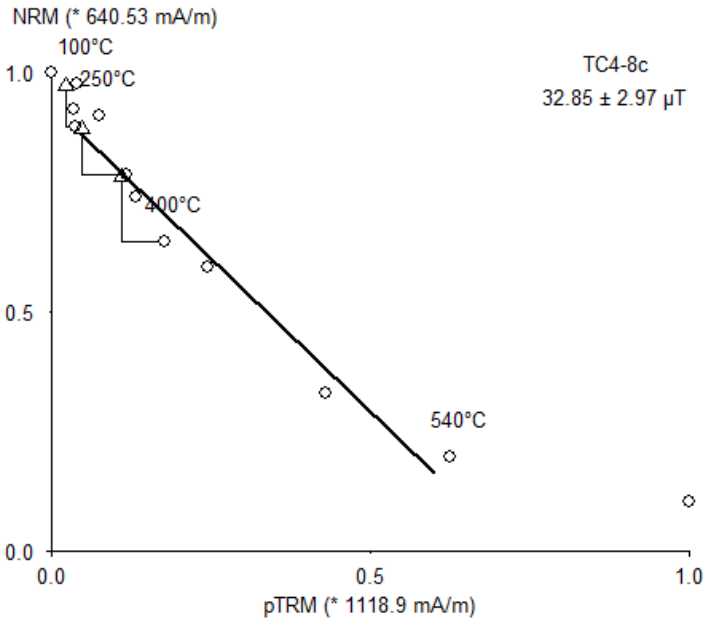

TC4-8c
32.85 ± 2.97 µT

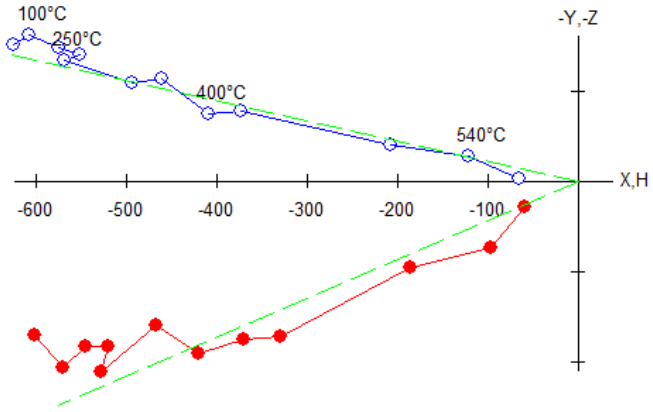

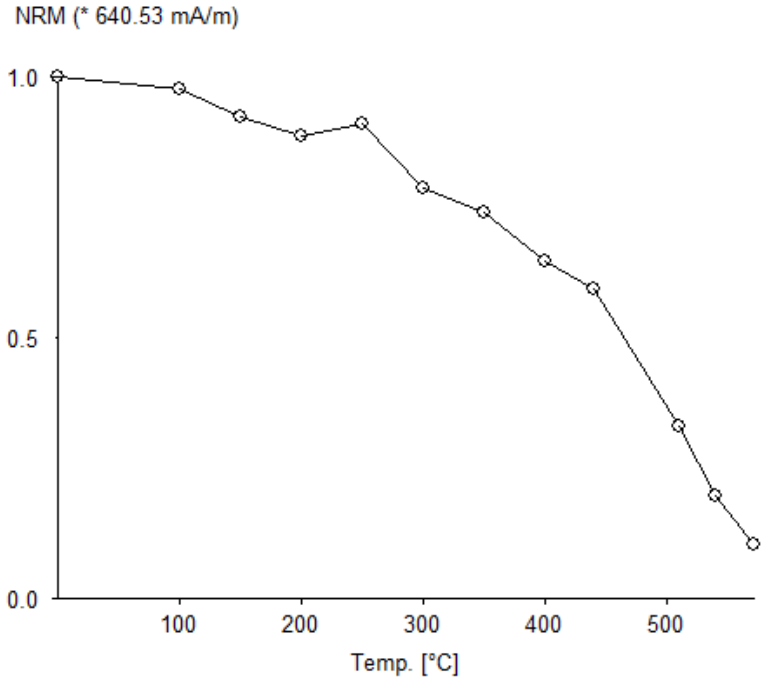

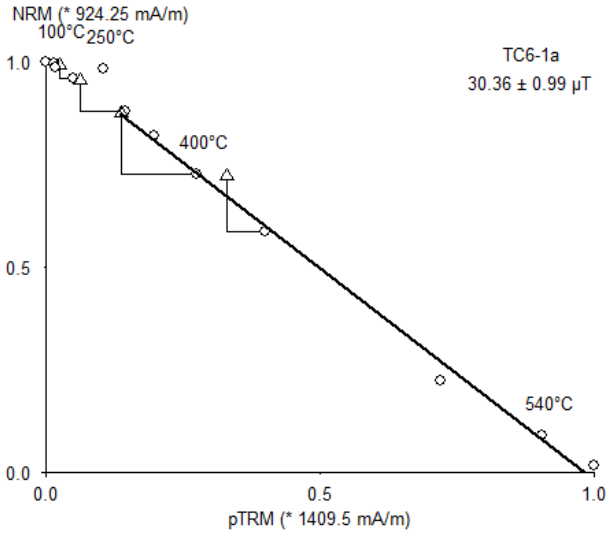
NRM (* 924.25 mA/m)
100°C 250°C
TC6-1a
30.36 ± 0.99 µT
400°C
540°C
1.0
0.5
0.0
0.0
0.5
1.0
pTRM (* 1409.5 mA/m)

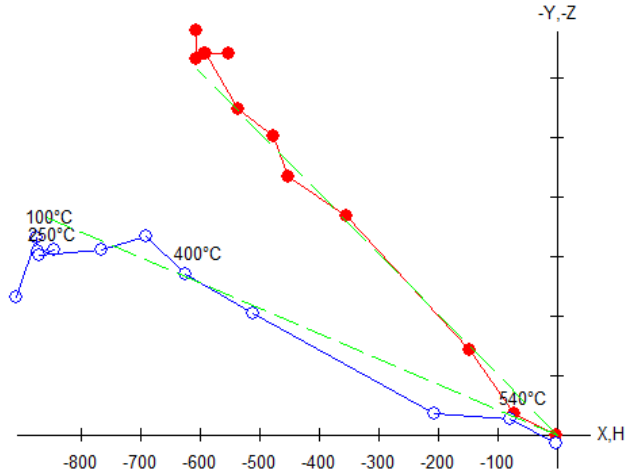
-Y,-Z
100°C
250°C
400°C
540°C
X,H
-800
-700
-600
-500
-400
-300
-200
-100

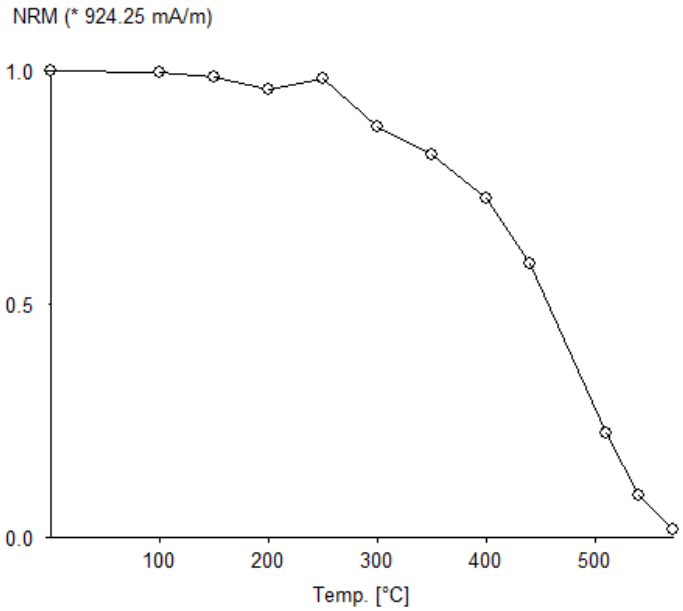
NRM (* 924.25 mA/m)
1.0
0.5
0.0
100
200
300
400
500
Temp. [°C]

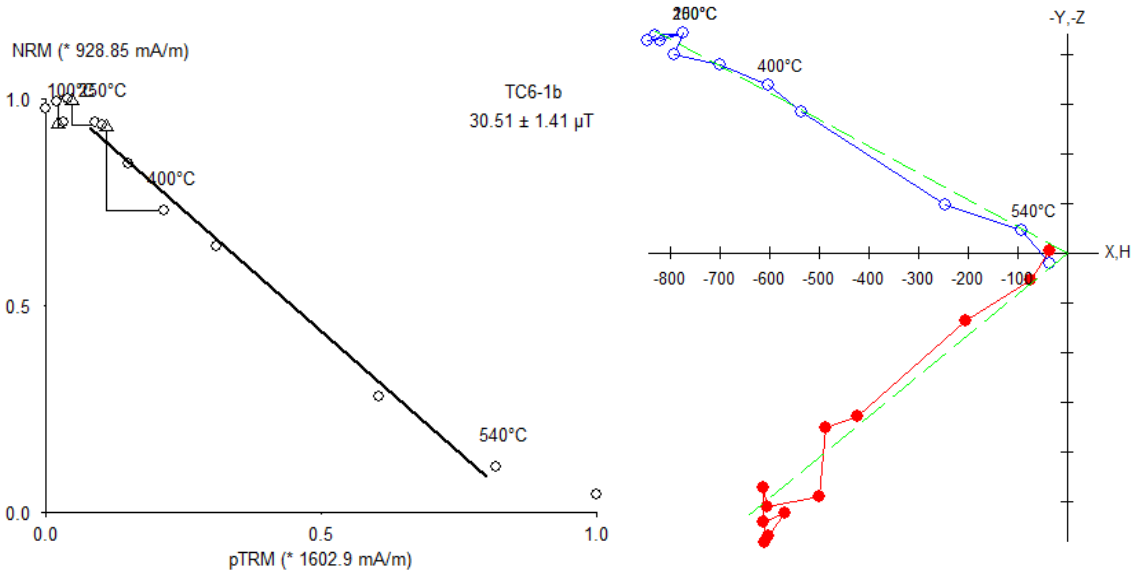
NRM (* 928.85 mA/m)
1.0
0.5
0.0
0.0
0.5
1.0
pTRM (* 1602.9 mA/m)
100°C
540°C
TC6-1b
30.51 ± 1.41 µT
400°C
540°C
-Y,-Z
X,H
-800
-700
-600
-500
-400
-300
-200

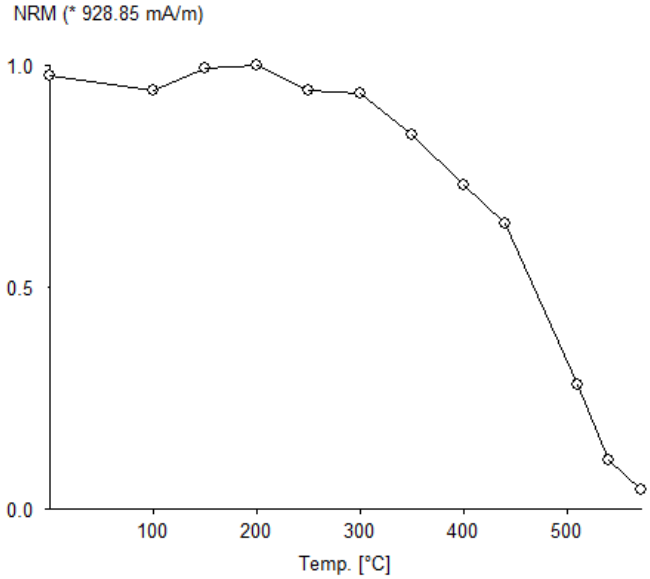
NRM (* 928.85 mA/m)
1.0
0.5
0.0
100
200
300
400
500
Temp. [°C]

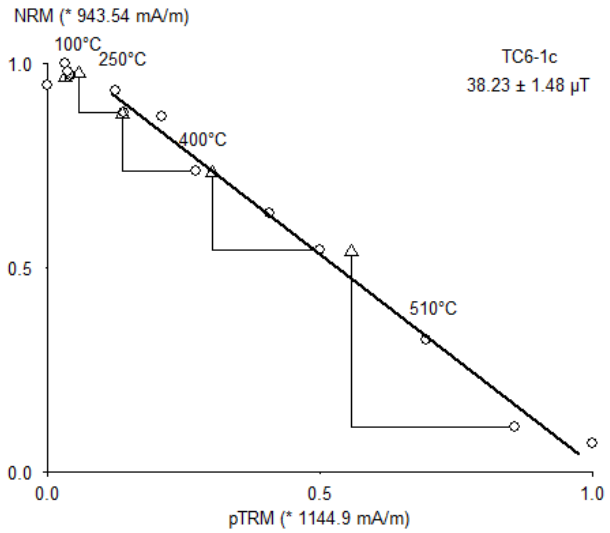
NRM (* 943.54 mA/m)
100°C
250°C
400°C
510°C
TC6-1c
38.23 ± 1.48 µT
1.0
0.5
0.0
0.0
0.5
1.0
pTRM (* 1144.9 mA/m)

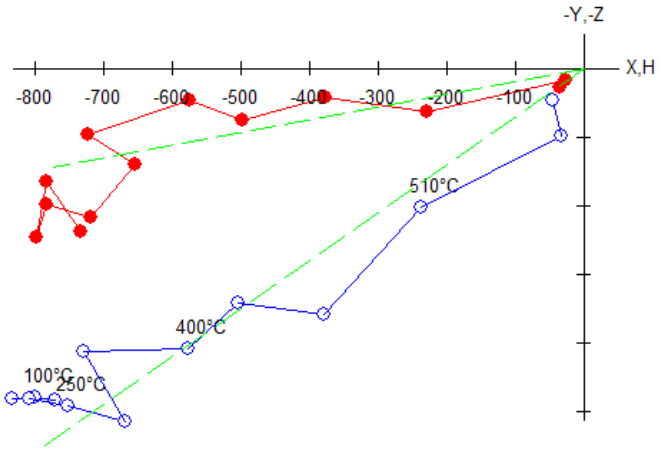
-Y,-Z
X,H
-800
-700
-600
-500
-400
-300
-200
-100
510°C
400°C
100°C
250°C

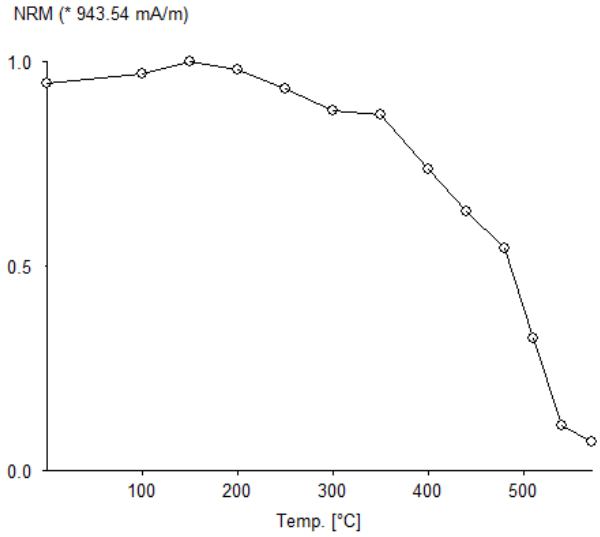
NRM (* 943.54 mA/m)
1.0
0.5
0.0
100
200
300
400
500
Temp. [°C]

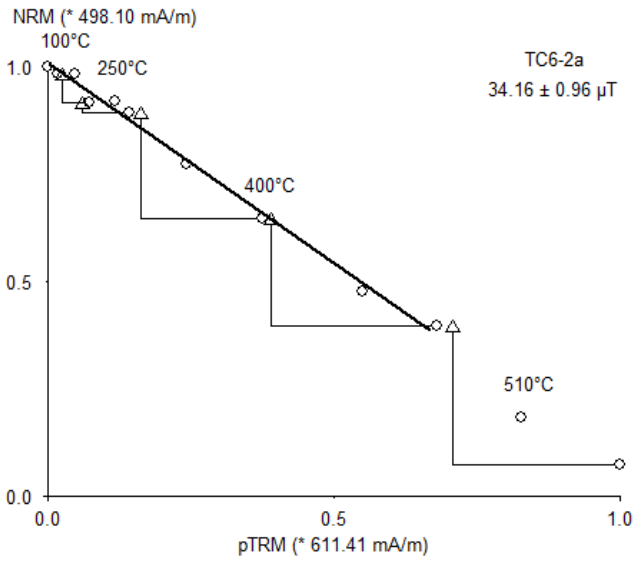
NRM (* 498.10 mA/m)
100°C
250°C
400°C
510°C
TC6-2a
34.16 ± 0.96 µT
1.0
0.5
0.0
0.0
0.5
1.0
pTRM (* 611.41 mA/m)

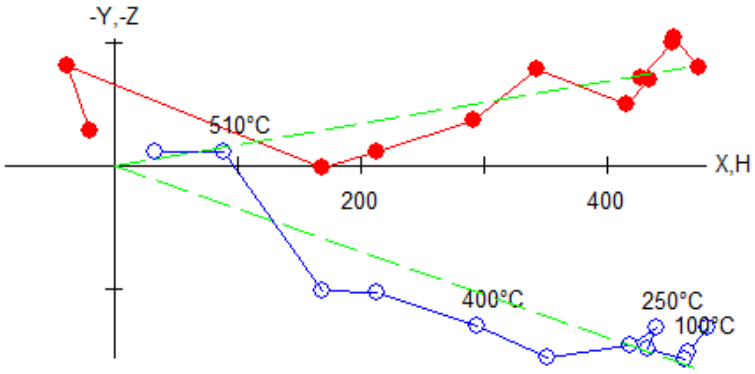
-Y,-Z
510°C
X,H
200
400
400°C
250°C
100°C

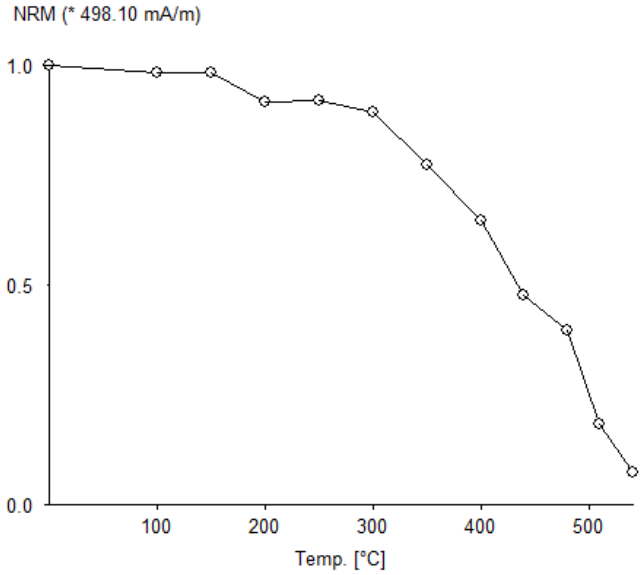
NRM (* 498.10 mA/m)
1.0
0.5
0.0
100
200
300
400
500
Temp. [°C]

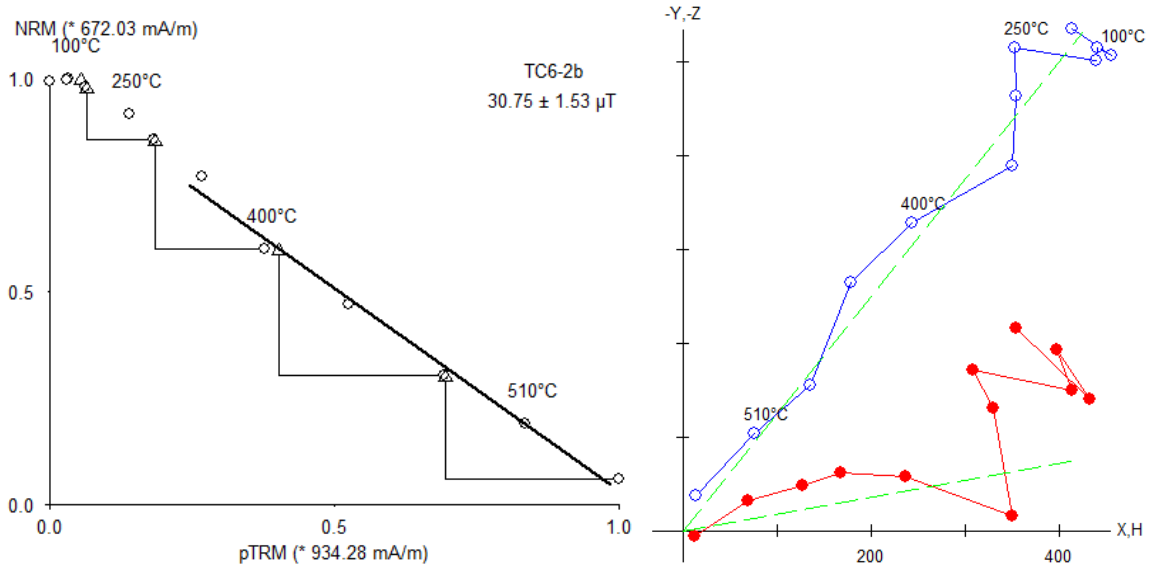
NRM (* 672.03 mA/m)
100°C
250°C
400°C
510°C
TC6-2b
30.75 ± 1.53 µT
1.0
0.5
0.0
0.0
0.5
1.0
pTRM (* 934.28 mA/m)
-Y,-Z
250°C
100°C
400°C
510°C
X,H
200
400

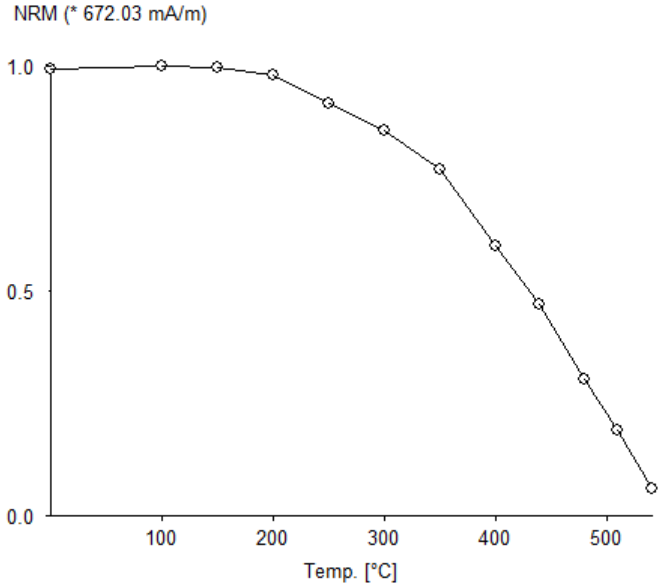
NRM (* 672.03 mA/m)
1.0
0.5
0.0
100
200
300
400
500
Temp. [°C]

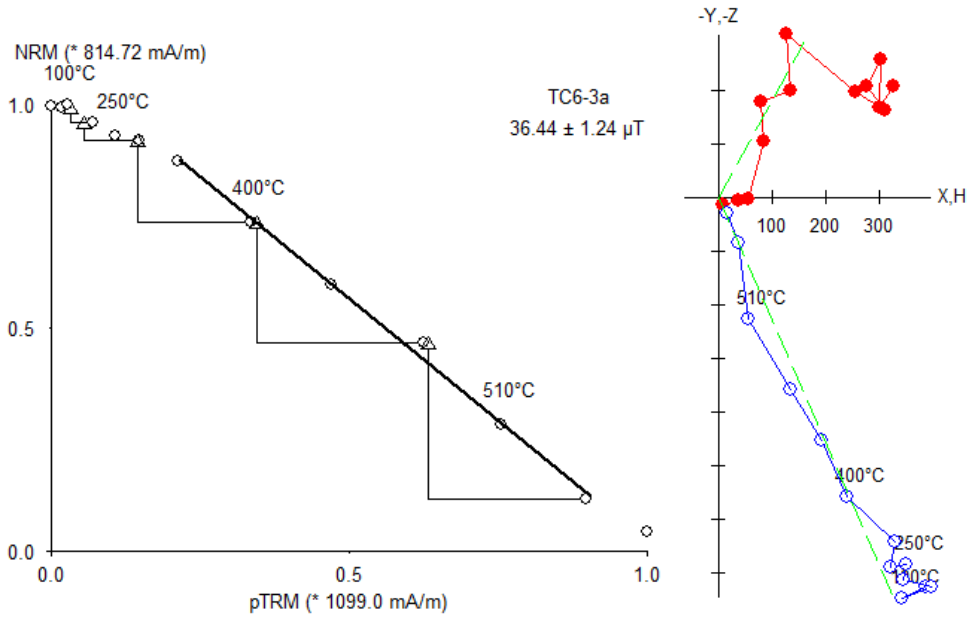
NRM (* 814.72 mA/m)
100°C
250°C
400°C
510°C
1.0
0.5
0.0
0.0
0.5
1.0
pTRM (* 1099.0 mA/m)
TC6-3a
36.44 ± 1.24 µT
-Y,-Z
X,H
100
200
300
510°C
400°C
250°C
100°C

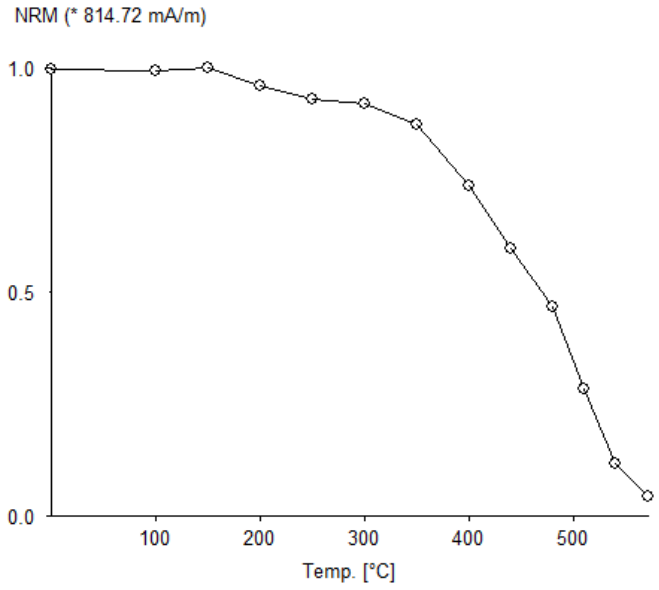
NRM (* 814.72 mA/m)
1.0
0.5
0.0
100
200
300
400
500
Temp. [°C]

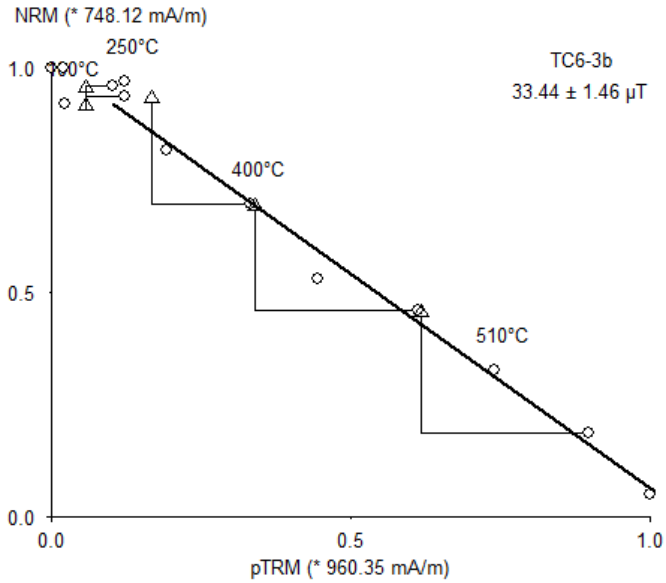
NRM (* 748.12 mA/m)
250°C
1.0
400°C
TC6-3b
33.44 ± 1.46 µT
0.5
510°C
0.0
0.0
0.5
1.0
pTRM (* 960.35 mA/m)

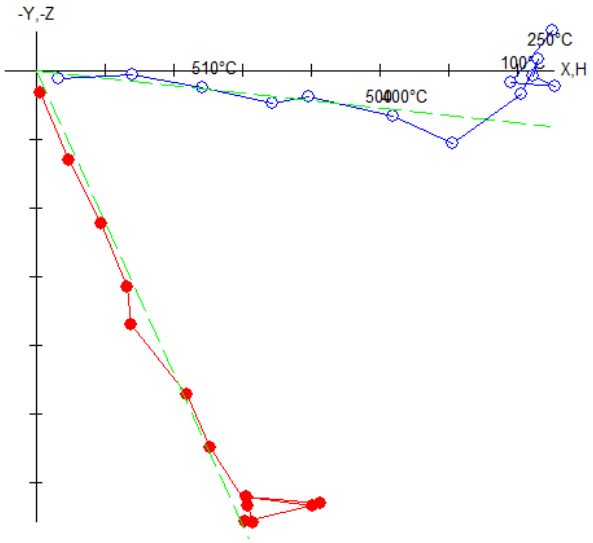
-Y,-Z
250°C
510°C
X,H
500°C

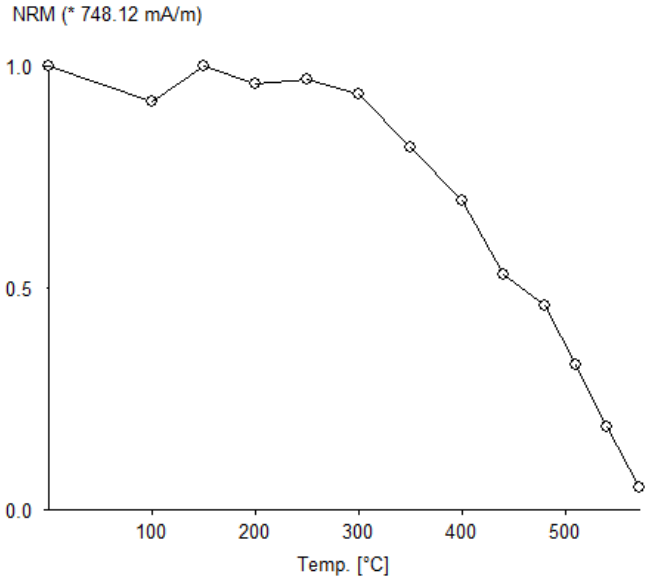
NRM (* 748.12 mA/m)
1.0
0.5
0.0
100
200
300
400
500
Temp. [°C]

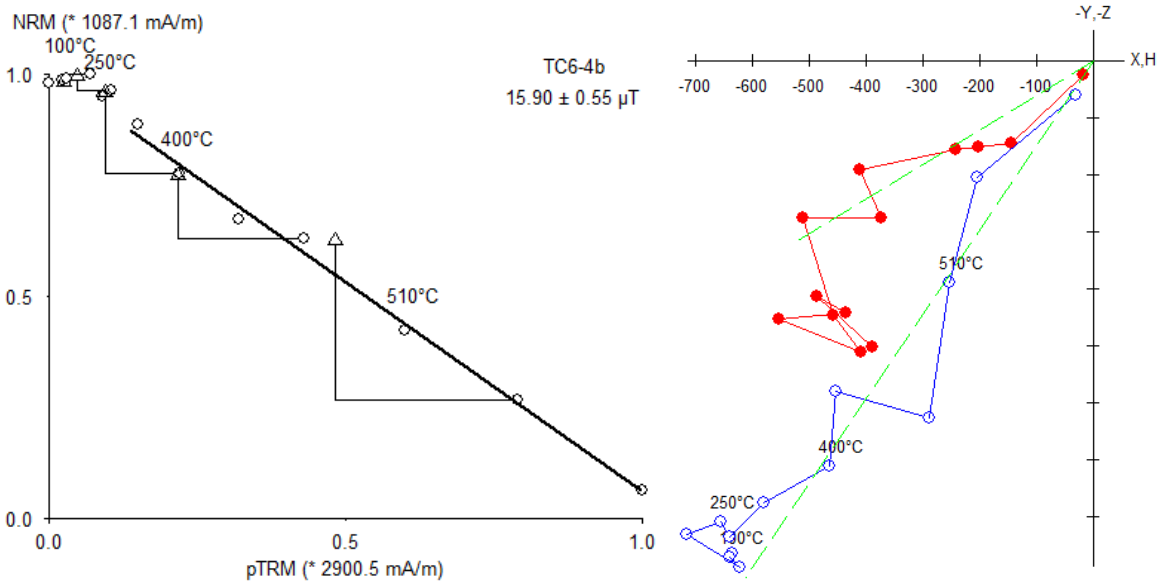
NRM (* 1087.1 mA/m)
100°C
250°C
400°C
510°C
1.0
0.5
0.0
0.0
0.5
1.0
pTRM (* 2900.5 mA/m)
TC6-4b
15.90 ± 0.55 µT
-Y,-Z
X,H
-700
-600
-500
-400
-300
-200
-100
510°C
400°C
250°C
100°C

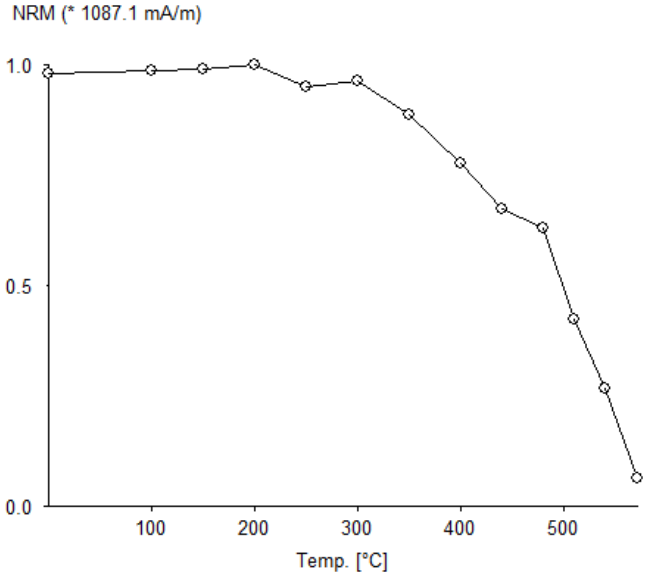
NRM (* 1087.1 mA/m)
1.0
0.5
0.0
100
200
300
400
500
Temp. [°C]

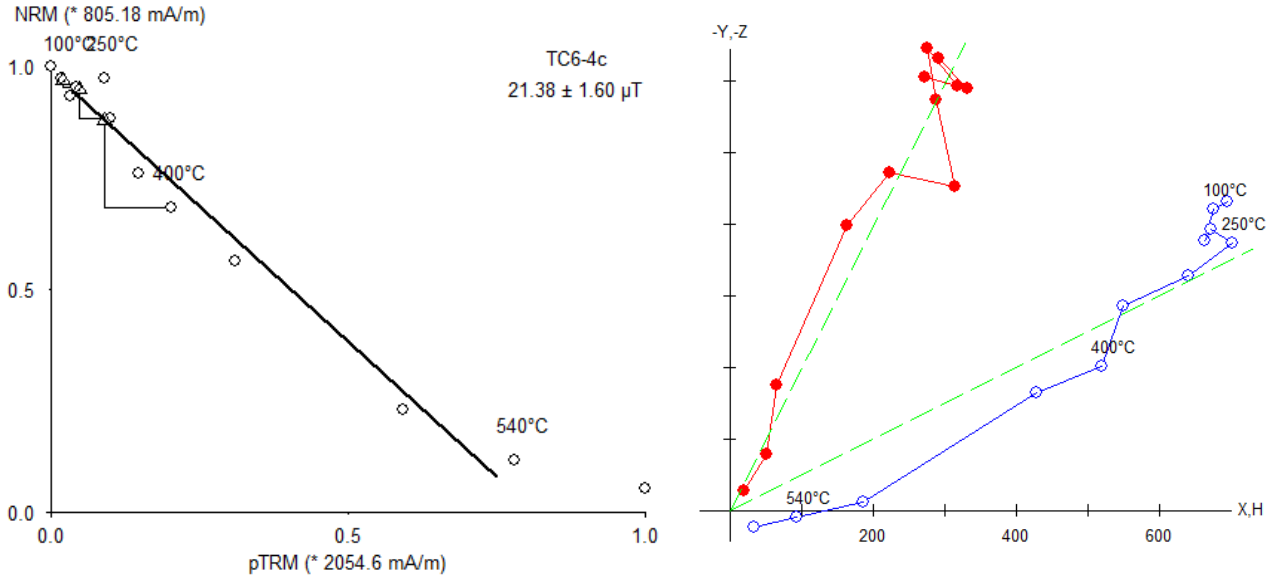
NRM (* 805.18 mA/m)
100°C
250°C
400°C
540°C
1.0
0.5
0.0
0.0
0.5
1.0
pTRM (* 2054.6 mA/m)
TC6-4c
21.38 ± 1.60 µT
-Y,-Z
100°C
250°C
400°C
540°C
X,H
200
400
600

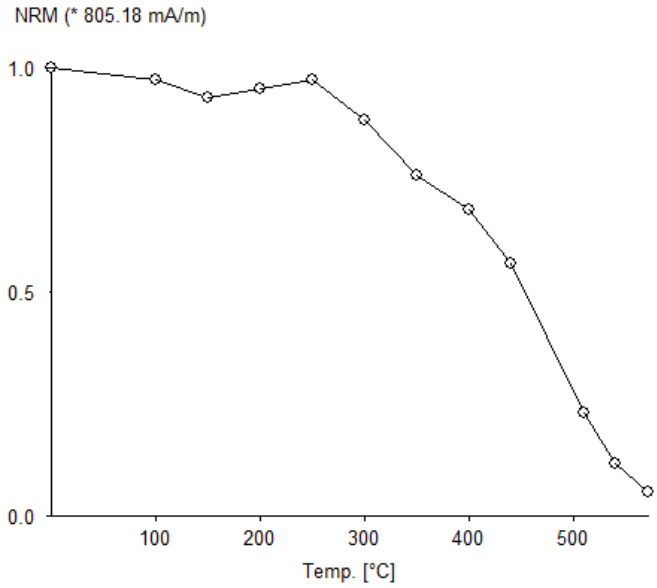
NRM (* 805.18 mA/m)
1.0
0.5
0.0
100
200
300
400
500
Temp. [°C]

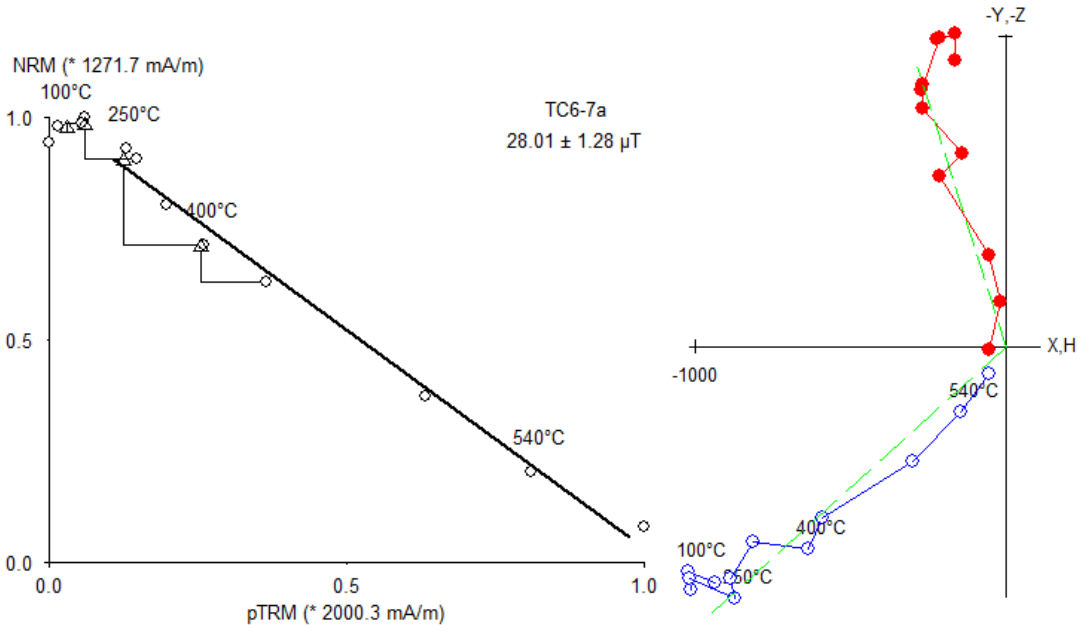
NRM (* 1271.7 mA/m)
100°C
250°C
400°C
540°C
1.0
0.5
0.0
0.0
0.5
1.0
pTRM (* 2000.3 mA/m)
TC6-7a
28.01 ± 1.28 µT
-Y,-Z
X,H
-1000
540°C
400°C
100°C
250°C

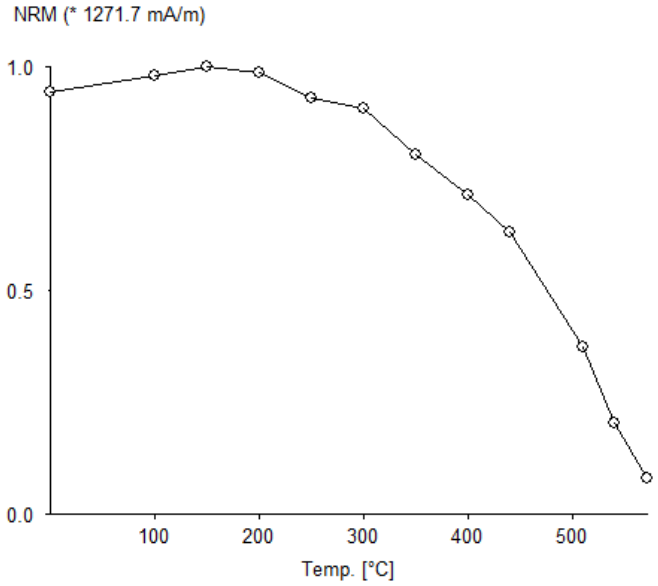
NRM (* 1271.7 mA/m)
1.0
0.5
0.0
100
200
300
400
500
Temp. [°C]

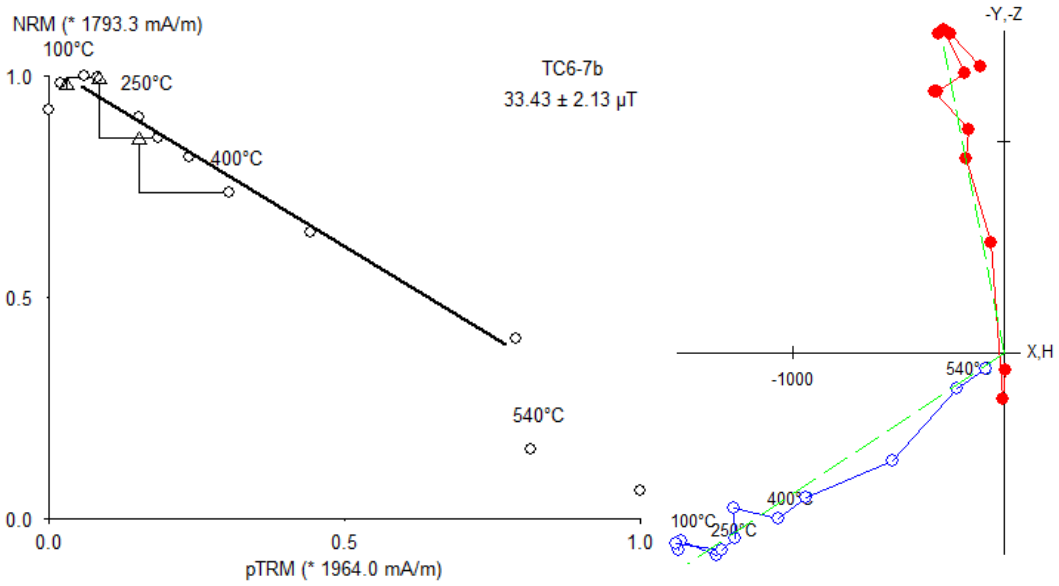
NRM (* 1793.3 mA/m)
100°C
250°C
400°C
540°C
1.0
0.5
0.0
0.0
0.5
1.0
pTRM (* 1964.0 mA/m)
TC6-7b
33.43 ± 2.13 µT
-Y,-Z
X,H
-1000
540°C
400°C
100°C
250°C

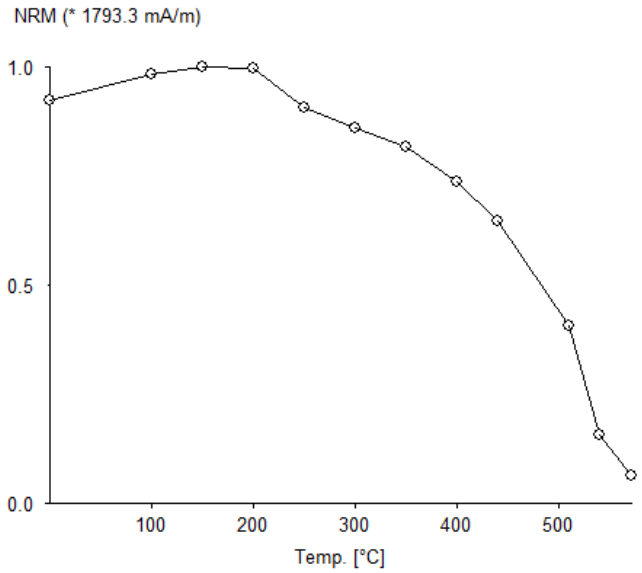
NRM (* 1793.3 mA/m)
1.0
0.5
0.0
100
200
300
400
500
Temp. [°C]

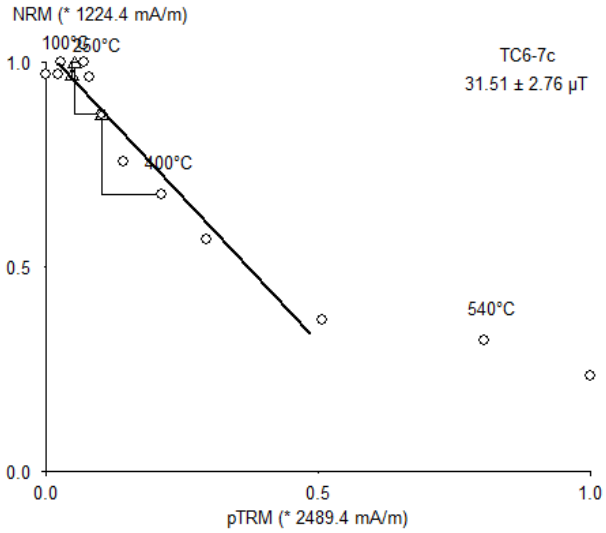

TC6-7c
31.51 ± 2.76 µT

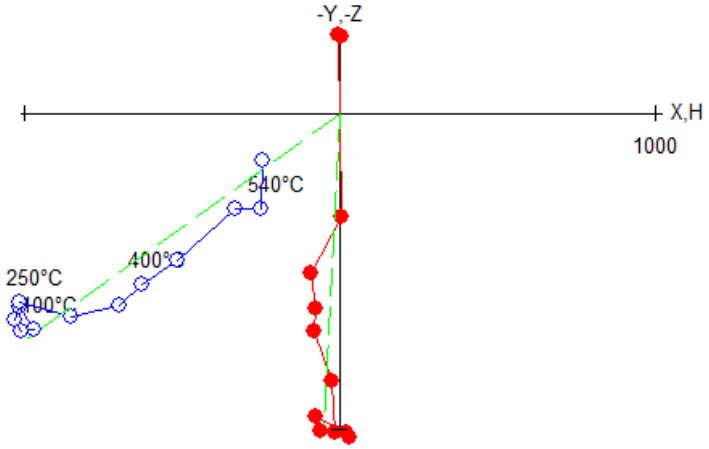

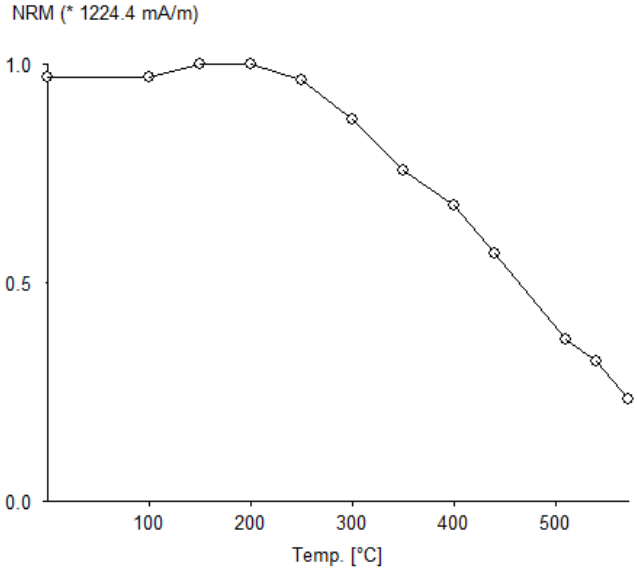

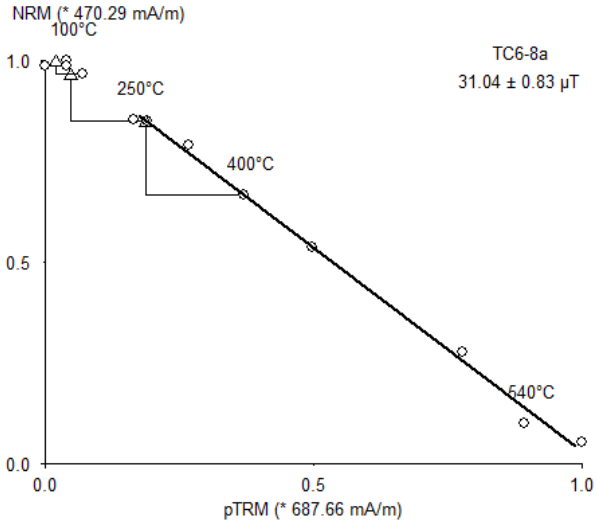
NRM (* 470.29 mA/m)
100°C
250°C
400°C
540°C
TC6-8a
31.04 ± 0.83 µT
1.0
0.5
0.0
0.0
0.5
1.0
pTRM (* 687.66 mA/m)

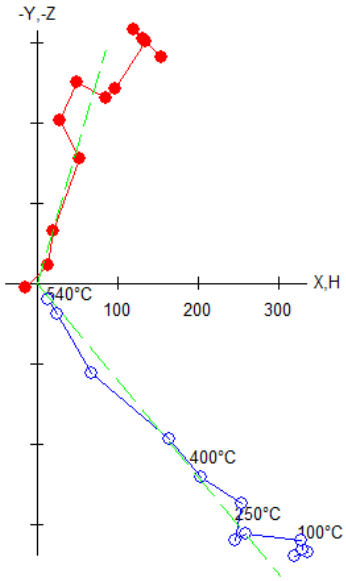
-Y,-Z
X,H
540°C
100
200
300
400°C
250°C
100°C

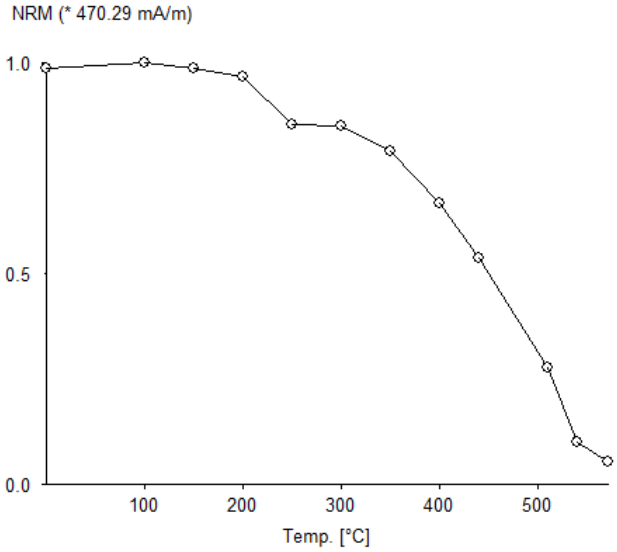
NRM (* 470.29 mA/m)
1.0
0.5
0.0
100
200
300
400
500
Temp. [°C]

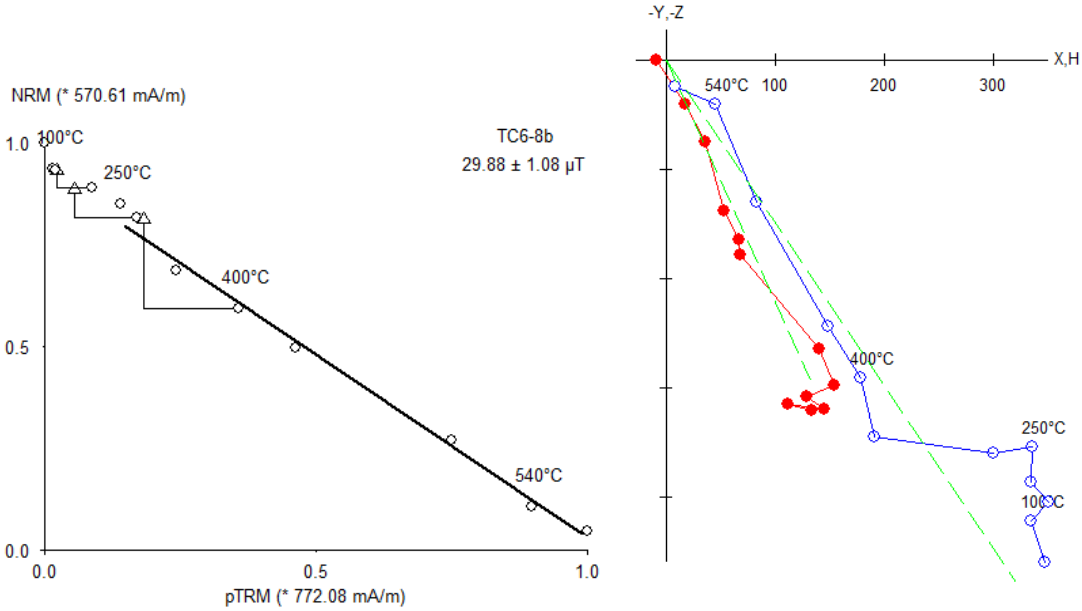
NRM (* 570.61 mA/m)
1.0
0.5
0.0
100°C
250°C
400°C
540°C
TC6-8b
29.88 ± 1.08 µT
0.0
0.5
1.0
pTRM (* 772.08 mA/m)
-Y,-Z
X,H
540°C
100
200
300
400°C
250°C
100°C

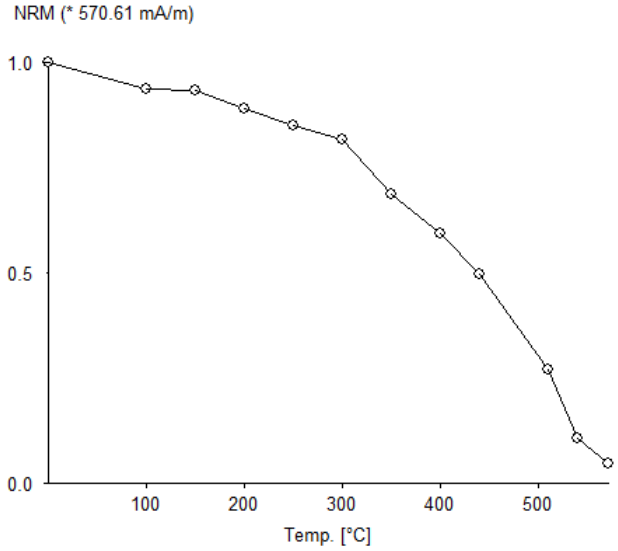
NRM (* 570.61 mA/m)
1.0
0.5
0.0
100
200
300
400
500
Temp. [°C]

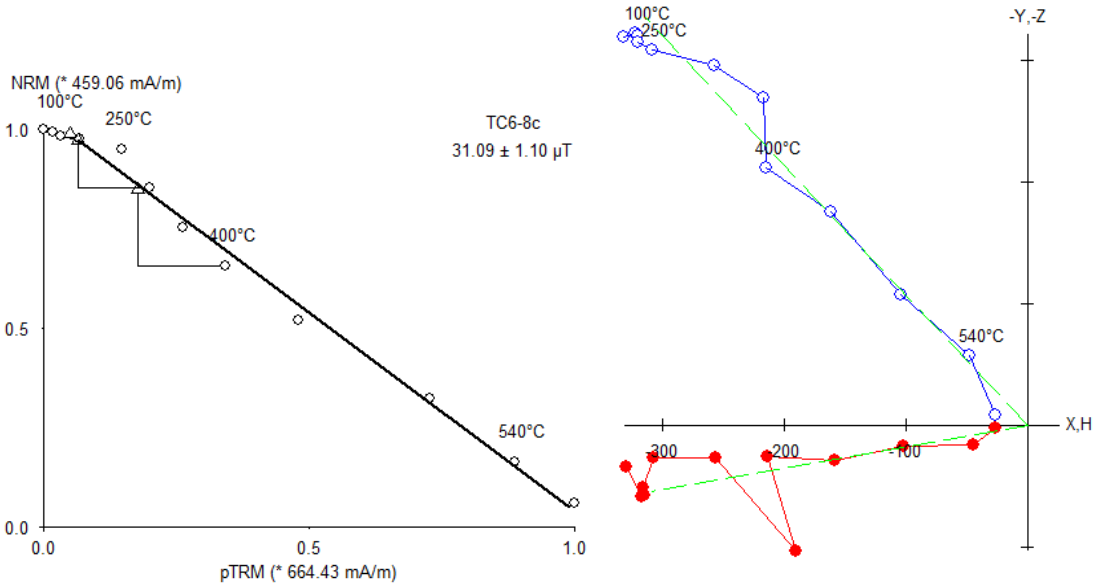
NRM (* 459.06 mA/m)
100°C
250°C
400°C
540°C
1.0
0.5
0.0
0.0
0.5
1.0
pTRM (* 664.43 mA/m)
TC6-8c
31.09 ± 1.10 µT
100°C
250°C
400°C
540°C
-Y,-Z
X,H
300
200
100

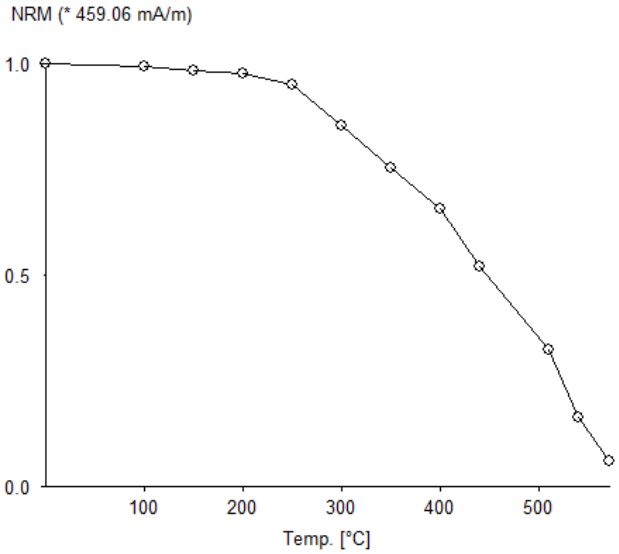
NRM (* 459.06 mA/m)
1.0
0.5
0.0
100
200
300
400
500
Temp. [°C]

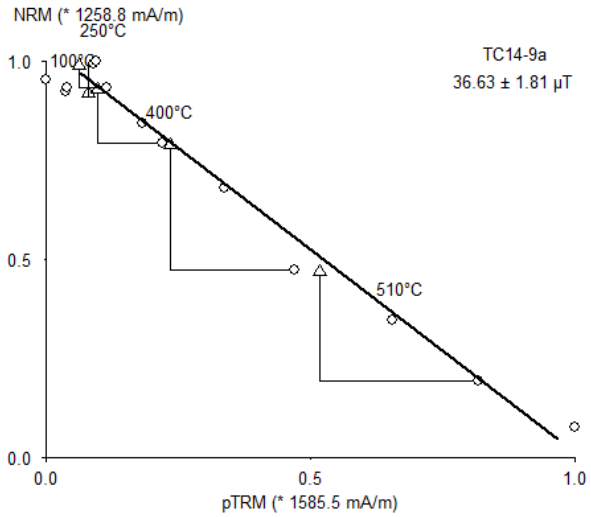

TC14-9a

36.63 ± 1.81 µT

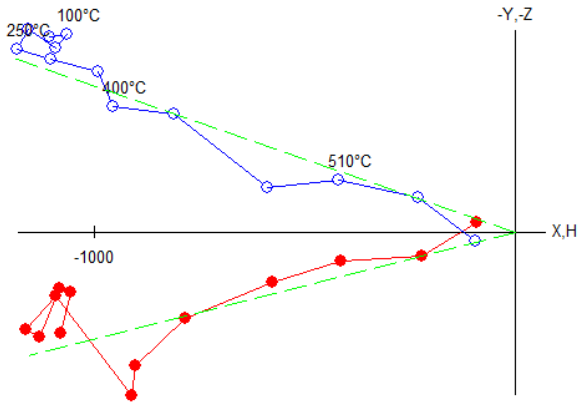

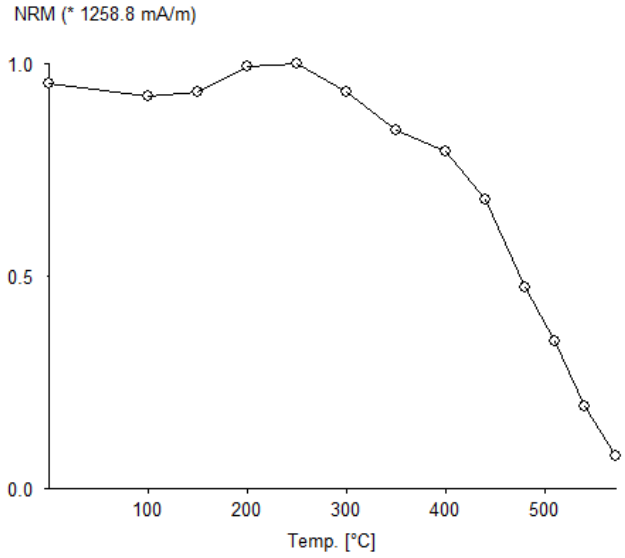

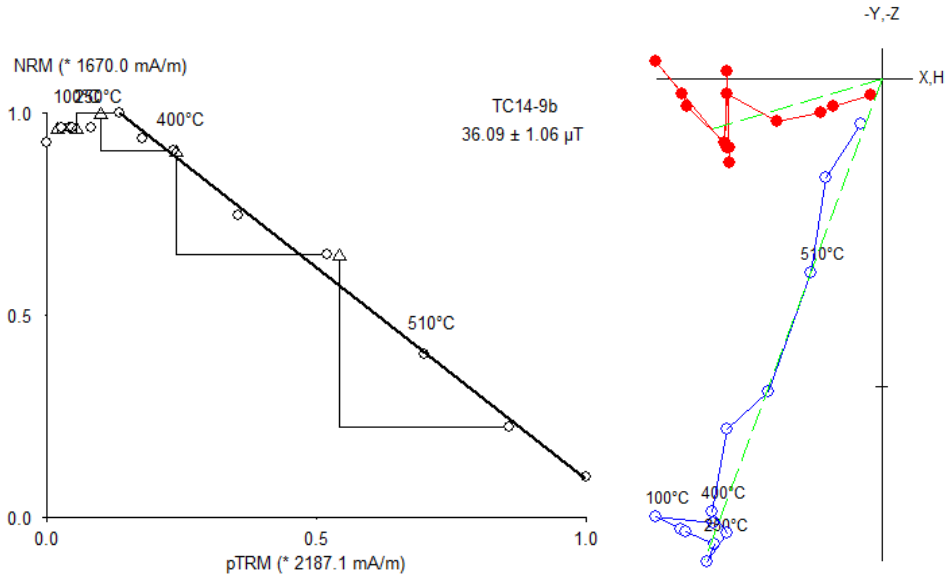
NRM (* 1670.0 mA/m)
100°C
400°C
510°C
1.0
0.5
0.0
0.0
0.5
1.0
pTRM (* 2187.1 mA/m)
TC14-9b
36.09 ± 1.06 µT
-Y,-Z
X,H
510°C
100°C
400°C

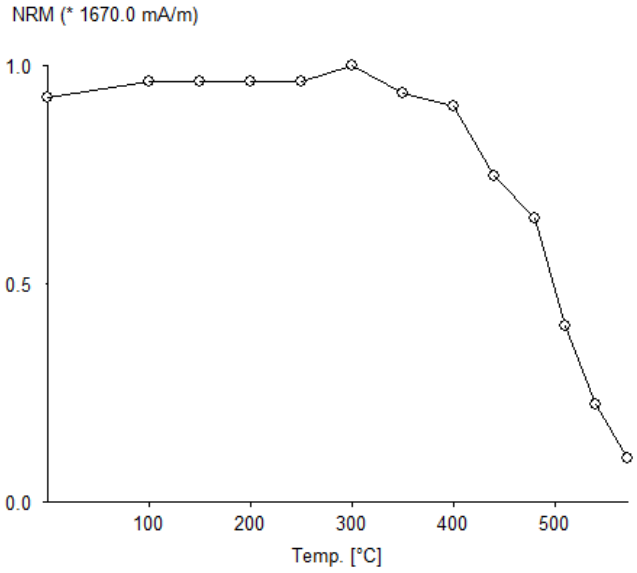
NRM (* 1670.0 mA/m)
1.0
0.5
0.0
100
200
300
400
500
Temp. [°C]

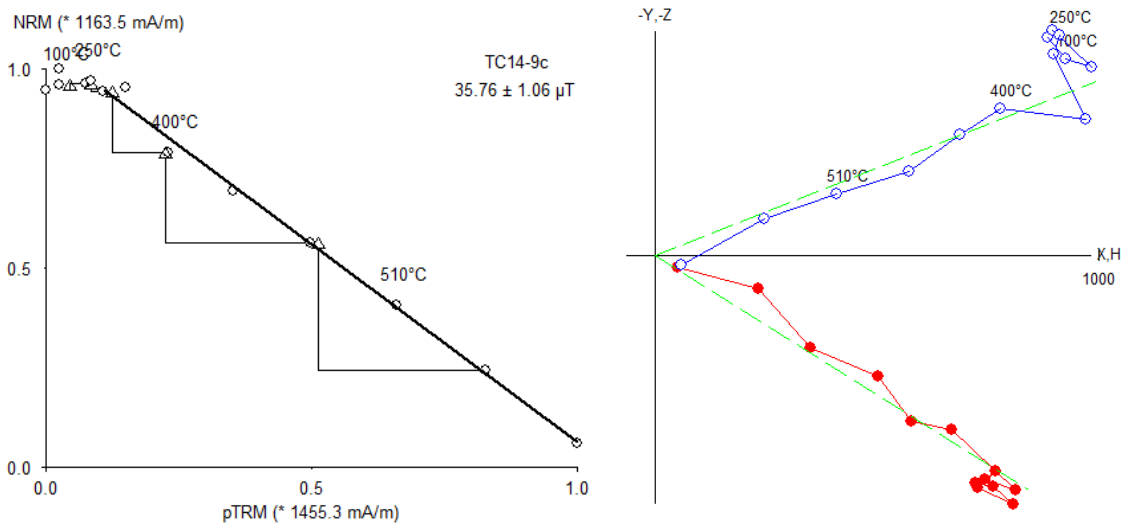
NRM (* 1163.5 mA/m)
100-250°C
1.0
0.5
0.0
400°C
510°C
TC14-9c
35.76 ± 1.06 µT
0.0
0.5
1.0
pTRM (* 1455.3 mA/m)
-Y,-Z
250°C
400°C
510°C
K,H
1000

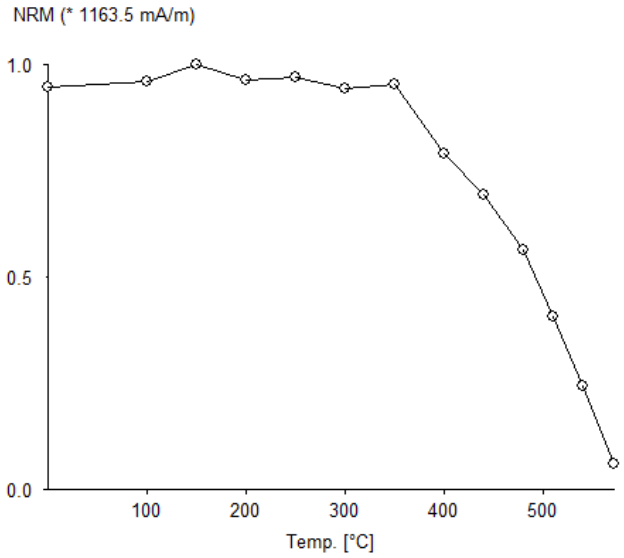
NRM (* 1163.5 mA/m)
1.0
0.5
0.0
100
200
300
400
500
Temp. [°C]

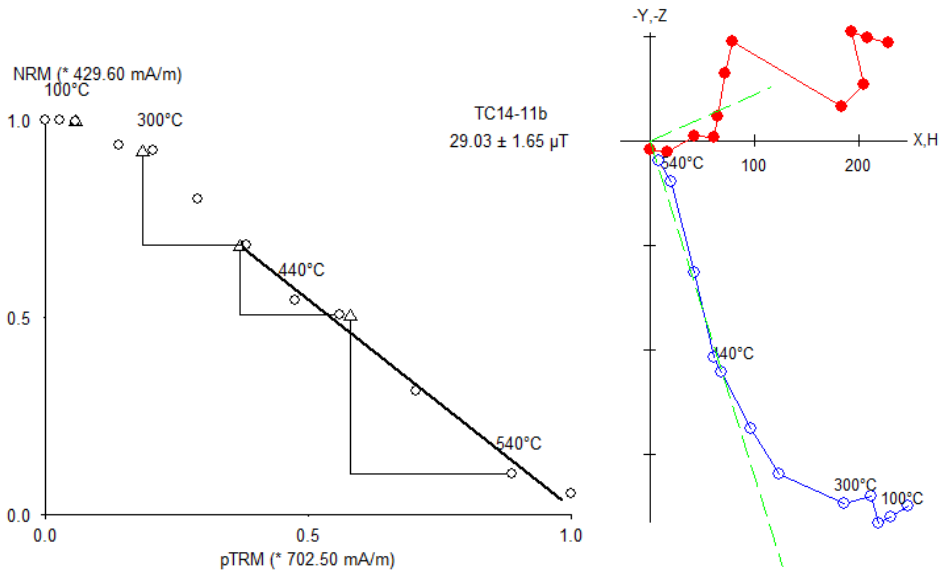
NRM (* 429.60 mA/m)
100°C
300°C
440°C
540°C
1.0
0.5
0.0
0.0
0.5
1.0
pTRM (* 702.50 mA/m)
TC14-11b
29.03 ± 1.65 µT
-Y,-Z
X,H
540°C
100
200
440°C
300°C
100°C

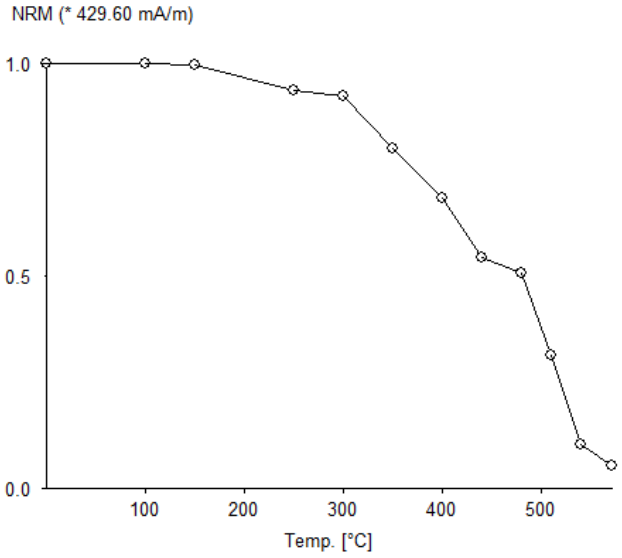
NRM (* 429.60 mA/m)
1.0
0.5
0.0
100
200
300
400
500
Temp. [°C]

- *Thin sections under the petrographic microscope*

Left images are samples under plain polarized light (PPL), right images are under cross polarized light (XPL).

TC4-3:

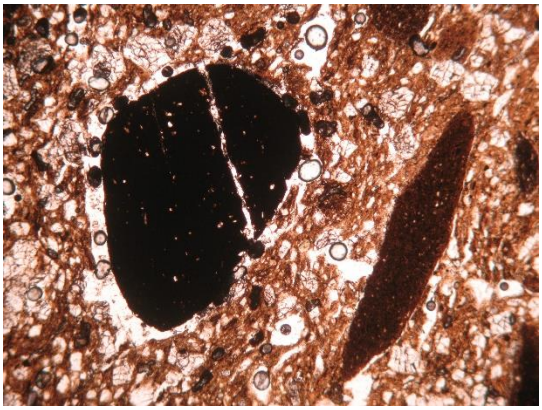

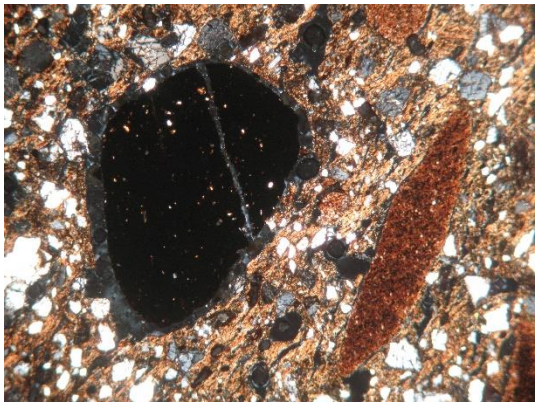

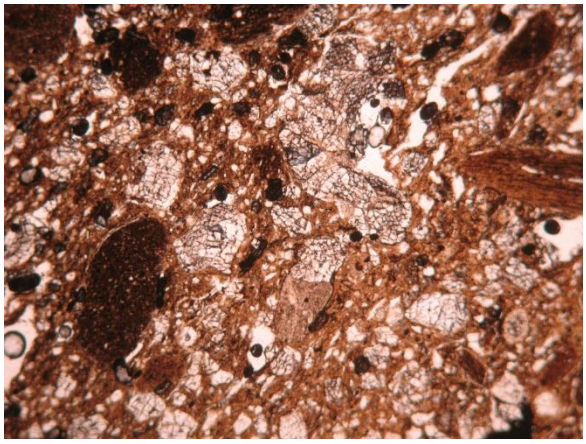

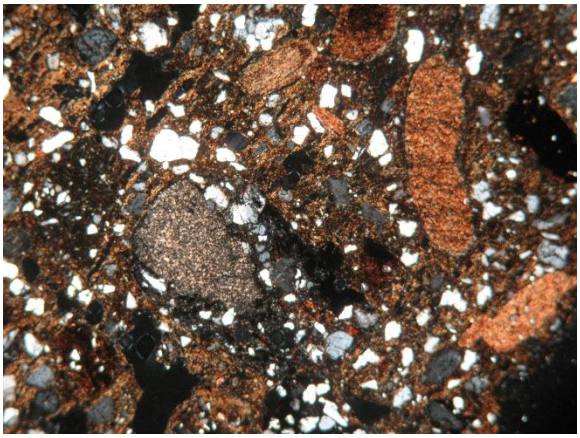

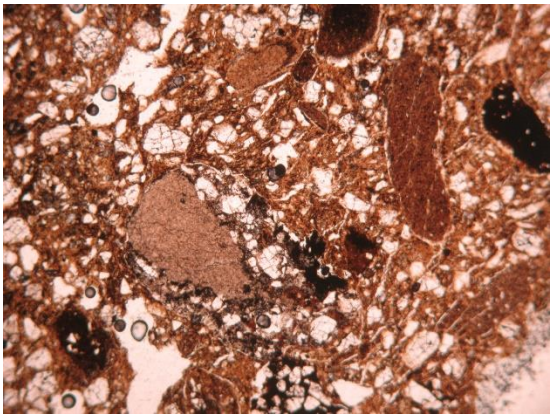

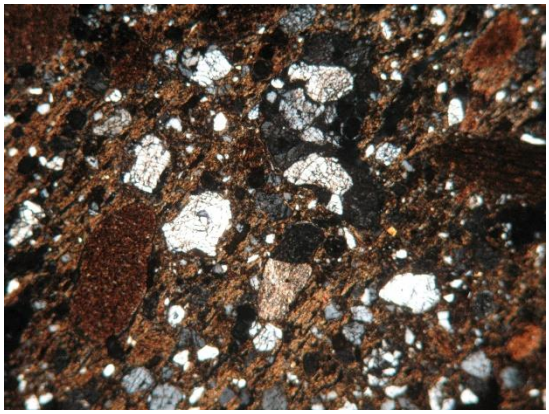

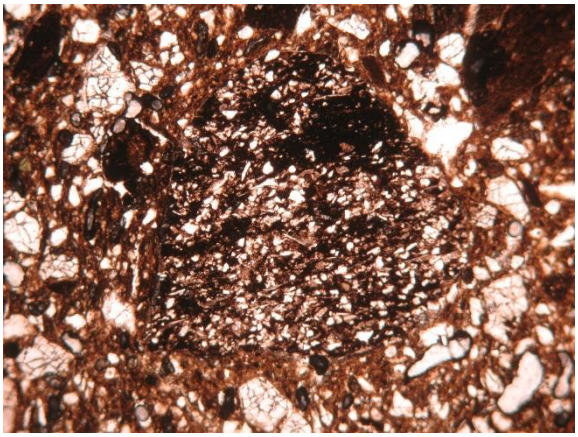
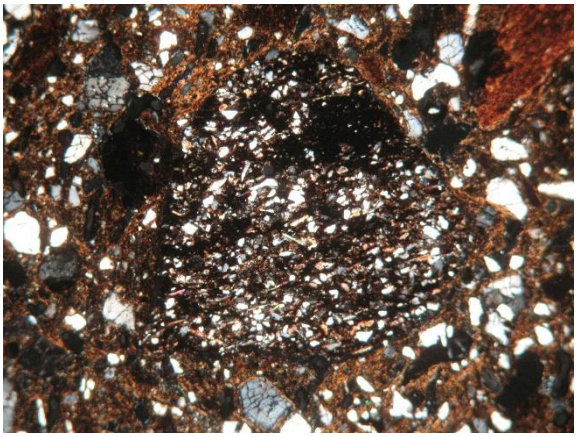
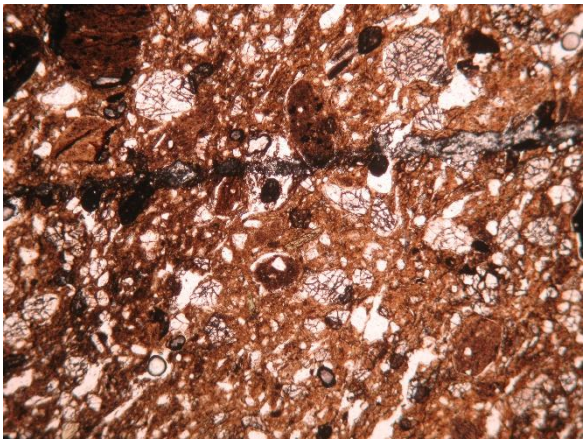
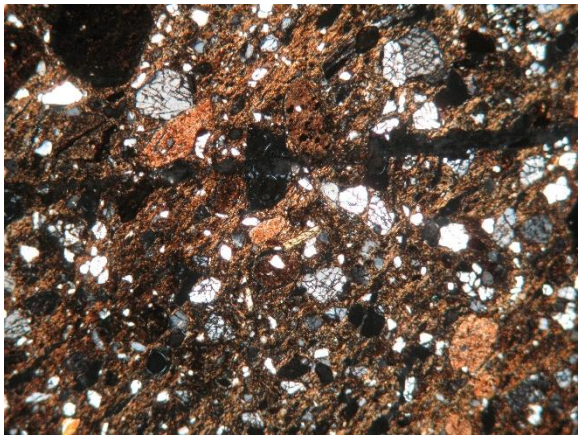

TC4-6:

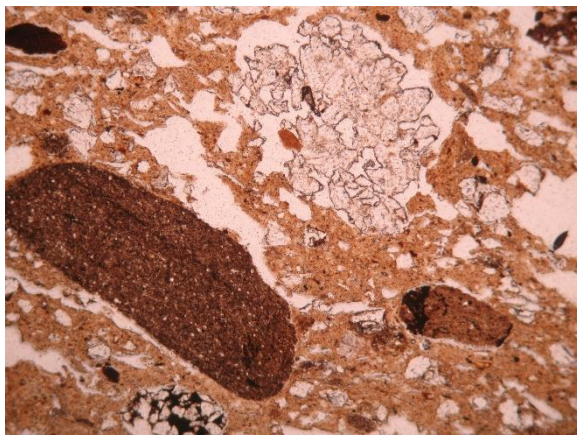
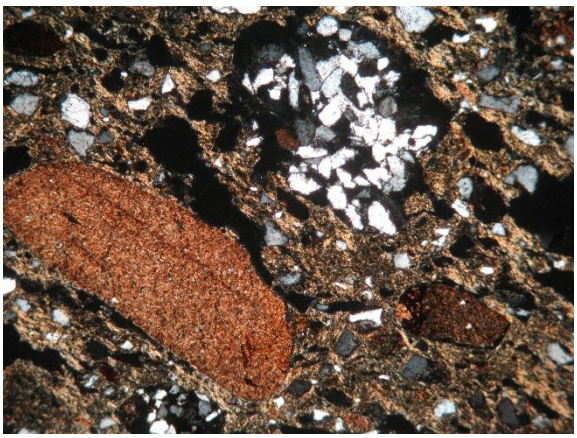
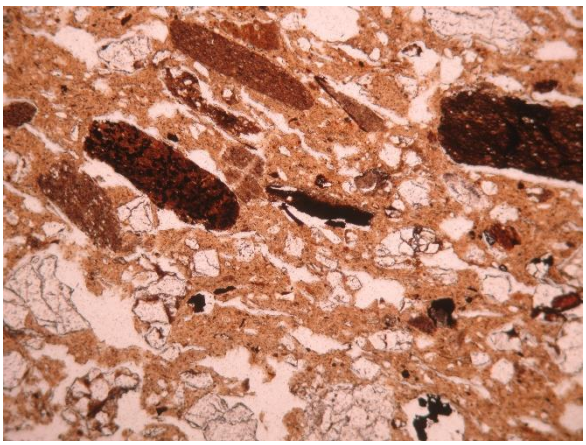
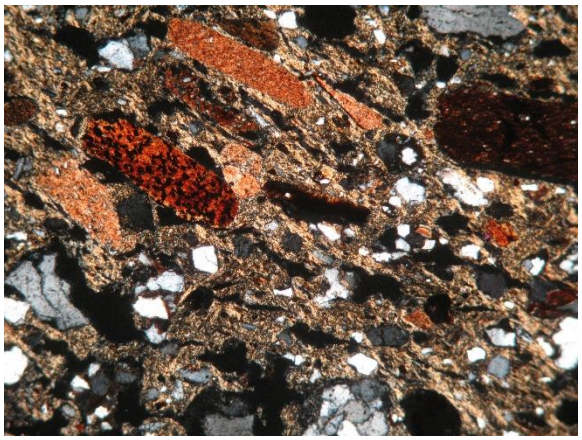
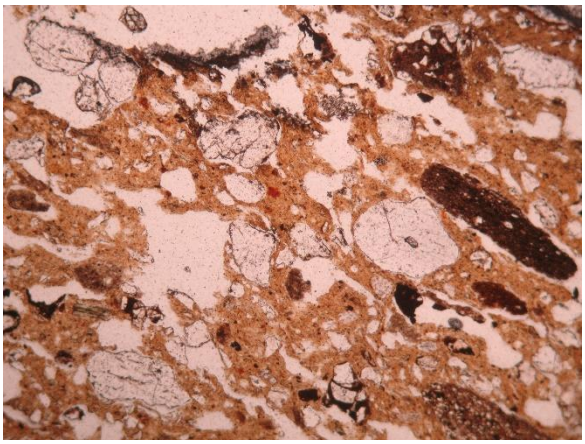
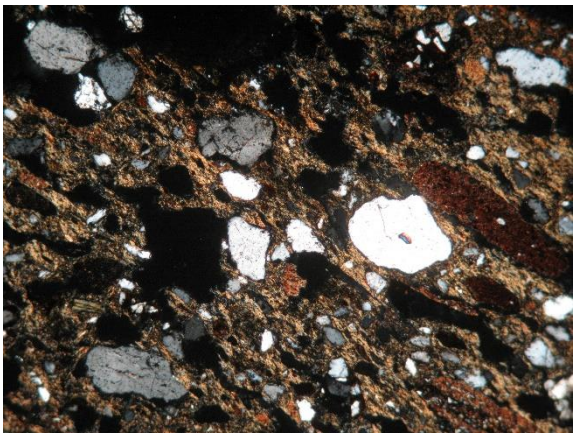

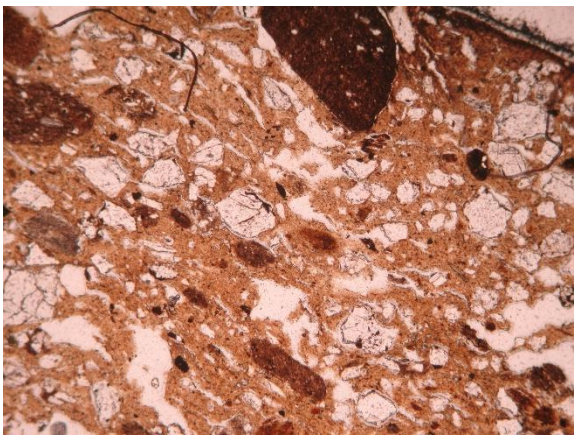

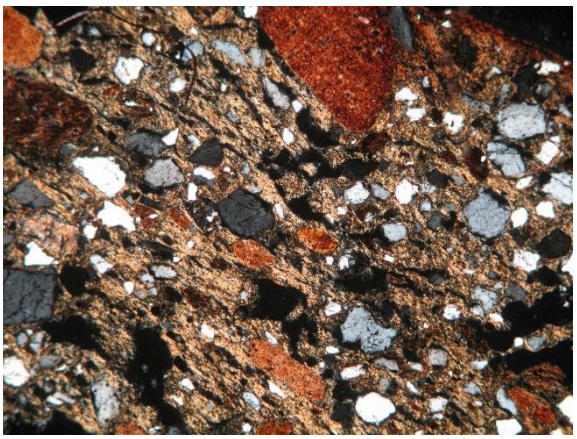

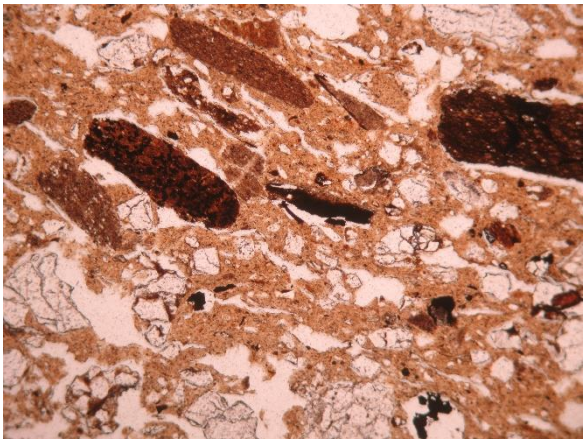

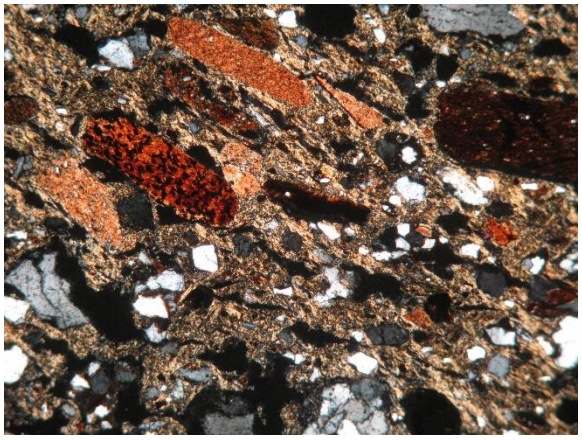

TC6-1:

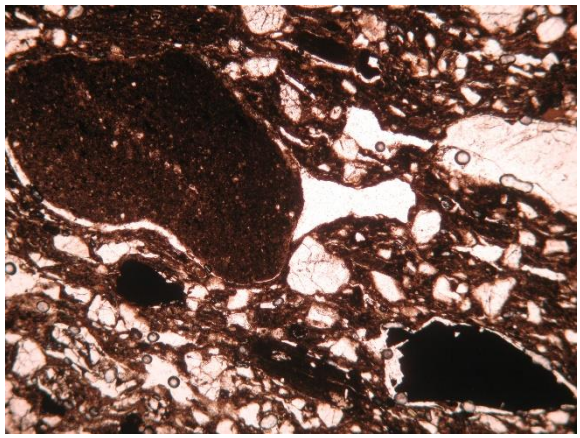

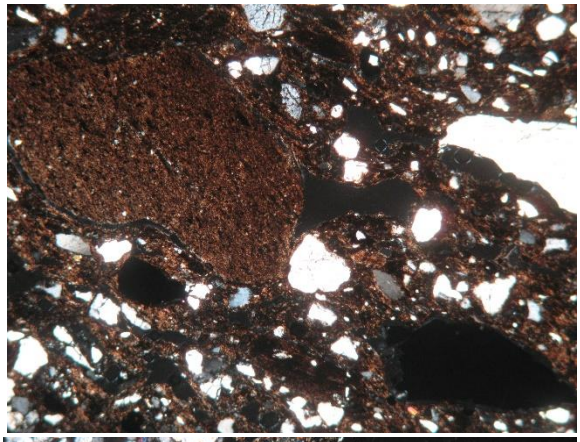

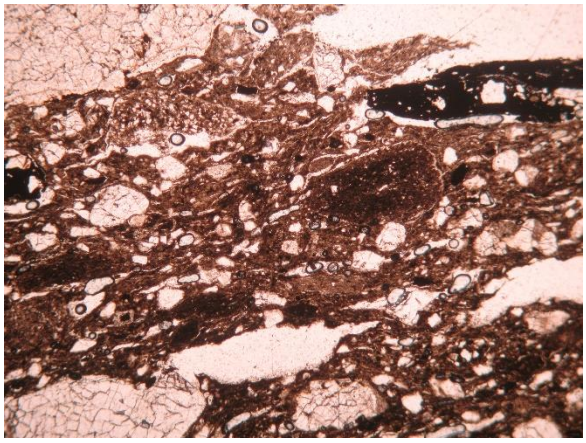

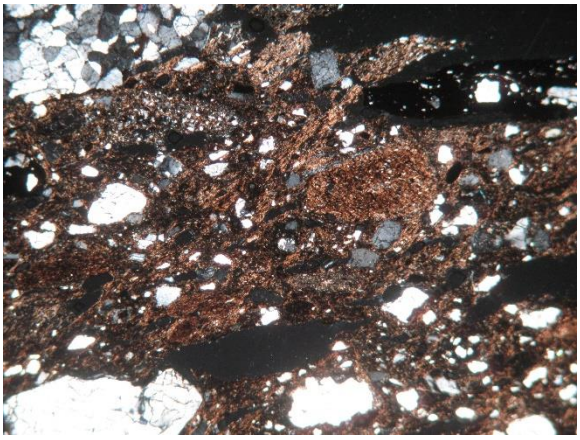

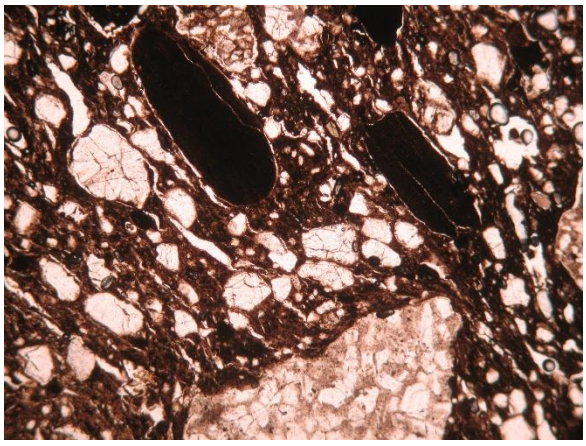

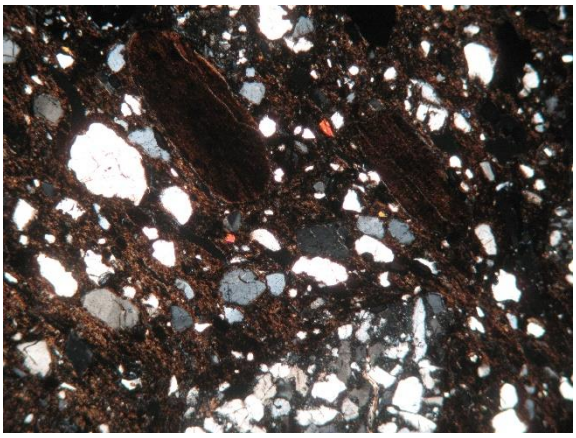

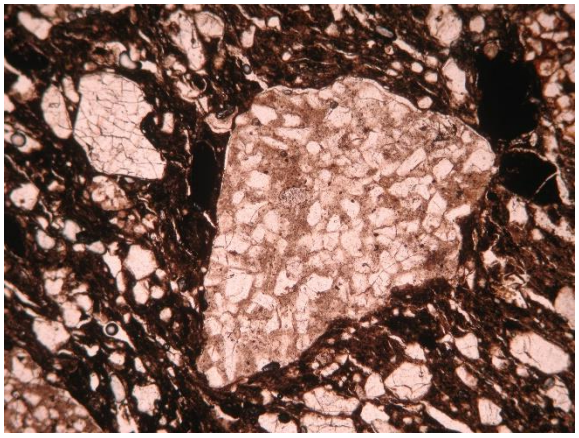

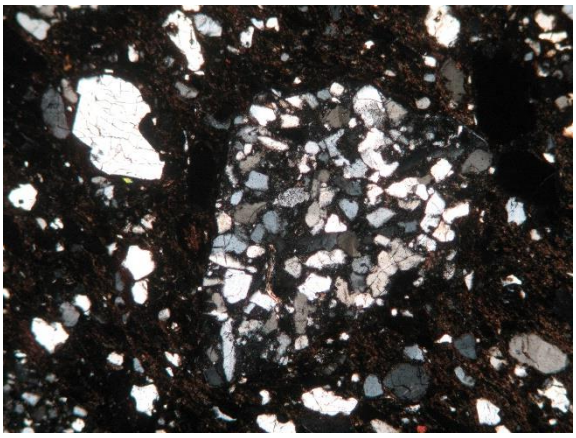

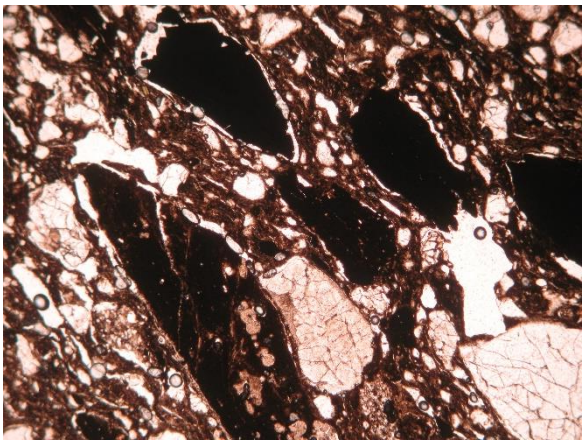

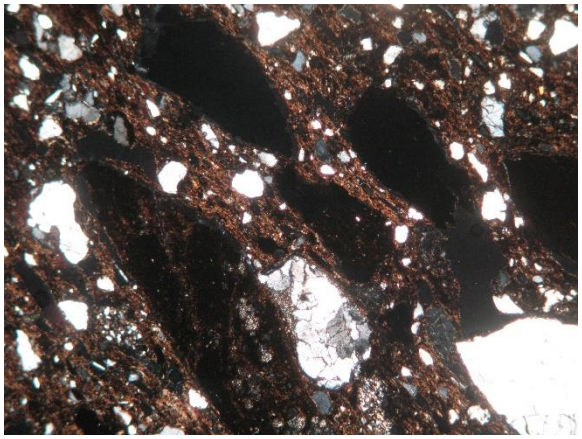

TC6-8:

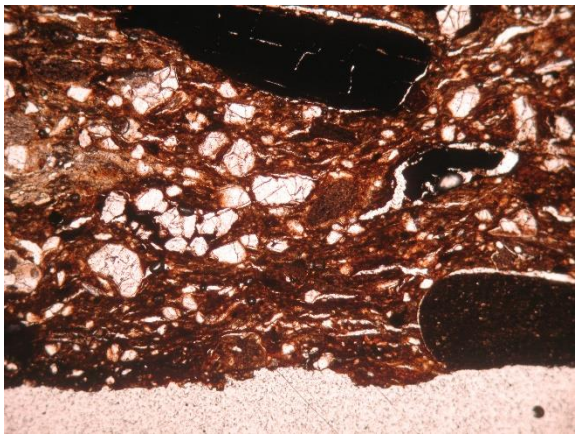
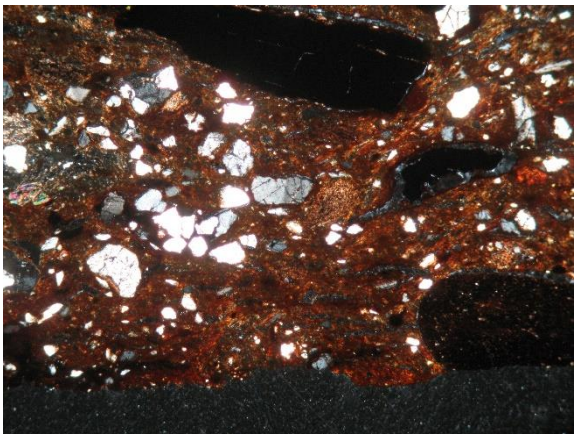
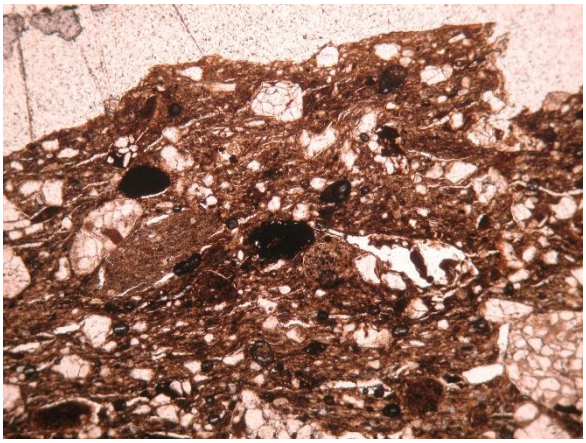

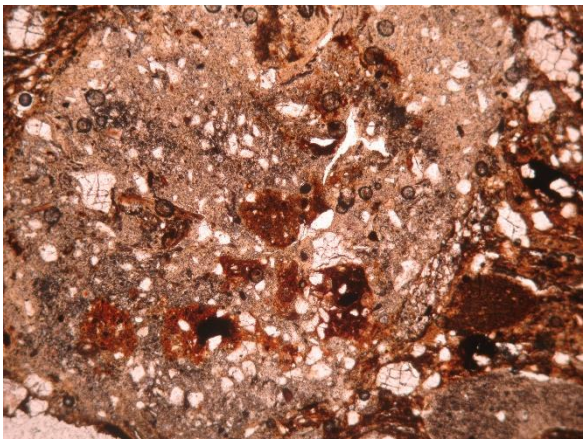
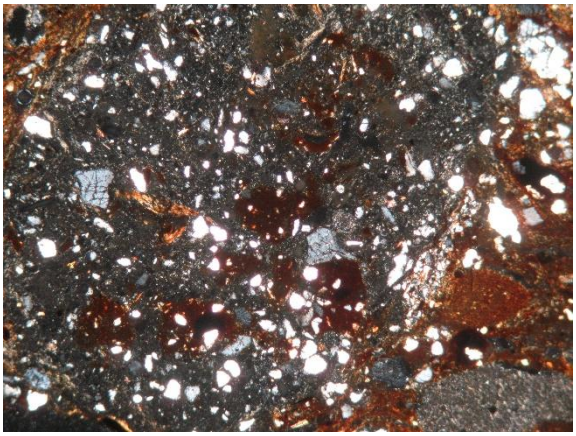

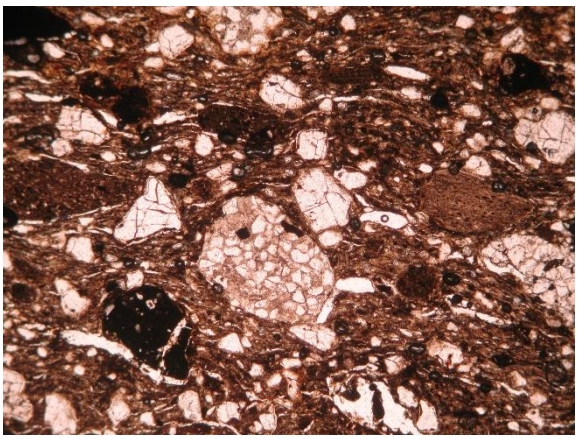
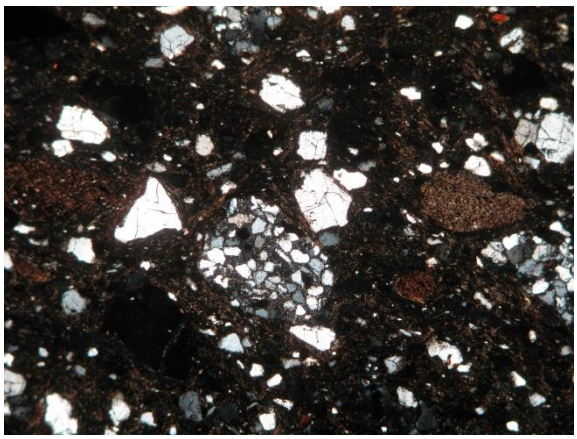
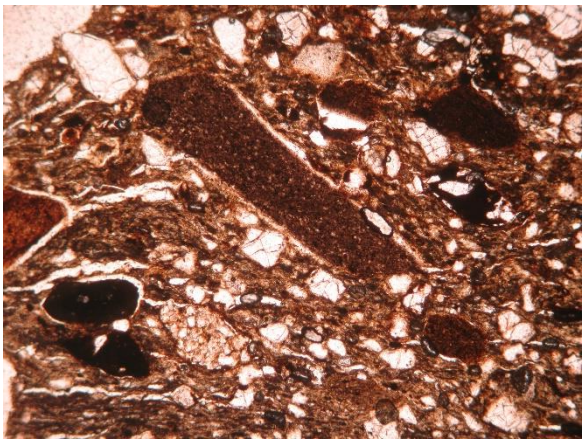
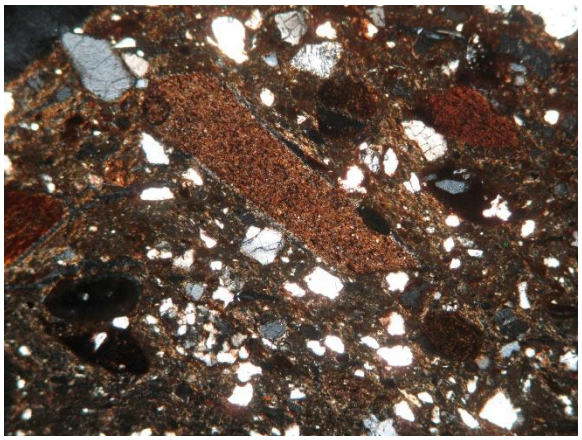
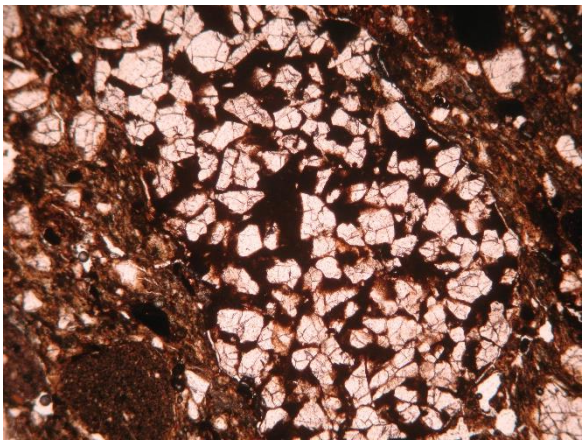
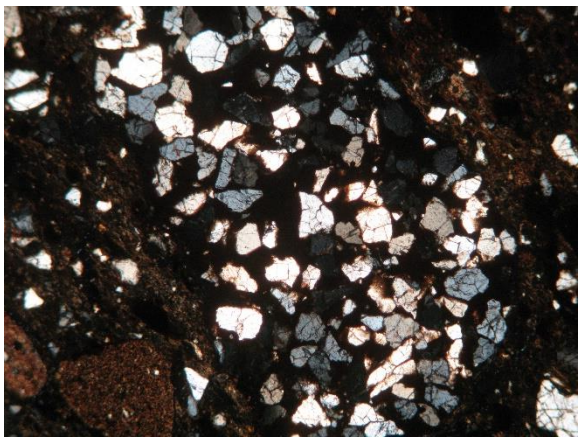

TC14-12: